Effects of self energy of the ions on the double layer structure and properties at the dielectric interface

Thesis by

Rui Wang

In Partial Fulfillment of the Requirements

for the Degree of

Doctor of Philosophy

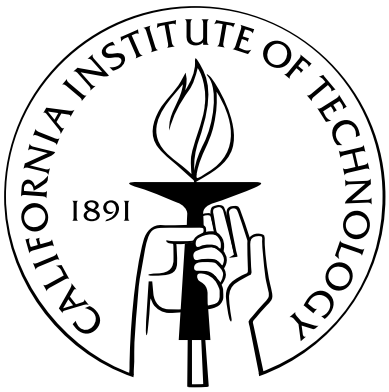

California Institute of Technology

Pasadena, California

2015

(Defended Octber 27, 2014)

To my wife, Lisha Zhang

Acknowledgments

Over the last six years, I have benefitted greatly from my interactions with many people in the Caltech community. Caltech is a very special place and I am fortunate to have had the opportunity to study here. For me, Caltech is a heaven in doing research, just like the magic journey of Harry Potter in hogwarts.

First and foremost, I am very grateful to my advisor, Professor Zhen-Gang Wang. As a teacher, he always encourage us to think about the same problem from different perspectives. I can still remember the first Statistical Mechanics lecture he gave us: he guided us to think about the collection between the ensemble average and the Lebesgue integration. In my twenty-year experience as a student, I have never had such amazing feeling as in his class. As a researcher, his depth of knowledge and insights impressed me from the very beginning of my research. I took almost five years to fully understand his general theory about the self energy of the ions. I can always find the solution from him when I have a question. He is the role model to me in my research career. As an advisor, he not only helps me solve specific problems in my projects, but also gives me a lot of priceless suggestion for my future career. I feel so lucky to be his student!

I am particularly grateful to the members of my committee, Professor John Brady, Professor David Tirrell, Professor Thomas Miller and Professor Rudolph Marcus for helpful discussions on the work done in this thesis. They will serve as guidance in my scientific development throughout the rest of my career.

I wish to thank Kathy Bubash for welcoming me to Caltech, and later for always being helpful. Kathy has been offering the most and best help I have ever experienced. I am also thankful to the past and present members of the Wang group, Dr. Bradley Olsen, Dr. Issei Nakamura, Dr. Christina Ting, Dr. Xiaofei Xu, Dr. Umi Yamamoto, Bilin Zhuang, Kevin Shen, Issac Fees and Ahmad Omar, for their support. Discussion with them is very helpful and gives me a lot of inspirations. I also wish to thank my friends, Jonathan Choi, Mu Wang and Ran Duan, for keeping my life fun at Caltech.

I am deeply appreciative of my parents' support; they have been both a source of motivation and an understanding outlet for frustration. I am also thankful for the support of my parents-in-law.

Finally, I want to express my gratitude my wife, Lisha Zhang, for her love, support, encouragement, critique, devotion, and wisdom. She has sacrificed a lot to let me fulfill my dream. I hope I

can help her to fulfill her own dream in the future just like what she is doing for me right now. I could not have done this without her.

Abstract

Although numerous theoretical efforts have been put forth, a systematic, unified and predictive theoretical framework that is able to capture all the essential physics of the interfacial behaviors of ions, such as the Hofmeister series effect, Jones-Ray effect and the salt effect on the bubble coalescence remain an outstanding challenge. The most common approach to treating electrostatic interactions in the presence of salt ions is the Poisson-Boltzmann (PB) theory. However, there are many systems for which the PB theory fails to offer even a qualitative explanation of the behavior, especially for ions distributed in the vicinity of an interface with dielectric contrast between the two media (like the water-vapor/oil interface). A key factor missing in the PB theory is the self energy of the ion.

In this thesis, we develop a self-consistent theory that treats the electrostatic self energy (including both the short-range Born solvation energy and the long-range image charge interactions), the nonelectrostatic contribution of the self energy, the ion-ion correlation and the screening effect systematically in a single framework. By assuming a finite charge spread of the ion instead of using the point-charge model, the self energy obtained by our theory is free of the divergence problems and gives a continuous self energy across the interface. This continuous feature allows ions on the water side and the vapor/oil side of the interface to be treated in a unified framework. The theory involves a minimum set of parameters of the ion, such as the valency, radius, polarizability of the ions, and the dielectric constants of the medium, that are both intrinsic and readily available. The general theory is first applied to study the thermodynamic property of the bulk electrolyte solution, which shows good agreement with the experiment result for predicting the activity coefficient and osmotic coefficient.

Next, we address the effect of local Born solvation energy on the bulk thermodynamics and interfacial properties of electrolyte solution mixtures. We show that difference in the solvation energy between the cations and anions naturally gives rise to local charge separation near the interface, and a finite Galvani potential between two coexisting solutions. The miscibility of the mixture can either increases or decreases depending on the competition between the solvation energy and translation entropy of the ions. The interfacial tension shows a non-monotonic dependence on the salt concentration: it increases linearly with the salt concentration at higher concentrations, and

decreases approximately as the square root of the salt concentration for dilute solutions, which is in agreement with the Jones-Ray effect observed in experiment.

Next, we investigate the image effects on the double layer structure and interfacial properties near a single charged plate. We show that the image charge repulsion creates a depletion boundary layer that cannot be captured by a regular perturbation approach. The correct weak-coupling theory must include the self-energy of the ion due to the image charge interaction. The image force qualitatively alters the double layer structure and properties, and gives rise to many non-PB effects, such as nonmonotonic dependence of the surface energy on concentration and charge inversion. The image charge effect is then studied for electrolyte solutions between two plates. For two neutral plates, we show that depletion of the salt ions by the image charge repulsion results in short-range attractive and long-range repulsive forces. If cations and anions are of different valency, the asymmetric depletion leads to the formation of an induced electrical double layer. For two charged plates, the competition between the surface charge and the image charge effect can give rise to like- charge attraction.

Then, we study the inhomogeneous screening effect near the dielectric interface due to the anisotropic and nonuniform ion distribution. We show that the double layer structure and interfacial properties is drastically affected by the inhomogeneous screening if the bulk Debye screening length is comparable or smaller than the Bjerrum length. The width of the depletion layer is characterized by the Bjerrum length, independent of the salt concentration. We predict that the negative adsorption of ions at the interface increases linearly with the salt concentration, which cannot be captured by either the bulk screening approximation or the WKB approximation. For asymmetric salt, the inhomogeneous screening enhances the charge separation in the induced double layer and significantly increases the value of the surface potential.

Finally, to account for the ion specificity, we study the self energy of a single ion across the dielectric interface. The ion is considered to be polarizable: its charge distribution can be self-adjusted to the local dielectric environment to minimize the self energy. Using intrinsic parameters of the ions, such as the valency, radius, and polarizability, we predict the specific ion effect on the interfacial affinity of halogen anions at the water/air interface, and the strong adsorption of hydrophobic ions at the water/oil interface, in agreement with experiments and atomistic simulations.

The theory developed in this work represents the most systematic theoretical technique for weak-coupling electrolytes. We expect the theory to be more useful for studying a wide range of structural and dynamic properties in physicochemical, colloidal, soft-matter and biophysical systems.

Contents

List of Figures

Chapter 1

Introduction

1.1 Background

Ions are essential in physical chemistry, colloidal science, electrochemistry, biology and many other areas of science and engineering[1, 2]. For example, salts are widely used in the separation of the azeotropes[3], and have also been found effective in the enhanced oil recovery (EOR) technology to increase the productivity and purity of crude oil[4]. The excessive rate of ozone depletion is closely related to the solvation of halide ions in sea salt aerosols[5]. In the energy arena, there is much current interest in lithium salt-doped polymers as new battery materials[6, 7]. For charged macromolecules (see Figure 1.1), such as the colloidal particles, polyelectrolyte solutions, membranes and biological polyelectrolytes (proteins, DNA and RNA), the dissociated ions typically form diffuse clouds which partially screening the electrostatic field around these charged macromolecules[8, 9, 10]. Protein stability and solubility are well known to be significantly affected by the addition of salts[11]. The interaction force between colloidal particles can be systematically tuned by controlling the salt concentration, as can be the size of micellar aggregates formed by ionic surfactants[12]. The kinetics of delivering nanoparticles through lipid membrane is also affected by electrostatic interactions[13]. The ions play a central role, mediating an effective interaction that differs from the direct Coulomb interaction in magnitude and in range (in some situations, even in sign), which affects a wealth of structural and dynamic properties[14].

The effects of ions can often be understood in terms of the translational entropy and electrostatic screening. Modulation of the colloidal forces by salt ions relies primarily on their screening of the Coulomb interaction between the colloidal particles, whereas the adsorption of a charged polymer on an oppositely charged surface is usually explained by the translational entropy gain upon the release of counterions. These effects are often described in the framework of the Poisson-Boltzmann (PB) theory, a mean-field theory that describes a system in terms of the mean electrostatic potential and the average concentration of the mobile ions. At large surface-charge density, high counter-ion valency and high ion concentration - the so-called strong coupling limit - it is well recognized that

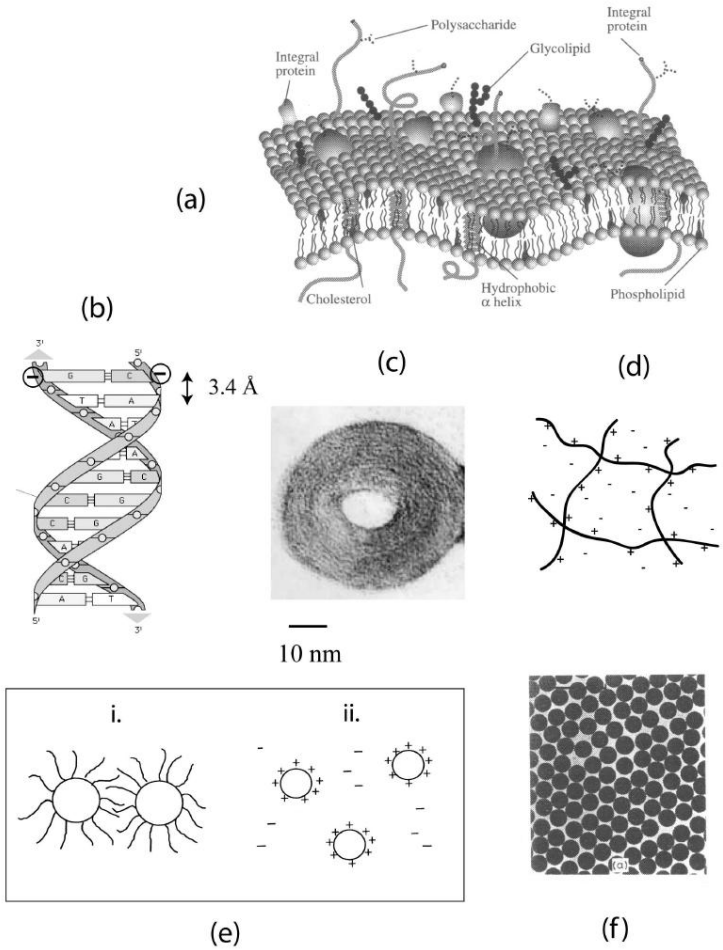

Figure 1.1: Charged macromolecules in solution. (a) Cell membrane (b) DNA structure (c) Electron micro-graph of DNA, collapsed into a toroidal structure in the presence of spermine (4+) ions[8] (d) Polyelectrolyte solution (e) Colloids: i. sterically stabilized ; ii. charge stabilized (f) Polystyrene latex particles in solution. Figures (a) and (f) are reproduced from Ref.[9] and Ref.[10], respectively.

PB theory fails to capture a number of qualitative effects observed in experiments and simulation, such as like-charge attraction[15, 16, 17] and charge inversion[18, 19, 20, 21]. Integral-equation methods[22, 23] and other strong-coupling theories[17, 24] have been employed to account for the strong ion-ion correlations in this regime. In the opposite limit - the weak-coupling regime - it is generally accepted that the electrostatics is well described by the PB theory[25, 26, 27, 28]. Performing a perturbation expansion approach, Netz[28] demonstrated that the PB theory is the leading-order theory in the weak-coupling limit, and becomes exact in the limit of zero coupling strength. Although these demonstrations were performed explicitly for counterion-only systems, the conclusions are generally believed to hold when salt ions are added. Thus, many researchers in the electrolyte community consider the weak-coupling theory to mean the PB theory; in other words,

weak-coupling is considered synonymous with the validity of the PB theory.

However, there are many systems in the weak-coupling regime for which the PB theory fails to offer even a qualitative explanation of the behavior, especially for ions distributed in the vicinity of an interface with dielectric contrast between the two media (like the water-vapor/oil interface). In the absence of a fixed surface charge, the PB theory predicts a trivial and erroneous solution of uniform ion distribution across the interface, which contradicts with the fact that there is an unequal partition of ions between the two media with dielectric difference. In addition, the PB theory predicts a constant electrostatic potential across the interface, which also contradicts with the phenomenon that there is a finite potential difference between the two media known as the Galvani potential. Another prominent example that the PB theory fails to explain is the Jones-Ray effect - discovered more than 70 years ago - that the surface/interface tension of salt solutions first decreases, reaches a minimum, and then increases again, as a linear function of salt concentration[29]. Some other examples include salt effects on bubble coalescence[30], and the ion conductivity in artificial and biological ion-channels[31, 32, 33]. Recently, Laanait et. al. observed condensation of the hydrophobic ion at the water-oil interface by X-ray reflectivity study, which is also inconsistent with the prediction of the PB theory[34, 35].

Another important phenomenon that cannot be captured by the PB theory is the specific ion effect[36] (which is also known as the Hofmeister series effect): many interfacial phenomena, such as the surface tension of electrolyte solution, salt effects on bubble coalescence and the effectiveness of salts on the stability of protein solutions and colloidal suspensions, exhibit strong dependence on the chemical identity of the ions. Over 120 years ago, Hofmeister[37] observed that different ions have a very different effects on the stability of protein solutions. While some electrolytes are very efficient at salting out proteins, others lead to protein precipitation only at much larger concentrations. A related mystery, which is also very old, has to do with the surface tension. Some hundred years ago Heydweiller[38] noted that adding a strong electrolyte to water leads to an increase in the surface tension of the water-air interface. While the dependence on the type of cation is weak, there is a strong variation of the excess surface tension with the type of anion - the lighter halides lead to larger excess surface tension than the heavier ones. The sequence is precisely the reverse of the Hofmeister one. Although this specific ion effect has been known for over a century, it is still a long-standing mystery in the fields of physical chemistry and biophysics.

A key factor missing in the PB theory is the self energy of the ion[39], which determines the ion distribution at the dielectric interface as well as other interfacial properties. The self energy of the ion is the reversible work required to assemble the charge and mass of the ion at the spatial location $\mathbf{r}$ by bringing in the constituent charges and masses from an infinitely dispersed state, where the interaction is zero. The self energy can be divided into the electrostatic contribution and non-electrostatic contribution. The electrostatic contribution includes the local Born solvation

energy, the ion-ion correlation and the long-range image charge effect, whereas the non-electrostatic contribution includes the cavity energy, the hydration and some other effects. Retaining only the short-range Born solvation energy, Nakamura et. al.[40, 41] showed that adding a small amount of lithium salt to a (polyethylene oxide)-b-polystyrene (PEO-PS) block copolymers significantly affects the order-disorder-transition temperature of the block copolymer.

Theoretical efforts to account for the effect of self energy near an interface were pioneered by Wagner, Onsager and Samaras (WOS)[42, 43]. The WOS theory predicts depletion of ions from the surface due to the image force repulsion and can qualitatively explain the increase of surface tension with the salt concentration. However, the surface tension predicted by the WOS theory deviates sharply from the experiment data in the high salt concentration regime as shown in Figure 1.2[44, 45, 46]. In addition, it fails to capture both the Jones-Ray effect and the Hofmeister series effect.

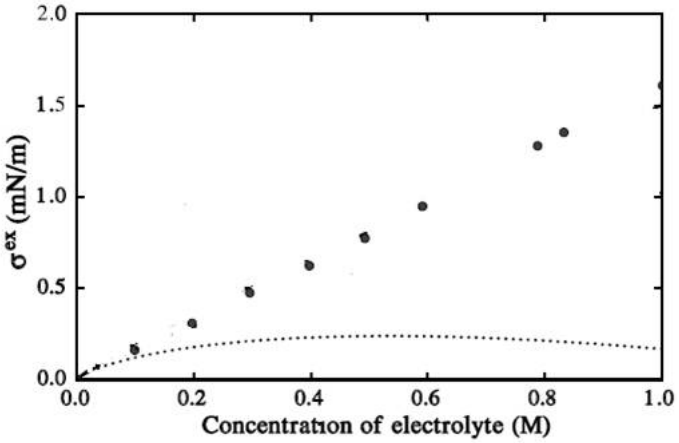

Figure 1.2: The surface tension of 1:1 electrolyte solution calculated by WOS theory (the dot line) in comparison with the experiment data (the filled circles).

There are several drawbacks in the WOS theory. First, the WOS theory assumes that the image charge repulsion is screened by the constant bulk screening strength, which fails to capture the fact that the screening is spatially varying near the dielectric interface. The bulk screening approximation obviously overestimates the screening effect on this ion, giving rise to a concave downwards curve when the the surface tension of the electrolyte solution is plotted against the salt concentration as shown in Figure 1.2, which contradicts with the linear increase of the surface tension observed in experiment.

Another drawback of the WOS theory and its subsequent modifications is modeling the ion as a point charge, which results in the self energy being discontinuous at the dielectric interface. The self energy diverges to positive infinity when the ion approaches the interface from the water side, giving rise to complete absence of ions. The picture of ion-free zone obtained from WOS theory

fails to explain the effect of ion specificity on the surface/interface tension. It also contradicts with experiment[47] and simulation[48] results that anions are able to approach the interface closer than cations, or even be adsorbed to it. On the other hand, the self energy diverges to negative infinity when the ion approaches the interface from the vapor/oil side, which would lead to unlimited accumulation of ions there. To avoid this unrealistic behavior, the ion distribution is artificially restricted to lie only in the water phase. However, it has been pointed out that some distribution of ions in the vapor/oil phase is essential in order to explain the existence of the electrostatic potential gradient at the interface and the initial drop of the surface tension in the Jones-Ray effect. In addition, the point charge model of the ion excludes the probability of charge polarization[49]. Polarizability is an intrinsic property of specific ions, and can be very different from one ion to another. Computer simulation by Jungwirth and Tobias showed that the polarizability of different ions is a key contribution to their affinity to the interface[48].

1.2 Motivation and Organization of the Thesis

Although numerous theoretical efforts have been put forth, the understanding of the interfacial behaviors of the ions, such as the Jones-Ray effect, the specific ion effect and the salt effect on the bubble coalescence remains an outstanding challenge. The focus of this thesis is on the effect of the self energy of the ions on the double layer structure and interfacial properties near the dielectric interface. We want to achieve the following goals through this work:

1. It is desirable to develop a self-consistent theory that can treat both the short-range and long-range electrostatic self energy, the nonelectrostatic contribution of the self energy, the ion-ion correlation and the screening effect systematically in a single framework, instead of a piecewise *ad hoc* construction as in previous work[50, 51]. The new theory should capture both the non-meanfield effect and the specific ion effect. The theory should involve a minimum set of parameters of the ion, such as the valency, radius, polarizability of the ions, and the dielectric constants of the medium, that are both intrinsic and readily available.

2. The model for the self energy of the ion in the theory needs to be free of the divergence problems and give a continuous self energy across the interface, which naturally allows the existence of ions in the vapor/oil phase. This continuous feature of this new self-energy model represents an essential improvement over existing models and allows ions on the water side and the vapor/oil side of the interface to be treated in a unified framework.

3. It is necessary to clarify what is the correct theory for the weakly charged surfaces. In the the weak-coupling regime, it is generally accepted that the electric double layer is well described by the PB theory. Kanduc and Podgornik[52, 53] concluded that, under the weak-coupling condition, the image force only enters as a small correction to the leading PB theory, which vanishes in the limit

of zero coupling. Physically, however, a single ion in solution next to a surface of a lower dielectric plate obviously should feel the image charge repulsion even in the absence of any surface charge, and the ion distribution - the probability of finding the ion at any location - should reflect the image charge interaction through the Boltzmann factor. This was the case studied in the pioneering work of Wagner, and Onsager and Samaras for the surface tension of electrolyte solutions. The discrepancy between different theories in treating the same *physical* weak-coupling condition need to be clarified.

4. It is still debated the existence and relative importance of the nonelectrostatic contributions of the self energy, such as cavity energy, hydration, and dispersion forces[36]. Although the constituent components in the electrostatic self energy have become clear in recent years, the problem is then in the accurate and consistent treatment of the electrostatic effects. Such a treatment is essential both because the electrostatic part is a major component in the self energy of an ion, and because the relative importance of the nonelectrostatic contributions can only be evaluated when the electrostatic contribution is treated accurately.

The issues discussed in this thesis are organized in six chapters. Chapter 2 presents the general theory, chapter 3 studies the effect of the local Born solvation energy, chapters 4 and 5 study the image charge effect, chapter 6 studies the effect of the inhomogeneous screening, and chapter 7 studies the specific ion effect. Each chapter either has been published or is in preparation as one scientific paper which can be read independently of the others.

In chapter 2, we develop a general theory for electrolyte solutions with dielectric inhomogeneity by using the renormalized Gaussian variational approach. The key result of the theory is a set of self- consistent equations for the mean electrostatic potential, the correlation function (Green function), the self energy of ions (including both the short-range Born solvation energy and the long-range image charge effect) and the incompressible field due to the nonelectrostatic ion-size effect. The general theory is applied to study the thermodynamic property of the bulk electrolyte solution by comparing the activity coefficient and the osmotic coefficient predicted by our theory with the experimental data.

In chapter 3, we first investigate the effect of local Born solvation energy on the bulk thermodynamics of electrolyte solution mixtures. The spinodal and phase boundary for the phase separation of the mixture are calculated. Then, the theory is applied to study the effect of Born solvation energy on the interfacial structure and interfacial tension of the electrolyte solution mixture. Both the salt concentration effect and the ion size effect on the interfacial tension are considered.

In chapter 4, we apply the general theory to electrolyte solution in contact with a single weakly-charged surface. We discuss whether the image charge effect should appear in the Boltzmann factor, which is different from the previous theoretical treatments. Then we study the image charge effect on the double layer structure for both the system containing only counterions and the system with added salts. The salt effect on the surface excess free energy is also investigated.

In chapter 5, we examine the image charge effects on the electrical double layer structure and forces between two plates. First, the ion depletion and depletion force for symmetric salt solution between two neutral plates is studied. Then, we investigate the induced double layer formed by asymmetric salt. We also consider the complex ion depletion when the salt solution is a mixture of 1:1 electrolyte and 2:1 electrolyte. Finally, the double layer structure and forces between two weakly-charged plates is studied. We show that the competition between the surface charge and the image charge effect can give rise to like- charge attraction and charge inversion.

In chapter 6, we theoretically study the inhomogeneous screening effect of electrolyte solution near the dielectric interface. By comparing the results from fully solving the Green function with the approximated methods (the bulk screening approximation and the WKB approximation), we show the nature of inhomogeneous screening and its effect on the depletion layer structure and interfacial properties.

In chapter 7, we present a unified model for the self energy of an ion that treats all the electrostatic contributions: the Born solvation energy, the image charge interaction, and ion polarizability in a single, consistent framework. Along with the relevant nonelectrostatic contributions, we apply our theory to study the specific ion effect on the interfacial affinity of halogen anions at the water/air interface and the strong adsorption of hydrophobic ions at the water/oil interface.

Bibliography

[1] J. N. Israelachvili, *Intermolecular and surface forces*, 2nd Ed. (Academic, London, 1992).

[2] D. Andelman, in *Soft Condensed Matter Physics in Molecular and Cell Biology*, W. C. K. Poon and D. Andelman, eds. (Taylor and Francis, Boca Raton, Florida, 2000).

[3] W. J. Moore, *Physical Chemistry*, 3nd ed. (Prentice Hall, NJ, 1962).

[4] M. Baviere, *Basic Concepts in Enhanced Oil Recovery Processes*, (Elsevier Applied Science, London, 2007).

[5] E. M. Knipping, M. J. Lakin, K. L. Foster, P. Jungwirth, D. J. Tobias, R. B. Gerber, D. Dabdub, and B. J. Finlayson-Pitts, *Science*, **288**, 301-306 (2000).

[6] G. S. MacGlashan, Y. G. Andreev, P. G. Bruce, *Nature*, **398**, 792-794 (1999).

[7] E. D. Gomez et al., *Nano Letters*, **9**, 1212-1216 (2009).

[8] W. M. Gelbart, R. F. Bruinsma, P. A. Pincus and V. A. Parsegian, *Phys. Today*, **53**, 38-44 (2000).

[9] I. W. Hamley, *Introduction to Soft Matter. Polymers, Colloids, Amphiphiles, and Liquid Crystals*, (Wiley, Chichester, 2000).

[10] D. H. Everett, *Basic Principles of Colloid Science*, (Royal Society of Chemistry, Cambridge, 1988).

[11] S. Kumar and R. Nussinov, *Chembiochem*, **3**, 604 (2002).

[12] V. Dahirel and M. Jardat, *Curr. Opin. Colloid Interface Sci.*, **15**, 2C7 (2010).

[13] C. L. Ting and Z. -G. Wang, *Phys. Rev. Lett.*, **106** , 168101 (2011).

[14] Y. Levin, *Rep. Prog. Phys.*, **65**, 1577-1632, (2002).

[15] R. Kjellander, S. Marelja, R. M. Pashley and J. P. A. Quirk, *J. Chem. Phys.*, **92**, 4399-4407 (1990).

[16] W. R. Bowen and A. Q. Sharif, *Nature*, **393**, 663-665 (1998).

[17] Y. S. Jho, M. Kanduč, A. Naji, R. Podgornik, M. W. Kim and P. A. Pincus, *Phys. Rev. Lett.*, **101**, 188101 (2008).

[18] P. Kekicheff, S. Marcelja, T. J. Senden and V. E. Shubin, *J. Chem. Phys.*, **99**, 6098-6113 (1993).

[19] T. T. Nguyen, A. Y. Grosberg and B. I. Shklovskii, *Phys. Rev. Lett.*, **85**, 1568-1571 (2000).

[20] A. Y. Grosberg, T. T. Nguyen and B. I. Shklovskii, *Rev. Mod. Phys.*, **74**, 329-345 (2002).

[21] K. Besteman, M. A. G. Zevenbergen, H. A. Heering and S. G. Lemay, *Phys. Rev. Lett.*, **93**, 170802 (2004).

[22] R. Kjellander, T. Akesson, B. Jonsson and S. Marelja, *J. Chem. Phys.*, **97**, 1424-1431 (1992).

[23] J. W. Zwanikkena and M. Olvera de la Cruz, *Proc. Natl. Acad. Sci. USA*, **110**, 5301-5308 (2013).

[24] A. Naji, S. Jungblutb, A. G. Moreirac and R. R. Netz, *Physica A*, **352**, 131-170 (2005).

[25] P. Attard, D. J. Mitchell and B. W. Ninham, *J. Chem. Phys.*, **88**, 4987-4996 (1988).

[26] P. Attard, D. J. Mitchell and B. W. Ninham, *J. Chem. Phys.*, **89**, 4358-4367 (1988).

[27] J. C. Neu, *Phys. Rev. Lett.*, **82**, 1072-1074 (1999).

[28] R. R. Netz, *Eur. Phys. J. E*, **5**, 557-574 (2001).

[29] G. Jones and W. A. Ray, *J. Am. Chem. Soc.* **59**, 187 (1937).

[30] V. S. J. Craig, B. W. Ninham and R. M. Pashley, *Nature* **364**, 317 (1993).

[31] A. Parsegian, *Nature*, **221**, 844-846 (1969).

[32] T. Bastug and S. Kuyucak, *Biophys. J.*, **84**, 2871-2882 (2003).

[33] S. Buyukdagli, M. Manghi and J. Palmeri, *Phys. Rev, Lett.*, **105**, 158103, (2010).

[34] N. Laanait, et al., *J. Chem. Phys.*, **132**, 171101 (2010).

[35] G. M. Luo, S. Malkova, J. Yoon, D. G. Schultz, B. H. Lin, M. Meron, I. Benjamin, P. Vanysek and M. L. Schlossman, *Science*, **311**, 216-218 (2006).

[36] P. L. Nostro and B. W. Ninham, *Chem. Rev.*, **112**, 2286 (2012).

[37] F. Hofmeister, *Arch. Exp. Pathol. Pharmakol.*, **24**, 247 (1888).

[38] A. Heydweiller, *Ann. Phys.* (Leipzig) **33**, 145 (1910).

[39] Z. -G. Wang, *Phys. Rev. E*, **81**, 021501 (2010).

[40] I. Nakamura, N. P. Balsara, Z.-G. Wang, *Phys. Rev. Lett.*, 2011; **107**, 198301 (2011).

[41] I. Nakamura, Z.-G. Wang, *Soft Matter*, **8**, 9356-9367 (2012).

[42] C. Wagner, Phys. Z. **25**, 474 (1924).

[43] L. Onsager and N. N. T. Samaras, *J. Chem. Phys.*, **2**, 528 (1933).

[44] N. Matubayasi, K. Yamamoto, S. Yamaguchi, H. Matsuo and N. Ikeda, *J. Colloid Interface Sci.*, **214**, 101 (1999).

[45] N. Matubayasi, K. Tsunemoto, I. Sato, R. Akizuki, T. Morishita, A. Matuzawa, and Y. Natsukari, *J. Colloid Interface Sci.*, **243**, 444 (2001).

[46] Y. Levin and J. E. Flores-Mena, Europhys. Lett. 56, 187 (2001).

[47] S. Ghosal et al., *Science* **307**, 563 (2005).

[48] P. Jungwirth and D. J. Tobias, *J. Phys. Chem. B* **106**, 6361 (2002); P. Jungwirth and D. J. Tobias, *Chem. Rev.* **106**, 1256 (2006).

[49] Y. Levin, *Phys. Rev. Lett.* **102**, 147803 (2009).

[50] M. Bier, J. Zwanikken and R.van Roij, *Phys. Rev. Lett.* **101**, 046104 (2008).

[51] Y. Levin, A. P. dos Santos and A. Diehl, *Phys. Rev. Lett.* **103**, 257802 (2009); *Langmuir*, **26**, 10778 (2010).

[52] M. Kanduč and R. Podgornik, *Eur. Phys. J. E*, **23**, 265-274 (2007).

[53] A. Naji, M. Kanduč, J. Forsman and R. Podgornik, *J. Chem. Phys.*, **139**, 150901 (2013).

Chapter 2

General Theory

In this chapter, we develop a general theory for electrolyte solutions with dielectric inhomogeneity by using the renormalized Gaussian variational approach. Instead using the point-charge model, we assume the ion has a finite charge spread. The key result of the theory is a set of self-consistent equations for the mean electrostatic potential, the correlation function (Green function), the self energy of ions and the incompressible field due to the ion-size effect. The general theory is applied to study the thermodynamic property of the bulk electrolyte solution. By taking both the charge spread on the ion and the non-electrostatic ion-size effect into account, our theory shows good agreement with the experiment result for predicting the activity coefficient and osmotic coefficient. This chapter is adapted from our paper, R. Wang and Z.-G. Wang, *J. Chem. Phys.* **139**, 124702 (2013); R. Wang and Z.-G. Wang, in preparation.

2.1 Renormalized Gaussian Fluctuation Theory

We consider a general system with a fixed charge distribution $e\rho_{ex}(\mathbf{r})$ in the presence of small mobile cations of valency q_+ and anions of valency q_- in a dielectric medium of dielectric constant $\varepsilon(\mathbf{r})$. e is the elementary charge. The charge on the ion is assumed to have a finite spread given by a short-range distribution function $h_\pm(\mathbf{r}-\mathbf{r}_i)$ for the ith ion. The total charge density is

$$e\rho(\mathbf{r}) = e\rho_{ex}(\mathbf{r}) + e\int d\mathbf{r}'\left[q_+h_+(\mathbf{r}'-\mathbf{r})\hat{c}_+(\mathbf{r}') - q_-h_-(\mathbf{r}'-\mathbf{r})\hat{c}_-(\mathbf{r}')\right] \tag{2.1}$$

with $\hat{c}_\pm(\mathbf{r}) = \sum_{i=1}^{n_\pm}\delta(\mathbf{r}-\mathbf{r}_i)$ the particle density operator for the ions. The Coulomb energy of the system, *including the self energy*, is

$$H = \frac{e^2}{2}\int d\mathbf{r}d\mathbf{r}'\rho(\mathbf{r})G_0(\mathbf{r},\mathbf{r}')\rho(\mathbf{r}') \tag{2.2}$$

where $G_0(\mathbf{r},\mathbf{r}')$ is the Coulomb operator given by

$$-\nabla\cdot[\varepsilon_0\varepsilon(\mathbf{r})\nabla G_0(\mathbf{r},\mathbf{r}')] = \delta(\mathbf{r}-\mathbf{r}') \tag{2.3}$$

ε_0 is the vacuum permittivity. The grand canonical partition function of the system is

$$\begin{aligned}\Xi &= \sum_{n_{\{+,-,s\}}=0}^{\infty}\frac{\mathrm{e}^{\mu_+n_+ + \mu_-n_- + \mu_sn_s}}{n_+!n_-!n_s!v_+^{n_+}v_-^{n_-}v_s^{n_s}}\int\prod_{i=1}^{n_+}d\mathbf{r}_i\prod_{j=1}^{n_-}d\mathbf{r}_j\prod_{k=1}^{n_s}d\mathbf{r}_k \\ &\times \prod_{\mathbf{r}}\delta[1-\hat{c}_+(\mathbf{r})v_+ - \hat{c}_-(\mathbf{r})v_- - \hat{c}_s(\mathbf{r})v_s]\exp\left(-\beta H\right)\end{aligned} \tag{2.4}$$

where μ_α ($\alpha = +,-,s$) is the chemical potential of the ions and solvent, respectively. The functional delta is introduced for the local incompressibility constraint to avoid the over-crowding of the ions. $v_\pm$ and v_s is the volume of the cations, anions and solvent molecules, respectively. We perform the usual Hubbard-Stratonovich transformation and identity transformation to Eq. 2.4 by introducing a field variable $\phi(\mathbf{r})$ in couple with $\rho(\mathbf{r})$ and a field variable $\zeta(\mathbf{r})$ in couple with the impressibility, which yields

$$\Xi = \frac{1}{Z_0}\int D\phi\int D\zeta\exp\left\{-L[\phi,\zeta]\right\} \tag{2.5}$$

where the "action" L is

$$\begin{aligned}L &= \int d\mathbf{r}\left[\frac{1}{2}\epsilon(\nabla\phi)^2 + i\rho_{ex}\phi - \lambda_+\mathrm{e}^{-iq_+\hat{h}_+\phi - iv_+\zeta} - \lambda_-\mathrm{e}^{iq_-\hat{h}_-\phi - iv_-\zeta}\right] \\ &- \int d\mathbf{r}\left(\lambda_s\mathrm{e}^{-iv_s\zeta} + i\zeta\right)\end{aligned} \tag{2.6}$$

We take the saddle point approximation for ζ (setting $\eta = i\zeta^*$ with ζ^* denoting the saddle point value of ζ), which yields

$$v_+\lambda_+ \mathrm{e}^{-iq_+\hat{h}_+\phi - v_+\eta} + v_-\lambda_- \mathrm{e}^{iq_-\hat{h}_-\phi - v_-\eta} + v_s\lambda_s \mathrm{e}^{-v_s\eta} - 1 = 0 \tag{2.7}$$

The partition function can be rewritten as

$$\Xi = \frac{1}{Z_0}\int D\phi \exp\left\{-\int d\mathbf{r}\left[\frac{1}{2}\epsilon(\nabla\phi)^2 + i\rho_{ex}\phi - \eta - \lambda_+\mathrm{e}^{-iq_+\hat{h}_+\phi - v_+\eta} - \lambda_-\mathrm{e}^{iq_-\hat{h}_-\phi - v_-\eta} - \lambda_s\mathrm{e}^{-v_s\eta}\right]\right\} \tag{2.8}$$

$\lambda_\alpha = \mathrm{e}^{\mu_\alpha/v_\alpha}$ is the fugacity of the ions and solvent. We have used the short-hand notation $\hat{h}_\pm\phi$ to represent the local spatial averaging of ϕ by the charge distribution function: $\hat{h}_\pm\phi = \int d\mathbf{r}' h_\pm(\mathbf{r}' - \mathbf{r})\phi(\mathbf{r}')$.

To develop a nonperturbative theory, we perform a variational calculation[1, 2] of Eq. 2.8 using the Gibbs-Feynman-Bogoliubov bound for the grand free energy $W = -\ln\Xi$, which yields

$$W \leq -\ln\Xi_{ref} + \langle L[\phi] - L_{ref}[\phi]\rangle \tag{2.9}$$

where

$$\Xi_{ref} = \frac{1}{Z_0}\int D\phi \exp\left\{-L_{ref}\left[\phi\right]\right\} \tag{2.10}$$

The average $\langle\cdots\rangle$ is taken in the reference ensemble with action L_{ref}. We take the reference action to be of the Gaussian form centered around the mean $-i\psi$

$$L_{ref} = \frac{1}{2}\int d\mathbf{r}d\mathbf{r}'[\phi(\mathbf{r}) + i\psi(\mathbf{r})]G^{-1}(\mathbf{r},\mathbf{r}')[\phi(\mathbf{r}') + i\psi(\mathbf{r}')] \tag{2.11}$$

where G^{-1} is the functional inverse of the the Green's function G. ψ and G are taken to be variational parameters for the grand free energy functional. The introduction of i is to keep the mean electrostatic potential ψ real, as the saddle-point value of the field variable is purely imaginary. With the Gaussian reference action Eq. 2.11, all the terms on the r.h.s. of Eq. 2.9 can be evaluated analytically; the details are provided in the appendix (Section 2.4). The resulting variational free energy is:

$$\begin{aligned} W &= -\frac{1}{2}\ln\left(\frac{\det G}{\det G_0}\right) - \frac{1}{2}\int d\mathbf{r}d\mathbf{r}'\left[G^{-1}(\mathbf{r},\mathbf{r}') - G_0^{-1}(\mathbf{r},\mathbf{r}')\right]G(\mathbf{r},\mathbf{r}') - \frac{1}{2}\int d\mathbf{r}\epsilon(\nabla\psi)^2 \\ &- \int d\mathbf{r}\left[\lambda_+\mathrm{e}^{-q_+\psi - u_+ - v_+\eta} + \lambda_-\mathrm{e}^{q_-\psi - u_- - v_-\eta} + \lambda_s\mathrm{e}^{-v_s\eta} + \eta - \rho_{ex}\psi\right] \end{aligned} \tag{2.12}$$

where $u_\pm$ is the self energy of the ions

$$u_\pm(\mathbf{r}) = \frac{1}{2} q_\pm^2 \int d\mathbf{r}' d\mathbf{r}'' h_\pm(\mathbf{r}-\mathbf{r}') G(\mathbf{r}',\mathbf{r}'') h_\pm(\mathbf{r}''-\mathbf{r}) \tag{2.13}$$

Minimizing W with respect to ψ and G respectively gives rise to

$$-\nabla\cdot(\epsilon\nabla\psi) = \rho_{ex} + \lambda_+ q_+ \mathrm{e}^{-q_+\psi - u_+ - v_+\eta} - \lambda_- q_- \mathrm{e}^{q_-\psi - u_- - v_-\eta} \tag{2.14}$$

$$-\nabla\cdot[\epsilon\nabla G(\mathbf{r},\mathbf{r}')] + 2I(\mathbf{r})G(\mathbf{r},\mathbf{r}') = \delta(\mathbf{r}-\mathbf{r}') \tag{2.15}$$

where $I(\mathbf{r})$ is the local ionic strength,

$$I(\mathbf{r}) = \frac{1}{2}\left(\lambda_+ q_+^2 \mathrm{e}^{-q_+\psi - v_+\eta - u_+} + \lambda_- q_-^2 \mathrm{e}^{q_-\psi - v_-\eta - u_-}\right) \tag{2.16}$$

η is obtained by setting $\mu_s = 0$ and making use the equation of incompressibility,

$$\eta = -\frac{1}{v_s}\ln\left[1 - v_+ c_+(\mathbf{r}) - v_- c_-(\mathbf{r})\right] \tag{2.17}$$

with the salt concentration given by

$$c_\pm(\mathbf{r}) = \lambda_\pm \exp\{\mp q_\pm\psi(\mathbf{r}) - u_\pm(\mathbf{r}) - \frac{v_\pm}{v_s}\ln\left[1 - v_+ c_+(\mathbf{r}) - v_- c_-(\mathbf{r})\right]\} \tag{2.18}$$

Equations 2.13 - 2.18 forms a set of self-consistent equations for the mean electrostatic potential $\psi(\mathbf{r})$, the correlation function (Green function) $G(\mathbf{r},\mathbf{r}')$, the self energy $u_\pm(\mathbf{r})$ of the ions and the incompressibility field η, which are the key equations for weakly coupled electrolytes. Eq. 2.14 has the same form as the PB equation, but now with the self-energy of the ions appearing in the Boltzmann factor. The appearance of the self energy in the Boltzmann factor reflects the nonlinear feedback of the fluctuation, an aspect that was missing in a perturbation expansion. The self-energy given by Eq. 2.13 is a unified expression that includes the Born energy of the ion, the interaction between the ion and its ionic atmosphere, as well as the distortion of the electric field by a spatially varying dielectric function, the latter taking the form of image charge interaction near a dielectric discontinuity. In general, the self energy is spatially varying if there is spatial inhomogeneity in either the dielectric constant or the ionic strength. The grand free energy can be derived by using the charging method (as shown in Appendix), which yields:

$$
\begin{aligned}
W &= \frac{1}{2}\int d\mathbf{r}\psi\left[\rho_{ex} - q_+c_+ + q_-c_-\right] \\
&- \int d\mathbf{r}\left[c_+ + c_- + \frac{1 - c_+v_+ - c_-v_-}{v_s} - \frac{\ln(1 - c_+v_+ - c_-v_-)}{v_s}\right] \\
&+ \frac{1}{2}\int d\mathbf{r}_1 \int d\mathbf{r} \int d\mathbf{r}' \int_0^1 d\tau [G(\mathbf{r}, \mathbf{r}', \tau) - G(\mathbf{r}, \mathbf{r}')] \\
&\times \left[c_+(\mathbf{r}_1)q_+^2 h_+(\mathbf{r} - \mathbf{r}_1)h_+(\mathbf{r}_1 - \mathbf{r}') + c_-(\mathbf{r}_1)q_-^2 h_-(\mathbf{r} - \mathbf{r}_1)h_-(\mathbf{r}_1 - \mathbf{r}')\right] \qquad (2.19)
\end{aligned}
$$

2.2 Thermodynamic Properties of Bulk Electrolyte Solution

In Section 2.1, we derive a general theory for electrolyte solution in a dielectric medium, which includes the contributions from the local Born energy, the ion-ion correlation, the long-range image charge effect and the excluded volume effect due to incompressibility. Here, we will apply the general theory to the bulk electrolyte solution, in which the mean-electrostatic potential is zero everywhere. For an isolated ion in a uniform dielectric medium with scaled dielectric constant ϵ,

$$G(\mathbf{r}, \mathbf{r}') = \frac{1}{4\pi\epsilon|\mathbf{r} - \mathbf{r}'|} \qquad (2.20)$$

We assume the charge of the ion is uniformly distributed on the ion surface:

$$h_\pm(\mathbf{r} - \mathbf{r}') = \frac{1}{4\pi a_\pm^2}\delta(|\mathbf{r} - \mathbf{r}'| - a_\pm) \qquad (2.21)$$

Then, the self energy of the ion can be calculated from Eq. 2.13,

$$u_\pm = \frac{q_\pm^2}{8\pi\epsilon a_\pm} \qquad (2.22)$$

which reproduce the Born energy of a single ion.

For the bulk electrolyte solution with concentration of cations and anions $c_\pm^b$, the local charge separation is absent; thus, $\psi = 0$.

$$G(\mathbf{r}, \mathbf{r}') = \frac{\mathrm{e}^{-\kappa_b|\mathbf{r}-\mathbf{r}'|}}{4\pi\epsilon|\mathbf{r} - \mathbf{r}'|} \qquad (2.23)$$

where $\kappa_b = [(z_+^2 c_+^b + z_-^2 c_-^b)/\epsilon]^{1/2}$ is the inverse of the bulk Debye screening length. Substituting Eq. 2.23 into Eq. 2.13 gives rise to the self energy of the ion in the bulk electrolyte solution as

$$u_\pm = \frac{q_\pm^2}{8\pi\epsilon a_\pm}\left(\frac{1 - \mathrm{e}^{-2\kappa_b a_\pm}}{2\kappa a_\pm}\right) \qquad (2.24)$$

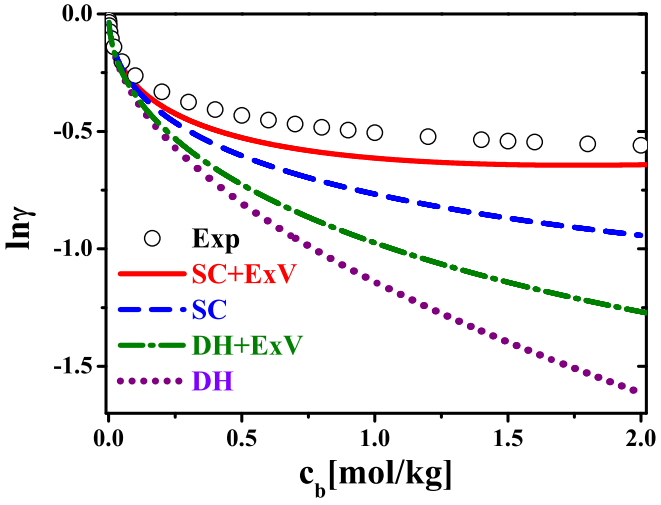

Figure 2.1: Activity coefficient of KCl solution calculated by different theoretical models in comparison with the experiment data. $a_{K^+} = 2.18\mathring{A}$ and $a_{Cl^-} = 1.91\mathring{A}$. The notation "Exp" denotes the experiment data from Ref[7]. "SC+ExV" denotes the result calculated by using the charge-spread model and taking the non electrostatic ion-size effect into account. "SC" denotes the result calculated by using the charge-spread model while the ion is treated as volumeless. "DH+ExV" denotes the result calculated by using the Debye-Hückel point-charge model and taking the non electrostatic ion-size effect into account. "DH" denotes the result calculated by only using the Debye-Hückel point-charge model.

Applying Eq. 2.18 to the bulk solution, we have

$$\mu_\pm = \mu_\pm^\circ + \ln(c_\pm^b) + \ln\gamma_\pm \tag{2.25}$$

where $\mu_\pm^\circ = \ln v_\pm + q_\pm^2/(8\pi\epsilon a_\pm)$ is the standard chemical potential for the ions which is independent of the salt concentration. The first two terms on the r.h.s of Eq. 2.25 are the contributions from the ideal solution, whereas the third term is the excess part which describes the deviation from the ideal solution. $\gamma_\pm$ is the activity coefficient of the ions, which is given by combining Eq. 2.18 and Eq. 2.25

$$\ln\gamma_\pm = \frac{q_\pm^2}{8\pi\epsilon a_\pm}\left(\frac{1-\mathrm{e}^{-2\kappa_b a_\pm}}{2\kappa_b a_\pm} - 1\right) - \frac{v_\pm}{v_s}\ln(1 - v_+c_+ - v_-c_-) \tag{2.26}$$

The first term on the r.h.s of Eq. 2.26 is the electrostatic contribution from the ion-ion correlation at the level of Debye-Hückel theory. However, our theory takes the charge-spread of the ion into account, which avoids the overestimation of the correlation in the point-charge limit of the Debye-Hückel theory[3, 4, 5]. In the point-charge limit of the Debye-Hückel theory, the activity coefficient is given by $\ln\gamma_\pm = -q_\pm^2\kappa_b/(8\pi\epsilon)$[6]. The second term on the r.h.s of Eq. 2.26 is the non-electrostatic contribution due to the ion size effect. Individual activity coefficients cannot be measured experimentally. We need to measure the mean activity coefficient, which for binary salt is defined by

$\gamma_{\pm} = \left(\gamma_{+}^{q_+} + \gamma_{-}^{q_-}\right)^{1/(q_+ + q_-)}$.

Figure 2.1 shows the activity coefficient of the KCl solution calculated by different theoretical models in comparison with the experiment data[7]. In the low salt concentration regime ($c_b < 0.01M$), the activity coefficient predicted by different models coincide with each other, which is also in agreement with the experiment. Therefore, the Debye-Hückel limiting theory is accurate in the low salt concentration regime. However, the Debye-Hückel point-charge model severely overestimate the activity coefficient as the salt concentration increases ($c_b > 0.1M$). By using the charge-spread model instead of the point-charge model, the effect of short-range ion-ion correlation is reduced, which increases the activity coefficient as shown in Figure 2.1. By fully accounting for both the charge-spread effect and the non-electrostatic ion-size effect, the activity coefficient predicted by our theory is in good agreement with the experiment result in a wide range of salt concentration (up to 2M).

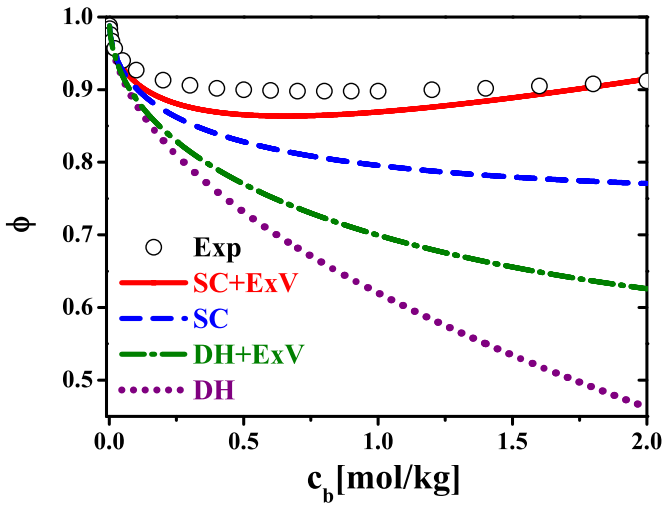

Figure 2.2: Osmotic coefficient of KCl solution calculated by different theoretical models in comparison with the experiment data[7]. $a_{K^+} = 2.18\mathring{A}$ and $a_{Cl^-} = 1.91\mathring{A}$.

Another thermodynamic property that can be measured in experiment is the osmotic coefficient, which is defined as $\phi = -\frac{W - W^\circ}{V(c_+ + c_-)}$, where W° is the grand free energy for the pure solvent. By applying the solution of the Green function (Eq. 2.23) into the grand free energy (Eq. eq2.19), we obtain

$$\phi = 1 - \frac{\frac{1}{v_s}[v_+c_+ + v_-c_- + \ln(1 - v_+c_+ - v_-c_-)] + \frac{q_+^2 c_+}{2} g(a_+, \kappa_b) + \frac{q_-^2 c_-}{2} g(a_-, \kappa_b)}{c_+ + c_-} \tag{2.27}$$

where

$$g(a_\pm, \kappa_b) = \frac{\kappa_b a_\pm + \mathrm{e}^{-2\kappa_b a_\pm} + \kappa_b a_\pm \mathrm{e}^{-2\kappa_b a_\pm} - 1}{8\pi\epsilon\kappa_b^2 a_\pm^3} \tag{2.28}$$

is the contribution from ion-ion correlation. The osmotic coefficient predicted by Debye-Hückel point-charge model decreases monotonically as c_b increases, which drastically differs from the experiment data as shown in Figure 2.2. By taking both the effect of charge spread and the effect of ion-size into account, our theory predicts the nonlinear dependence of the osmotic coefficient on c_b, in good agreement with the experiment data.

2.3 Appendix: Derivation of the key equations in Section 2.1

We approximate the grand free energy by the lower bound of the right hand side of Eq. 2.9, which yields

$$\begin{aligned} W &= -\frac{1}{2}\ln\left(\frac{\det G}{\det G_0}\right) - \frac{1}{2}\int d\mathbf{r}d\mathbf{r}' \left\{\delta(\mathbf{r}'-\mathbf{r})\left[\epsilon(\nabla\psi)^2 - \epsilon\langle(\nabla\chi)^2\rangle\right] + G^{-1}(\mathbf{r},\mathbf{r}')\langle\chi(\mathbf{r})\chi(\mathbf{r}')\rangle\right\} \\ &+ \int d\mathbf{r}\left[\rho_{ex}\psi - \lambda_+\mathrm{e}^{-z_+\psi - v_+\eta}\langle\mathrm{e}^{-iz_+\hat{h}_+\chi}\rangle - \lambda_-\mathrm{e}^{z_-\psi - v_-\eta}\langle\mathrm{e}^{iz_-\hat{h}_-\chi}\rangle - \lambda_s\mathrm{e}^{-v_s\eta} - \eta\right] \end{aligned} \tag{2.29}$$

where $\chi \equiv \phi + i\psi$. Because the distribution of χ is Gaussian by our ansatz, the averages in Eq. 2.12 can be evaluated exactly. Noting that

$$\langle\chi(\mathbf{r})\chi(\mathbf{r}')\rangle = G(\mathbf{r},\mathbf{r}') \tag{2.30}$$

we have,

$$\int d\mathbf{r}d\mathbf{r}'\delta(\mathbf{r}-\mathbf{r}')\epsilon\langle(\nabla\chi)^2\rangle = \int d\mathbf{r}d\mathbf{r}'\nabla_{\mathbf{r}}\cdot\left[\epsilon(\mathbf{r})\nabla_{\mathbf{r}'}\delta(\mathbf{r}-\mathbf{r}')\right]G(\mathbf{r},\mathbf{r}') \tag{2.31}$$

and

$$\langle\mathrm{e}^{\mp iz_\pm\hat{h}_\pm\chi}\rangle = \exp\left[-\frac{1}{2}z_\pm^2\int d\mathbf{r}'d\mathbf{r}''h_\pm(\mathbf{r}'-\mathbf{r})G(\mathbf{r}',\mathbf{r}'')h_\pm(\mathbf{r}''-\mathbf{r})\right] \tag{2.32}$$

Substituting equations 2.30 - 2.32 into Eq. 2.30 gives rise to Eq. 2.12.

Minimizing W in Eq. 2.12 with respect to G yields,

$$\begin{aligned} 0 &= -G^{-1}(\mathbf{r},\mathbf{r}') + \nabla_{\mathbf{r}}\cdot\left[\epsilon(\mathbf{r})\nabla_{\mathbf{r}'}\delta(\mathbf{r}-\mathbf{r}')\right] \\ &+ \lambda_+ q_+^2\int d\mathbf{r}_1 h_+(\mathbf{r}-\mathbf{r}_1)h_+(\mathbf{r}_1-\mathbf{r}')\mathrm{e}^{-q_+\psi(\mathbf{r}_1)-v_+\eta(\mathbf{r}_1)-u_+(\mathbf{r}_1)} \\ &+ \lambda_- q_-^2\int d\mathbf{r}_1 h_-(\mathbf{r}-\mathbf{r}_1)h_-(\mathbf{r}_1-\mathbf{r}')\mathrm{e}^{-q_-\psi(\mathbf{r}_1)-v_-\eta(\mathbf{r}_1)-u_-(\mathbf{r}_1)} \end{aligned} \tag{2.33}$$

Inverting the above matrix equation

$$\begin{aligned} 0 &= -\delta(\mathbf{r}-\mathbf{r}') - \nabla_{\mathbf{r}} \cdot [\epsilon(\mathbf{r})\nabla_{\mathbf{r}} G(\mathbf{r},\mathbf{r}')] \\ &+ \lambda_+ q_+^2 \int d\mathbf{r}_1 d\mathbf{r}_2 h_+(\mathbf{r}-\mathbf{r}_1) h_+(\mathbf{r}_1-\mathbf{r}_2) \mathrm{e}^{-q_+\psi(\mathbf{r}_1)-v_+\eta(\mathbf{r}_1)-u_+(\mathbf{r}_1)} G(\mathbf{r}_2,\mathbf{r}') \\ &+ \lambda_- q_-^2 \int d\mathbf{r}_1 d\mathbf{r}_2 h_-(\mathbf{r}-\mathbf{r}_1) h_-(\mathbf{r}_1-\mathbf{r}_2) \mathrm{e}^{-q_-\psi(\mathbf{r}_1)-v_-\eta(\mathbf{r}_1)-u_-(\mathbf{r}_1)} G(\mathbf{r}_2,\mathbf{r}') \end{aligned} \tag{2.34}$$

Neglecting the change of the field within the ions, we obtain Eq.2.15.

The density of the solvent is:

$$c_s(\mathbf{r}) = \lambda_s \mathrm{e}^{-v_s\eta} \tag{2.35}$$

Therefore,

$$\eta = \frac{1}{v_s}\left[\mu_s - \ln(v_s c_s(\mathbf{r}))\right] \tag{2.36}$$

Since the three chemical potential $\mu_\pm$ and μ_s are not independent with each other, we can set $\mu_s = 0$ (the value of μ_s only shift the standard free energy of the pure solvent). From the incompressibility, we have

$$v_+ c_+(\mathbf{r}) + v_- c_-(\mathbf{r}) + v_s c_s(\mathbf{r}) = 1 \tag{2.37}$$

Substituting Eq. 2.37 into Eq. 2.36, we obtain Eq. 2.17.

Then we will derive the expression for the fluctuation contribution in the free energy which is the first two terms on the r.h.s of Eq. 2.12. We note that Eq. 2.33 can be written in the matrix form as

$$\begin{aligned} \mathbf{G}^{-1} - \mathbf{G}_0^{-1} &= \int d\mathbf{r}_1 \int d\mathbf{r}_2 G(\mathbf{r}_2,\mathbf{r}') \\ &\times \left[c_+(\mathbf{r}_1) q_+^2 h_+(\mathbf{r}-\mathbf{r}_1) h_+(\mathbf{r}_1-\mathbf{r}') + c_-(\mathbf{r}_1) q_-^2 h_-(\mathbf{r}-\mathbf{r}_1) h_-(\mathbf{r}_1-\mathbf{r}')\right] \end{aligned} \tag{2.38}$$

Note also that

$$\begin{aligned} \ln\left(\frac{\det \mathbf{G}}{\det \mathbf{G}_0}\right) &= \ln\det \mathbf{G} - \ln\det \mathbf{G}_0 \\ &= \int d\mathbf{r} \int d\mathbf{r}' \int_{G_0^{-1}}^{G^{-1}} \frac{\delta \ln\det \mathbf{G}}{\delta G^{-1}(\mathbf{r},\mathbf{r}')} \delta G^{-1}(\mathbf{r},\mathbf{r}') \end{aligned} \tag{2.39}$$

The innermost integral is a functional integration over G^{-1} from G_0^{-1} to G^{-1}. Since $\ln\det \mathbf{G}$ is the result of a Gaussian functional integral, we have

$$\frac{\delta \ln\det \mathbf{G}}{\delta G^{-1}(\mathbf{r},\mathbf{r}')} = -G(\mathbf{r},\mathbf{r}') \tag{2.40}$$

Therefore,

$$\ln\left(\frac{\det \mathbf{G}}{\det \mathbf{G}_0}\right) = -\int d\mathbf{r}\int d\mathbf{r}'\int_{G_0^{-1}}^{G^{-1}} G(\mathbf{r},\mathbf{r}')\delta G^{-1}(\mathbf{r},\mathbf{r}') \tag{2.41}$$

As the integration goes from G_0^{-1} to G^{-1}, the integrand changes from G_0 to G. From Eq. 2.38, a convenient path for integrating Eq. 2.41 is to introduce a continuous "charging" variable τ that goes from 0 to 1, while keeping the density profile fixed. Obviously the Green function is G_0 for $\tau = 0$ and is G for $\tau = 1$. For any intermediate value, we denote the Green function as $G(\mathbf{r},\mathbf{r}';\tau)$. Using Eq. 2.38, the above integral becomes,

$$\ln\left(\frac{\det \mathbf{G}}{\det \mathbf{G}_0}\right) = -\int d\mathbf{r}_1\int d\mathbf{r}\int d\mathbf{r}'\int_0^1 d\tau G(\mathbf{r},\mathbf{r}',\tau)$$
$$\times\left[c_+(\mathbf{r}_1)q_+^2 h_+(\mathbf{r}-\mathbf{r}_1)h_+(\mathbf{r}_1-\mathbf{r}') + c_-(\mathbf{r}_1)q_-^2 h_-(\mathbf{r}-\mathbf{r}_1)h_-(\mathbf{r}_1-\mathbf{r}')\right] \tag{2.42}$$

Substituting Eq. 2.42 into Eq.2.12 yields the final expression of the grand free energy as shown in Eq.2.19.

Bibliography

[1] R.R. Netz and H. Orland, *Eur. Phys. J. E*,**11**, 301C311, (2003).

[2] Z. -G. Wang, *Phys. Rev. E*, **81**, 021501 (2010).

[3] D. A. McQuarrie, *Statistical Mechanics*, (University Science Books, Mill Valley, CA, 2000).

[4] M. E. Fisher and Y. Yan, *Phys. Rev. Lett.*, **71**, 3826 (1993).

[5] D. Chandler and H. C. Anderson, *J. Chem. Phys.*, **54**, 26 (1971).

[6] P. Debye and E. Hückel, *Phys. Z.*, **24**, 185-206 (1923).

[7] R. A. Robinson and R. H. Stokes, *Electrolyte solutions*, 2nd Ed. (Butterworths, 1965).

Chapter 3

The effects of local Born solvation energy on Phase Equilibrium and Interfacial Tension of Liquid Mixtures

In this chapter, we study the bulk thermodynamics and interfacial properties of electrolyte solution mixtures by including the local contribution of the self energy – the Born solvation energy – into the mean-field Poisson-Boltzmann framework. Difference in the solvation energy between the cations and anions is shown to give rise to local charge separation near the interface, and a finite Donnan potential between two coexisting solutions. The ion solvation affects the phase equilibrium of the solvent mixture, depending on the dielectric constants of the solvents, reflecting the competition between the solvation energy and translation entropy of the ions. Miscibility is decreased if both solvents have low dielectric constants, and is enhanced if both solvents have high dielectric constant. At the mean-field level, the ion distribution near the interface is determined by two competing effects: accumulation in the electrostatic double layer and depletion in a diffuse interface. The interfacial tension shows a non-monotonic dependence on the salt concentration: it increases linearly with the salt concentration at higher concentrations, and decreases approximately as the square root of the salt concentration for dilute solutions, reaching a minimum near 1mM. We also find that, for a fixed cation type, the interfacial tension decreases as the size of anion increases. These results offer qualitative explanations within one unified framework for the long-known concentration and ion size effects on the interfacial tension of electrolyte solutions. This chapter is adapted from our paper, R. Wang and Z.-G. Wang, *J. Chem. Phys.* **135**, 014707 (2011).

3.1 Introduction

For soft matter and biological systems, ions and electrostatic interactions play an important role in the structural, dynamic and functional properties[1, 2, 3, 4]. The most common approach to treating electrostatic interactions in the presence of salt ions is the Poisson-Boltzmann (PB) equation[2]. It is a mean-field theory relating the average electrostatic potential to fixed charge densities and the average concentration of salt ions. Many modifications have been made in the recent years to the PB theory to include effects such as the excluded volume of the ions[5, 6, 7], nonlocality of dielectric constants[8, 9, 10] and the correlation between ions (manifested in the formation of bound ion pairs)[11].

An obvious effect that is missing in the PB theory is the solvation free energy of salt ions in the dissolving medium. While the solvation free energy can be absorbed into a redefinition of a reference state free energy for uniform systems and therefore becomes inconsequential, it must play a crucial role in spatially varying dielectric media. In a recent study, one of us developed a new theory that includes the solvation free energy in a general theory for treating fluctuation effects[12]. The solvation energy is shown to consist of a nonuniversal part in the form of local Born energy and an universal part that depends on the ion concentration, valency and the dielectric constant. Retaining the local Born energy while ignoring long wavelength fluctuations resulted in an improved mean-field theory, which was termed the Born-Energy Augmented Poisson Boltzmann (BEAPB) equation. If anions and cations have different ion radii and/or valency, the BEAPB theory predicts a spatially varying electrostatic potential and local charge separation.

In this chapter, we study the consequence of the solvation free energy on the miscibility and interfacial tension between two solvents using the BEAPB approach. Experimentally, the dependence of the liquid-gas surface tension on the electrolyte concentration has been measured for a long time[13, 14]. At high salt concentrations, the surface tension exhibits a linear increase with the salt concentration. However, Jones and Ray[13] showed that in very dilute solutions, the surface tension actually first decreases with the salt concentration and reaching a minimum near 1mM for several different salt solutions. To date, no theory has satisfactorily explained the full concentration dependence of the surface tension. In addition, the surface tension depends not only on the salt concentration, but also on the identity of cations and anions, which is often interpreted as the specific ion effect[15, 16]. For a fixed cation type, the water-air surface tension decreases according to the Hofmeister sequence: $F^- > Cl^- > Br^- > I^-$. Although there are fewer reported measurements of the liquid-liquid interfacial tension[17], its behavior is qualitatively similar to the liquid-gas surface tension, especially concerning the Jones-Ray effect and the specific ion effect.

Theoretically, great efforts have been made to understand the surface and interfacial tension of electrolyte solutions since the pioneering work of Wagner[18], and Onsager and Samaras[19]. By

assuming the absence of ions in the gas phase and considering the image charge repulsion as the dominant effect, Onsager and Samaras obtained the limiting law for the excess liquid-gas surface tension in the form $\Delta\gamma \sim c \ln c$ (c is the salt concentration in bulk solution). However, this theory fails to explain both the Jones-Ray effect and the specific ion effect. Nichols and Pratt[20] took the presence of ion in the gas phase into account (in this sense, there is no conceptual difference between the liquid-gas surfaces and the liquid-liquid interfaces) and found the excess interfacial tension decreases with the square root of the salt concentration $\Delta\gamma \sim -\sqrt{c}$ for dilute electrolyte solution. Recently, Bier et al.[21] assumed a shifted step-like form of the solvation potential and obtained analytical results by solving the linearized PB equation. Different scaling behaviors of the interfacial tension observed in experiments can be explained by adjusting the position of the interface in their model. However, the interfacial structure chosen in their work is artificial and the work does not explain the Jones-Ray effect. By means of Ginzburg-Landau approach, Onuki[22, 23] studied the ion distribution and the interfacial tension in the electrolyte mixture near the critical point. Both the solvation energy and the image interaction are taken into account. The behaviors of linear increase and square root decrease of $\Delta\gamma$ with the salt concentration are obtained in his work. However, the solvation energy and the image interaction were introduced phenomenologically, which makes it difficult to connect his model to the behavior of specific ions.

In this chapter, we provide a unified theoretical framework to describe the effect of ion solvation on the bulk thermodynamics and interfacial properties of electrolyte solution mixture at the mean-field level. We present our general model in Sec. 2A by accounting for the electrostatic interactions, the solvation effect and the inhomogeneous dielectric constant. The solvation energy retains the form of Born energy at the mean-field level, which is position-dependent in the inhomogeneous medium. In Sec. 2B, we present analytical results for a special case where the composition profile is a sharp step-like function. Some general phenomena caused by the difference in the solvation energy between the cations and anions, such as the finite electrostatic potential difference, the charge separation and the electrostatic double layer, are also illustrated here. In Sec. 3, we examine the effect of adding salt on the miscibility of the solvent mixture. Phase diagrams for different dielectric constants and temperatures are shown. In Sec. 4, we systematically investigate the interfacial structure and the interfacial tension of the electrolyte solution mixture. The effect of electrostatic double layer and the diffuse interface on the ion distribution is examined for different salt concentrations. The dependence of the interfacial tension on salt concentration and ion radius is also studied. Both the Jones-Ray effect and the specific ion effect are captured by our model. Finally, we summarize our key results and discuss possible extensions of the current model in Sec. 5.

3.2 Model and Theory

We consider a binary mixture consisting of solvents A and B, with dielectric constant ε_A and ε_B, respectively. We take A to be the component with higher dielectric constant, and write its volume fraction as $\phi(r)$ to denote the local composition of the mixture. We will use the subscripts α and β to denote the A-rich and B-rich phases, respectively, throughout this paper. The salt is composed of simple ions: cations and anions, with z_+ and z_+ denoting their valency (absolute value). In this work, ions are assumed to be volumeless particles; however, they are assigned sizes that capture the charge distribution in the ions. The number concentration of cations and anions are denoted by $c_+(r)$ and $c_-(r)$, respectively. $\rho(r) = ez_+c_+(r) - ez_+c_+(r)$ gives the local charge density where e is the elementary unit of charge. In the following subsection, we construct the free energy as a functional of the composition, ion concentration and electrostatic potential, in the mean-field framework.

3.2.1 Mean-field Theory

We treat our electrolyte solution as an open system: the ions and solvents are in contact with a reservoir of given chemical potentials. The grand potential G of the system can be divided into the electrostatic part (G_e) and the solution part (G_s) as:

$$G = \int d\mathbf{r} g(\mathbf{r}) = G_e + G_s \tag{3.1}$$

with $g(\mathbf{r})$ denoting the grand potential density. For the electrostatic part, we consider the Coulomb interaction between different ion species, the interaction between ions and the solvents (i.e. the solvation energy), and the translational entropy of the ions. Other effects, such as the polarization of ions[15, 24] and formation of bound ion pairs[11] are not taken into account in the present work. Thus, the electrostatic part of the grand potential functional can be written as:

$$\begin{aligned} G_e &\equiv \int d\mathbf{r} g_e(\mathbf{r}) \\ &= \int d\mathbf{r} \left[\rho\psi - \frac{\varepsilon_0 \varepsilon(\phi)}{2} (\nabla\psi)^2 + c_+u_+ + c_-u_- \right] \\ &+ kT \int d\mathbf{r} \left[c_+ \ln\left(c_+/c_+^R\right) - c_+ + c_- \ln\left(c_-/c_-^R\right) - c_- \right] \\ &- \int d\mathbf{r} (c_+\mu_+ + c_-\mu_-) \end{aligned} \tag{3.2}$$

where ψ is the electrostatic potential, ε_0 is the vacuum permittivity, $\varepsilon(\phi)$ is the local dielectric constant, μ_+ and μ_+ are respectively the chemical potential of the cations and anions in the reservoir, and c_+^R and c_-^R are their respective reference concentration. u_+ and u_- are respectively the solvation

energy of the cations and anions, the form of which will be specified later.

For the solution part of the grand potential, we combine a regular solution expression for homogeneous mixing and a square-gradient expression for the penalty of composition change to write[25, 26]:

$$\begin{aligned} G_s &\equiv \int d\mathbf{r} g_s(\mathbf{r}) \\ &= kT \int d\mathbf{r} \frac{1}{v_s} \left[\phi \ln \phi + (1-\phi) \ln (1-\phi) + \chi \phi (1-\phi)\right] \\ &+ kT \int d\mathbf{r} \left[\frac{1}{2} C(\phi) (\nabla \phi)^2 - \beta \mu_s \phi\right] \end{aligned} \tag{3.3}$$

where v_s is the volume of the solvents molecules (assumed for simplicity to be the same for the two solvents) and χ is the interaction parameter dependent on temperature. $C(\phi)$ scales the composition gradient and is set to be $a_s^2/\left[18 v_s \phi(1-\phi)\right]$ in analogy to binary polymer blends with a_s the radius of the solvent molecules[27] ; it determines the width of the interface. μ_s is the exchange chemical potential on a per unit volume basis (i.e. $\mu_s = (\mu_A - \mu_B)/v_s$) that is conjugate to the composition variable .

Within the mean-field framework, the equilibrium profiles of the electrostatic potential, ion concentrations and composition are obtained from extremalization of the grand potential, which results in the following equations:

$$\varepsilon_0 \nabla \cdot (\varepsilon \nabla \psi) = -\rho \tag{3.4}$$

$$c_+ = \lambda_+ \exp\left(-\beta e z_+ \psi - \beta u_+\right) \tag{3.5}$$

$$c_- = \lambda_- \exp\left(\beta e z_- \psi - \beta u_-\right) \tag{3.6}$$

$$\begin{aligned} \mu_s &= \frac{kT}{v_s} \left[\ln \phi - \ln (1-\phi) + \chi (1-2\phi)\right] \\ &- kT \left[\nabla \cdot (C \nabla \phi) - \frac{1}{2} \frac{\partial C}{\partial \phi} (\nabla \phi)^2\right] \\ &- \frac{\varepsilon_0}{2} \frac{\partial \varepsilon}{\partial \phi} (\nabla \psi)^2 + c_+ \frac{\partial u_+}{\partial \phi} + c_- \frac{\partial u_-}{\partial \phi} \end{aligned} \tag{3.7}$$

where λ_+ and λ_+ are the fugacity of cations and anions, respectively. From Eq. (3.7), we can see a shift of the exchange chemical potential caused by the electrostatic interaction and the ion solvation. Based on equations (3.4) (3.5) and (3.6), the equilibrium grand potential density can be rearranged to:

$$g(\mathbf{r}) = -\frac{\varepsilon_0 \varepsilon(\phi)}{2} (\nabla \psi)^2 - kT (c_+ + c_-) + g_s \tag{3.8}$$

which can be viewed as consisting of three contributions: the electrostatic interaction, the ion

distribution and the solution part. The interfacial tension for the planar interface is the excess grand potential per unit area:

$$\gamma = \int dz \left[g(z) - g^{\infty} \right] \tag{3.9}$$

where g^{∞} is the grand potential density in the bulk phase, which is equal for the two coexisting bulk phases, and integration is along the normal of the interface.

Substituting equations (3.5) and (3.6) into Eq. (3.4) results in the following Solvation-Energy Augmented Poisson-Boltzmann equation[12]:

$$\begin{aligned} - \quad & \varepsilon_0 \nabla \cdot (\varepsilon \nabla \psi) = e\lambda_+ z_+ \exp\left(-\beta e z_+ \psi - \beta u_+\right) \\ - \quad & e\lambda_- z_- \exp\left(\beta e z_- \psi - \beta u_-\right) \end{aligned} \tag{3.10}$$

This equation captures the effect of solvation energy on the electrostatic potential and ion distribution at the mean-field level.

An immediate application of Eq. (3.10) is the determination of the electrostatic potential difference between two coexisting bulk phases (also called Donnan potential or Giovanni potential). Eq. (3.10) for the bulk (i.e. $\nabla\psi = 0$) combined with the requirement of charge neutrality gives the Donnan potential ψ_D as:

$$\begin{aligned} \psi_D &= \psi_\beta - \psi_\alpha \\ &= \frac{1}{(z_+ + z_-)\, e} \left[(u_{+,\alpha} - u_{+,\beta}) - (u_{-,\alpha} - u_{-,\beta}) \right] \end{aligned} \tag{3.11}$$

From Eq. (3.11) we see that a finite potential difference develops if the cations and anions have unequal solvation energy. The difference in solvation energy also gives rise to an unequal partition of ions between the two coexisting bulk phases:

$$\begin{aligned} \frac{c^{\infty}_{+,\alpha}}{c^{\infty}_{+,\beta}} &= \frac{c^{\infty}_{-,\alpha}}{c^{\infty}_{-,\beta}} \\ &= \exp\left[\frac{\beta z_- \left(u_{+,\beta} - u_{+,\alpha}\right) + \beta z_+ \left(u_{-,\beta} - u_{-,\alpha}\right)}{z_+ + z_-} \right] \end{aligned} \tag{3.12}$$

These results were previously derived by Onuki[23, 22] and Kung et al.[31].

To solve the coupled equations (3.4)-(3.7) for a spatially inhomogeneous system, we need to specify the expression for the solvation energy. In Ref. 12, the solvation energy is shown to consist of a nonuniversal part accounting for the local interaction between the ion and the solvent, and a universal part due to correlations at longer length scales. For the present treatment at the mean-field

level, we ignore the long length scale effects and retain only the nonuniversal part of the solvation energy which takes the form of a local Born energy[28]:

$$u_+ = \frac{z_+^2 e^2}{8\pi a_+ \varepsilon_0 \varepsilon(\phi)} \quad and \quad u_- = \frac{z_-^2 e^2}{8\pi a_- \varepsilon_0 \varepsilon(\phi)} \tag{3.13}$$

where a_+ and a_- are respectively the radius of the cations and anions. The local dielectric constant of the solvent mixture is assumed to be a simple volume fraction weighted average of its two components[29]:

$$\varepsilon(\phi) = \varepsilon_A(\phi) + \varepsilon_B(1-\phi) \tag{3.14}$$

We note that other mixing rules, such as that based on the Clausius-Mossotti equation [30] can also be used. However, qualitatively similar results are expected [33]. In spite of its simplicity, the Born model captures the essential feature of the solvation energy that an ion dissolved in a more polar medium has lower free energy than in a less polar medium. More importantly, the Born solvation energy can be different for cations and anions. This is the key factor that causes the formation of the Donnan potential and charge separation near an interface.

3.2.2 Analytical solution for the case of sharp interface

Equations (3.4)-(3.6) (or equivalent Eq. (3.10)) and (3.7) are coupled and non-linear, which require numerical solution in general. However, an idealized case where solvent A and B form an infinitely sharp interface permits analytical solution for the electrostatic potential profile and ion concentration profile. We briefly discuss the behavior of the excess interfacial tension due to salt ions for this idealized case because the results help understand, and provide a basis for comparison with, results for the case of finite interfacial width to be described later.

The composition as well as the dielectric profiles for the sharp interface model are just step functions. The electrostatic potential and ion profiles in this case were first studied by Nielssen and Verwey[32], and more recently by Kung et al.[31]. We refer the readers to these references for the details and merely present the results. We use a system of coordinates where the interface between media coincides with the z=0 plane and the A-rich phase resides in the region $z < 0$. We assume $a_+ < a_-$ through out this paper. For monovalent salts, the nondimensionalized electrostatic potential $\bar{\psi} = \beta e \psi$ is given by:

$$\bar{\psi}(z) = -4 \tanh^{-1}\left[I_\alpha \exp(\kappa_\alpha z)\right] \quad for\ z < 0 \tag{3.15}$$

$$\bar{\psi}(z) = \bar{\psi}_D + 4 \tanh^{-1}\left[I_\beta \exp(-\kappa_\beta z)\right] \ for\ z > 0 \tag{3.16}$$

where $\kappa_\alpha = \sqrt{2c_\alpha^\infty/\bar{\varepsilon}_A}$ and $\kappa_\beta = \sqrt{2c_\beta^\infty/\bar{\varepsilon}_B}$ are the inverse of the Debye screening length in the

two bulk regions, with c_α^∞ and c_β^∞ the salt concentration in solvent A and B respectively far away from the interface, and $\bar{\varepsilon} = \varepsilon_0\varepsilon/(\beta e^2)$ the nondimensionalized dielectric constant. I_α and I_β are integration constants determined from the boundary conditions on $\bar{\psi}$ at the interface; they are given by:

$$I_\alpha = \frac{\sqrt{1+\tau^2+2\tau\cosh(\bar{\psi}_D/2)} - 1 - \tau\cosh(\bar{\psi}_D/2)}{\tau\sinh(\bar{\psi}_D/2)} \tag{3.17}$$

$$I_\beta = \frac{\sqrt{1+\tau^2+2\tau\cosh(\bar{\psi}_D/2)} - \tau - \cosh(\bar{\psi}_D/2)}{\sinh(\bar{\psi}_D/2)} \tag{3.18}$$

where $\tau = \sqrt{\varepsilon_B c_\beta^\infty/(\varepsilon_A c_\alpha^\infty)}$ and is independent of the salt concentration as can be seen from Eq. (3.12). Based on equations (3.5) and (3.6), the concentration profiles for cations and anions can be straightforwardly calculated as:

$$c_\pm(z) = c_\alpha^\infty \left(\frac{1 \pm I_\alpha \exp(\kappa_\alpha z)}{1 \mp I_\alpha \exp(\kappa_\alpha z)}\right)^2 \quad for\ z < 0 \tag{3.19}$$

$$c_\pm(z) = c_\beta^\infty \left(\frac{1 \mp I_\beta \exp(-\kappa_\beta z)}{1 \pm I_\beta \exp(-\kappa_\beta z)}\right)^2 \quad for\ z > 0 \tag{3.20}$$

In equations (3.19) and (3.20), we can see that the concentration of cations is different from the concentration of anions at the same position. The difference in concentration becomes more significant when $|z|$ gets smaller (i.e. approaching the interface). The charge separation is caused by the spatial varying electrostatic potential, which in turn originates from the unequal solvation energy between cations and anions. In addition, the concentration of the cations is higher than the anions (i.e. net negative charge accumulates) on the solvent-A side, while lower than the anions (i.e. net positive charge accumulates) on the solvent-B side. Therefore, an electrostatic double layer forms around the sharp interface. As indicated in equations (3.19) and (3.20), the length scale of the electrostatic double layer is characterized by the corresponding Debye screening length on each side: the layer on solvent-B side is thicker than the layer on solvent-A side because $\kappa_\alpha^{-1} > \kappa_\beta^{-1}$. The thickness of the electrostatic double layer increases as the electrolyte solution becomes dilute.

Equations (3.19) and (3.20) also lead to the following inequality:

$$c_+(z) + c_-(z) > 2c_\alpha^\infty = c_{+,\alpha}^\infty + c_{-,\alpha}^\infty \quad for\ z < 0 \tag{3.21}$$

$$c_+(z) + c_-(z) > 2c_\beta^\infty = c_{+,\beta}^\infty + c_{-,\beta}^\infty \quad for\ z > 0 \tag{3.22}$$

which indicates that the total ion concentration around the interface is higher than that in the bulk region; in other words, there is an excess of ions accumulating at the sharp interface. The charge separation, electrostatic double layer and excess ion adsorption at the interface, are shown in Fig. 3.1.

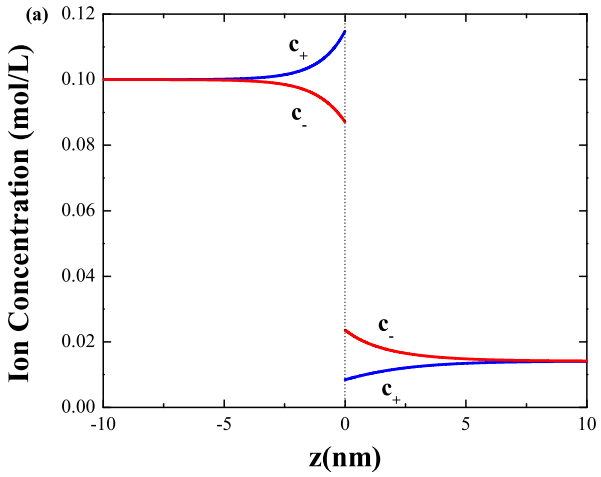

We note that similar expressions of electrostatic potential and ion concentration were given in the work of Kung et al.[31]. However, in this section, we emphasize their effect on the excess interfacial tension of the sharp interface, and will compare it to the results of the diffuse interface in section 4. The change in the interfacial tension for the sharp interface γ_{sh} can be divided into the electrostatic interaction part (γ_1) and the ion distribution part (γ_2) based on equations (3.8) and (3.9):

$$\begin{aligned} \gamma_{sh} &= \gamma_1 + \gamma_2 \\ &= -kT \int_{-\infty}^{\infty} dz \left[(\bar{\varepsilon}/2) \left(d\bar{\psi}/dz \right)^2 \right] \\ &- kT \int_{-\infty}^{\infty} dz \left(c_+ + c_- - c_+^{\infty} - c_-^{\infty} \right) \end{aligned} \tag{3.23}$$

From the expressions of the electrostatic potential and the ion concentration, the two contributions to the interfacial tension can be obtained by some straightforward algebra. The results are:

$$\begin{aligned} \gamma_1 &= \gamma_2 = -2kT\kappa_\alpha \bar{\varepsilon}_A \left[1 + \tau - \sqrt{1 + \tau^2 + 2\tau \cosh(\bar{\psi}_D/2)} \right] \\ &\sim -\left(c_\alpha^{\infty} \right)^{1/2} \end{aligned} \tag{3.24}$$

γ_1 and γ_2 are equal and both are negative. $\gamma_1 < 0$ can be easily seen in Eq. (3.23) whereas $\gamma_2 < 0$ comes from the accumulation of ions at the sharp interface. Therefore, the interfacial tension for a sharp interface decreases as the square root of the salt concentration ($\gamma_{sh} \sim -\left(c_\alpha^{\infty} \right)^{1/2}$) at the mean-field level. This result is in agreement with the theoretical results of Nichols and Pratt[20], and also with the experiment results measured by Guest and Lewis[17] at low salt concentrations. However, the results for this idealized composition profile fails to explain the linear increase with salt

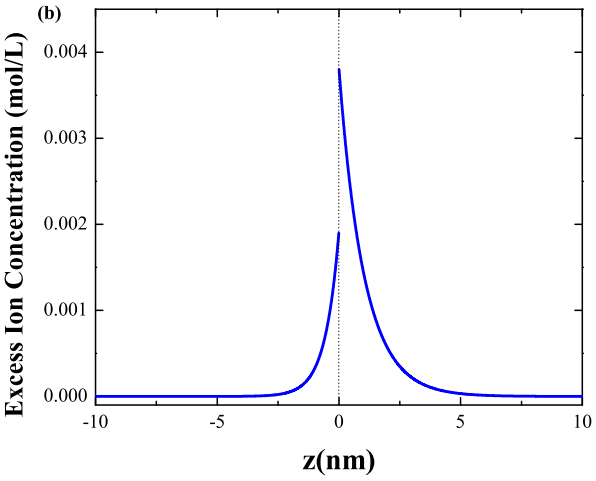

Figure 3.1: (a) The distribution of ions (c_+ and c_-) and (b) excess ion concentration ($c_+ + c_- - c_+^\infty - c_-^\infty$) between two immiscible solvents with $\varepsilon_A = 80$, $\varepsilon_B = 40$. $c_\alpha^\infty = 0.1$mol/L. $z_+ = z_- = 1$, $a_+ = 0.1nm$ and $a_- = 0.2nm$. The dot line indicates location of the sharp interface.

concentration at higher concentrations. More realistic description of the composition profile (such as Eq. (3.7)) is necessary to explain the complex behavior of the interfacial tension in the full range of the salt concentration.

3.3 Bulk Thermodynamics

The equilibrium interfacial profile is formed under the condition of equilibrium between two coexisting phases, which will in general be shifted by the addition of salt ions. Therefore, before discussing the interfacial properties, we first examine the thermodynamics of the bulk electrolyte solution in this section. The shift in the spinodal has been studied previously by one of us[33]. Here we calculate the full phase diagram.

It can be seen from Eq. (3.7) that the electrostatic interaction and the ion solvation alter the chemical potential of the solvent. The expression of the Born model (Eq. (3.13)) indicates that ions have lower solvation energy in the medium with higher dielectric constant, implying a higher solubility. The tendency for ions to be preferentially solvated by the solvent with the higher dielectric constant creates a driving force for phase separation of the two solvent components. On the other hand, the translational entropy of ions favors a uniform distribution, i.e. a single phase state.

To quantitatively analyze this effect, we write the exchange chemical potential and the grand

potential density in the bulk phase according to equations (3.7) and (3.8) as:

$$\begin{aligned}\mu_s &= \frac{kT}{v_s}\left[\ln\phi - \ln(1-\phi) + \chi(1-2\phi)\right] \\ &- \left[c_+^\infty(\phi)u_+(\phi) + c_-^\infty(\phi)u_-(\phi)\right]\frac{\Delta\varepsilon}{\varepsilon(\phi)}\end{aligned} \tag{3.25}$$

$$\begin{aligned}g^\infty &= \frac{kT}{v_s}\left[\phi\ln\phi + (1-\phi)\ln(1-\phi) + \chi\phi(1-\phi)\right] \\ &- kT\left[c_+^\infty(\phi) + c_-^\infty(\phi)\right] - \mu_s\phi\end{aligned} \tag{3.26}$$

where the concentration of the cations and anions is calculated from equations (3.5) and (3.6). Theoretically, phase equilibrium of the solvents mixture is best studied at a given chemical potential of cations and anions. The choice of the reservoir is arbitrary; for convenience, we choose the reservoir to be a salt solution in the pure solvent A. The chemical potential of ions is controlled by adjusting the salt concentration in the reservoir.

The phase boundary (binodal line) is determined by the respective equality of the chemical potential and the grand potential density in the two coexisting phases (denoted by α and β, respectively): $\mu_{s,\alpha} = \mu_{s,\beta}$ and $g_\alpha^\infty = g_\beta^\infty$. The spinodal is determined by the vanishing of the second derivative of g^∞ with respect to the composition, i.e. $\partial^2 g^\infty/\partial\phi^2 = 0$. The spinodal condition is found to be:

$$\frac{1}{v_s}\left(\frac{1}{\phi} + \frac{1}{1-\phi}\right) = 2(\chi + \Delta\chi) \tag{3.27}$$

where $\Delta\chi$ is the change of the interaction parameter resulting from adding the salt, given by:

$$\begin{aligned}\Delta\chi = \; & c^\infty \quad (\phi)\left[\beta u_+(\phi) + \beta u_-(\phi)\right]\left(\frac{\Delta\varepsilon}{\varepsilon(\phi)}\right)^2 \\ & \times \quad \left[\frac{z_-\beta u_+(\phi) + z_+\beta u_-(\phi)}{z_+ + z_-} - 2\right]\end{aligned} \tag{3.28}$$

$\Delta\chi > 0$ indicates that the miscibility between the two solvents decreases due to addition of salt, whereas $\Delta\chi < 0$ indicates increased miscibility. We see that $\Delta\chi$ is proportional to the salt concentration. We note that the sign of $\Delta\chi$ is determined by the terms in the square brackets in Eq. (3.28), reflecting the competition between the solvation energy and translational entropy.

In most cases, the solvation energy of cations and anions is more than $10kT$, which means $\Delta\chi$ is positive, resulting in phase separation at lower values of χ. Fig. 3.2(a) shows that both the binodal and the spinodal move downward in the ion-containing system compared to the ion-free system. When the solvation energy is less than $2kT$, a negative $\Delta\chi$ is obtained. From the Born model, this condition can be accomplished by high dielectric constant, high temperature, and/or large ion radius. Fig. 3.2(b) shows a phase diagram at high dielectric constant and high temperature; miscibility is

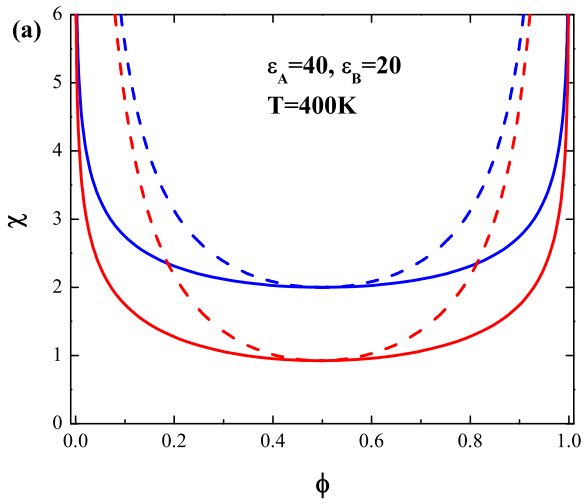

enhanced in this case. Moreover, we can see that the effect of the ion solvation on miscibility is more significant for the case of positive $\Delta\chi$ than negative $\Delta\chi$, because the correction depends not only on the difference in the dielectric constant but also on the dielectric constant itself. Eq. (3.28) indicates that the correction becomes less noticeable as ε increases.

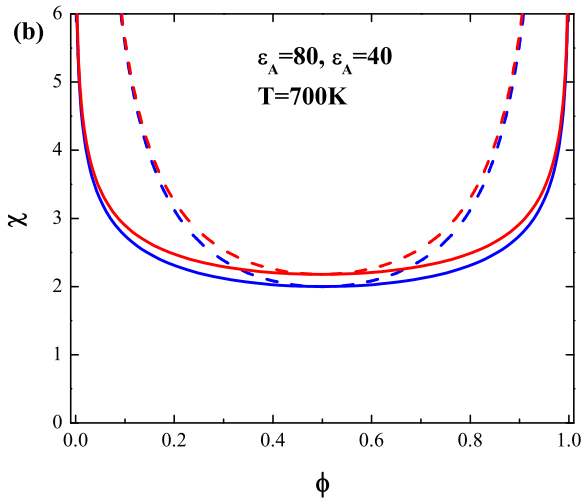

In the case where the dielectric constant of one solvent is high and of the other is low, the effect of adding salt on miscibility depends on the composition of the mixture. Miscibility increases if the high dielectric constant component is the majority, while it decreases if the low dielectric constant component is the majority. This kind of phase diagram is shown in Fig. 3.2(c).

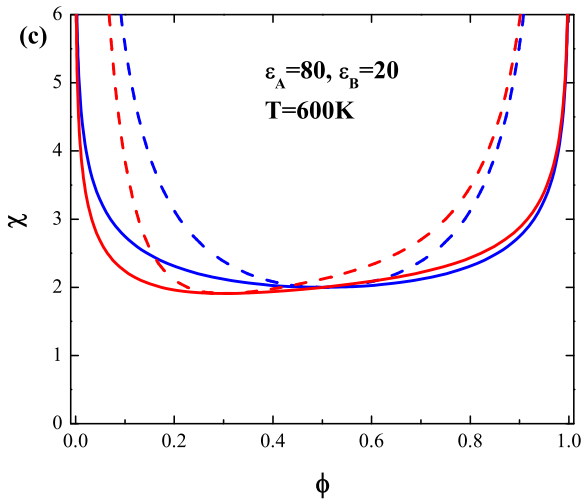

Figure 3.2: (Color online) Effect of the ion solvation on the phase diagram of the binary mixture. Solid lines are the binodal and dash lines are the spinodal. The red lines are for the ion-containing system and the blue lines are for the ion-free system. The salt concentration in the reservoir is 2mol/L. $z_+ = z_- = 1$, $a_+ = 0.1nm$, and $a_- = 0.3nm$. $a_s = 0.5nm$.

3.4 Interfacial Properties

The interfacial profiles of electrostatic potential, ion concentration and composition are obtained by simultaneously solving equations (3.4)-(3.7) with boundary conditions provided by the bulk thermodynamics discussed above. Compared to the case of sharp interface, the additional Eq. (3.7) gives rise to a finite composition gradient or, physically, a diffuse interface. For the mixture well below the critical temperature, the width of the diffuse interface scales as C^{-1}. Thus, C^{-1} becomes another length scale of the system in addition to the Debye screening length (κ^{-1}) that scales the electrostatic double layer. The interplay between these two length scales makes the interfacial structure and properties more complex, which we discuss below.

3.4.1 Interfacial structure

As discussed in Sec. 3.2.2, the electrostatic double layer is formed because of the finite potential difference between the two coexistent phases. Charge separation occurs within the electrostatic double layer. Excess ions accumulate near the interface. On the other hand, the composition of the mixture changes within the diffuse interface, which results in a significant change of the solvation energy. Ions will be preferentially distributed in the region of lower solvation energy as discussed in Sec. 3. The interfacial structure is determined by these two effects.

From the expression of C, we see that the length scale of the diffuse interface is approximately

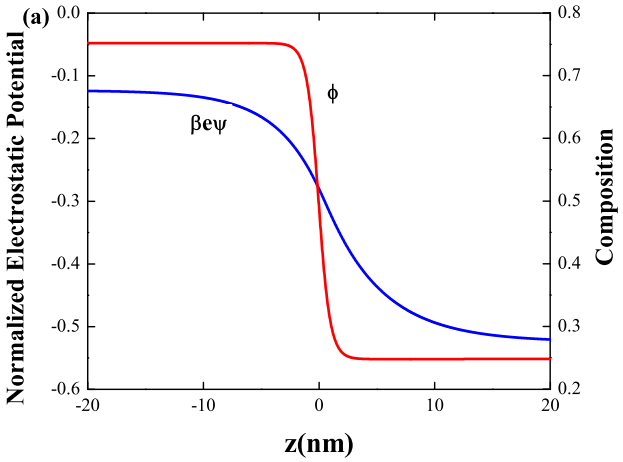

several a_s, that is on the order of 1nm. However, the Debye screening length can vary from nanometer to micrometer, depending on salt concentration. Fig. 3 shows the structure of the interface for the electrolyte solution with intermediate salt concentration ($c_\alpha^\infty = 0.01$ mol/L). From the composition profile in Fig. 3.3(a), we can see a diffuse interface with the width of 7nm between the two coexisting bulk solutions. The change of the electrostatic potential profile is smoother than the composition profile, which indicates that the electrostatic double layer is significantly wider than the composition interface ($C^{-1} < \kappa^{-1}$).

The concentration of cations and anions, and the total ion concentration ($c_+ + c_-$) are shown respectively in Figures 3(b) and 3(c), from which we can see the behavior of ion distribution in different regions. Beyond the electrostatic double layer (i.e. $|z| > \kappa^{-1}$), the concentration of cations and anions maintain its bulk value. Charge neutrality is satisfied in this bulk region (as denoted

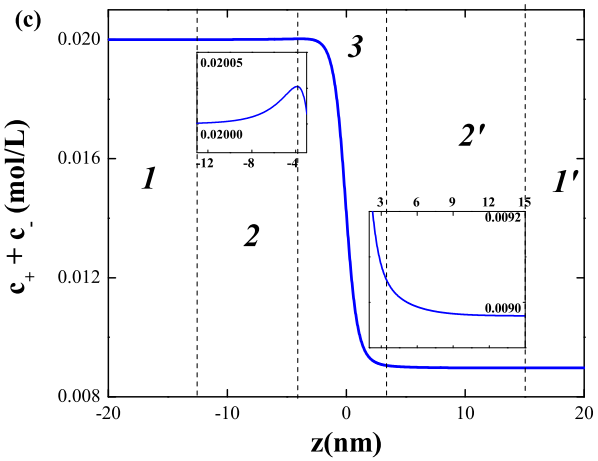

Figure 3.3: The interfacial structure for the electrolyte solution with $c_\alpha^\infty = 0.01$mol/L, (a) profiles of normalized electrostatic potential and composition, (b) the concentration of cations and anions, and (c) total ion distribution. The inserts in (c) show the excess ion accumulation in regions 2 and 2'. $\varepsilon_A = 80$, $\varepsilon_B = 40$. $z_+ = z_- = 1$, $a_+ = 0.1nm$, $a_- = 0.2nm$, $a_s = 0.5nm$, $\chi = 2.2$ and $T = 400K$.

by 1 and 1' in Fig. 3.3(c)). In the intermediate region that is inside the electrostatic double layer but outside the diffuse interface ($\kappa^{-1} > |z| > C^{-1}$), the composition is nearly constant while the electrostatic potential changes smoothly. The behavior of the ion distribution in this region (denoted by 2 and 2' as in Fig. 3.3(c)) is qualitatively the same as the case of the sharp interface. Charge separation becomes more significant as $|z|$ decreases. There are also excess ions accumulating (see the insets of Fig. 3.3(c)) in this region. Within the diffuse interface ($|z| < C^{-1}$), the composition profile changes more dramatically than the electrostatic potential profile. Solvation energy is the dominant effect on the ion distribution in this region (denoted by 3 as in Fig. 3.3(c)). The concentration of both cations and anions decreases when entering from region 2, because of the penetration of the solvent molecules with low dielectric constant in the diffuse interface. Similarly, the ion concentration increases when entering from region 2'. To calculate the net change of the ion concentration in region 3 compared to the bulk region, the exact position of the interface is needed. Onuki[22] pointed out that ions are repelled from the diffuse interface by defining the interface position with the Gibbs construction on the composition profile[34]. With the composition profile, cation and anion profiles all different, an unambiguous Gibbs construction is not obviously possible. Nevertheless, the conclusion that ions are slightly depleted in region 3 still stands, which is reflected by the behavior of the interfacial tension as will be discussed in Section 3.4.2.

The length scale of the electrostatic double layer strongly depends on the salt concentration, which leads to differences in the interfacial structure for the concentrated and the dilute electrolyte solution. Fig. 3.4 and Fig. 3.5 show the profiles of electrostatic potential and composition, and

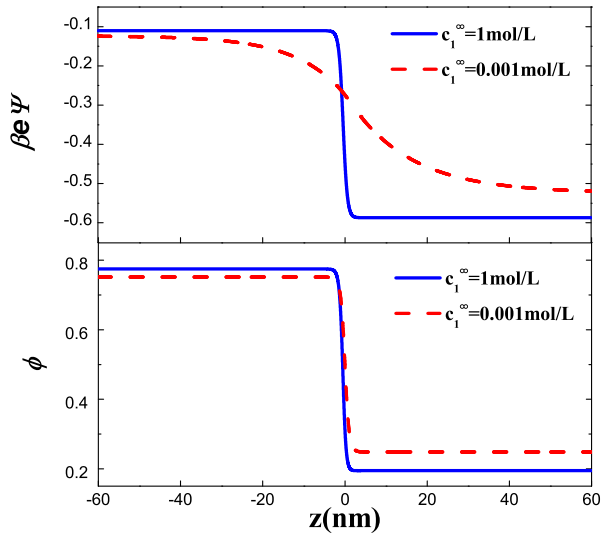

Figure 3.4: Profiles of normalized electrostatic potential and composition for $c_\alpha^\infty = 1$ mol/L and $c_\alpha^\infty = 0.001$ mol/L. $\varepsilon_A = 80$, $\varepsilon_B = 40$. $z_+ = z_- = 1$, $a_+ = 0.1nm$, $a_- = 0.2nm$, $a_s = 0.5nm$, $\chi = 2.2$ and $T = 400K$.

the ion distribution for these two cases ($c_\alpha^\infty = 1$ mol/L and $c_\alpha^\infty = 0.001$ mol/L). For $c_\alpha^\infty = 1$mol/L, both the electrostatic double layer and the diffuse interface have a length scale of a few nanometers ($\kappa^{-1} \cong C^{-1}$). Regions 2 and 2' shrink. The charge separation is greatly inhibited as shown in Fig. 3.5(a). The change of the solvation energy plays the main role in determining the ion distribution, which leads to ions being repelled from the interfacial area. For the case of very dilute electrolyte solution ($c_\alpha^\infty = 0.001$mol/L), the electrostatic double layer is about 100 times wider than the diffuse interface ($\kappa^{-1} \gg C^{-1}$). From the view of the electrostatic potential which changes very smoothly, the composition profile behaves as a step function. The behavior of ion distribution is similar to the case of sharp interface, seen from the similarity between Figures 3.5(b) and 3.1(a). Excess ions accumulate in the interface area.

3.4.2 Interfacial tension

The interfacial structure of the electrolyte solution mixture has direct consequences on the behavior of the interfacial tension. The excess interfacial tension can be divided into two parts:

$$\Delta\gamma = \gamma - \gamma_0 = \gamma_1 + \gamma_2 \tag{3.29}$$

where γ_0 is the interfacial tension of the salt-free system ($\gamma_0 = \int dz\,[g_0 - g_0^\infty]$). Based on Eq. (3.8), γ_1 and γ_2 are expressed respectively as:

$$\gamma_1 = -kT \int_{-\infty}^{\infty} dz \left[(\bar{\varepsilon}/2) \left(d\bar{\psi}/dz \right)^2 \right] \tag{3.30}$$

$$\begin{aligned} \gamma_2 &= -kT \int_{-\infty}^{\infty} dz (c_+ + c_- - c_+^\infty - c_-^\infty) \\ &+ \int_{-\infty}^{\infty} dz\,[(g_s - g_s^\infty) - (g_0 - g_0^\infty)] \end{aligned} \tag{3.31}$$

γ_1 is due to the electrostatic interactions, and γ_2 combines the influences of the ion distribution and the solution free energy. As pointed out by Onuki[22], the contribution of the second term in Eq. (3.31) to γ_2 is less important than the first term because the interfacial excess free energy of the ion-containing system is mostly cancelled out by the salt-free system. Therefore, γ_2 is mainly due to the change of ion concentration in the interfacial area compared to the bulk phase ($\gamma_2 \cong -kT \int_{-\infty}^{\infty} dz(c_+ + c_- - c_+^\infty - c_-^\infty)$). From equations (3.30) and (3.31), we see that γ_1 is always negative, while the sign of γ_2 depends on whether there is depletion or enrichment of ions in the interfacial region.

The change of γ_1, γ_2 and $\Delta\gamma$ as functions of the salt concentration in bulk phase 1 (c_α^∞) is shown in Fig. 3.6. γ_1 decreases approximately in proportion to $(c_\alpha^\infty)^{1/2}$ in the full range of the salt concentration, which is similar to its behavior in the sharp-interface case. γ_2 is positive and increases linearly with c_α^∞ when the salt concentration is high; this is due to the depletion of ions since the amount of depleted ions is proportional to the bulk salt concentration. This is consistent with the reasoning given in Sec. 4.1 that, for large c_α^∞, the repulsion of ions from the diffuse interface dominates over the accumulation of ions in the electrostatic double layer. However, γ_2 becomes negative in the very dilute regime ($c_\alpha^\infty < 0.005$mol/L), shown in the inset in Fig. 3.6. Excess ions are absorbed into the interfacial region because with the increase in the width of the electrostatic double layer due to decreased salt concentration, the composition profile behaves increasingly like a sharp interface.

With this qualitative understanding of the concentration dependence of γ_1 and γ_2, it is now easy to understand the behavior of $\Delta\gamma$. At high salt concentration, $|\gamma_1| < |\gamma_2|$; $\Delta\gamma \cong \gamma_2$, which is positive and increases linearly with the salt concentration. On the other hand, $|\gamma_1| > |\gamma_2|$ at low salt concentration; $\Delta\gamma \cong \gamma_1$, which is negative and decreases in proportional to the square root of the salt concentration. The different scaling behaviors of the interfacial tension with respect to the salt concentration (i.e. $\Delta\gamma \sim c_\alpha^\infty$ at large c_α^∞; $\Delta\gamma \sim -(c_\alpha^\infty)^{1/2}$ at small c_α^∞) is in agreement with the experiment results of the liquid-gas surface tension measured by Petersen and Saykally[14], and the liquid-liquid interfacial tension measured by Guest and Lewis[17]. Moreover, the $\Delta\gamma$ curve has

a small negative minimum ($\Delta\gamma_{min} \sim -10^{-3}\gamma_0$) in the dilute regime ($c_\alpha^\infty \sim 10^{-3}$mol/L). Both the location of the minimum and its magnitude are in the range of the Jones-Ray effect observed in the experiments.

To further demonstrate the effect of the interfacial structure on the interfacial tension, we investigate the behavior of γ_2 at three different values of the interaction parameter χ, as shown in Fig. 3.7. The value of χ determines the degree of phase separation and hence the width of the diffuse interface in combination with C^{-1}. As χ increases from 2.01 to 3, the width of the diffuse interface decreases from 20nm to 2nm. A narrower interface is less capable of depleting ions. For the case of $\chi = 3$, starting at high salt concentration and going in the direction of decreasing concentration, the effect of ion accumulation in the electrostatic double layer increases relative to the effect of ion depletion in the diffuse interface. γ_2 becomes negative at $c_\alpha^\infty = 0.018$mol/L as shown in Fig. 3.7. For small χ, especially near the critical point, the composition interface is quite wide. A larger width for the electrostatic double layer is required to counteract this effect. Thus, γ_2 remains positive even for very dilute electrolyte solution ($c_\alpha^\infty \sim 10^{-5}$mol/L), as shown for the case of $\chi = 2.01$ in Fig. 3.7.

Experimentally, the excess water-air surface tension is known to show a marked specific ion effect that decreases according to the Hofmeister sequence[15, 16]: $F^- > Cl^- > Br^- > I^-$. Similar dependence of the liquid-liquid interfacial tension on the cations and anions themselves has also been observed. Guest and Lewis found that[17], for K^+ as the cation, the interfacial tension between water and dekalin significantly decreases as the anion changes in the sequence of Cl^-, I^- and SCN^-. For the latter two anions, $\Delta\gamma$ is even negative up to a quite high salt concentration. This effect can also be explained by our model. The difference between the solvation energy of a specific ion in the two solvents decreases inversely with the ion radius. Let us first change the radius of anions by fixing the radius of cations under the precondition that $a_+ < a_-$. From equations (3.11) and (3.12), we can see that $|\psi_D|$ increases and $c_\alpha^\infty/c_\beta^\infty$ decreases as a_- increases. The increase of $|\psi_D|$ gives rise to a larger gradient of electrostatic potential, which causes γ_1 to become more negative. The decrease of $c_\alpha^\infty/c_\beta^\infty$ reduces the amount of ions that are depleted from the diffuse interface, and thus decreases γ_2. γ_1 and γ_2 change in the same direction, which makes $\Delta\gamma$ decrease as the radius of the anions increases. Fig. 8 shows the dependence of the interfacial tension on the radius of anions. For small ions, $\Delta\gamma$ has a linear relationship with the salt concentration in the concentrated region, while for large ions, $\Delta\gamma$ maintains the $-(c_\alpha^\infty)^{1/2}$ scaling in a wide range of the salt concentration. Similar analysis can also be made for the size change of cations under the condition that $a_+ < a_-$. However, γ_1 and γ_2 change in opposite directions in this case, which weakens the effect of a_+ on $\Delta\gamma$. This is consistent with the general experimental finding that the interfacial tension usually depends more strongly on anions than cations[15].

We note also that our results are consistent with the findings of Bhatt et al.[35] who studied the specific-ion effect on the surface tension of aqueous electrolytic solutions using molecular dynamics

simulation. In their work, it is found that when water molecules are treated explicitly and the ions are treated simply as charged Lennard-Jones particles, the surface tension shows a larger increase for the NaF solution than for the NaCl solution and the simulation data are in good agreement with experiment; this is consistent with the expectation from our theory based on the size dependence in the solvation energy of the ions. On the other hand, the opposite trend is obtained when water molecules are treated as a simple dielectric within the primitive model, which does not account for the solvation of ions. We therefore conclude that the size-dependent solvation energy of the ions is the key factor in determining the interfacial tension.

3.5 Conclusions

In this paper, we have presented a unified model in the mean-field framework to describe the bulk thermodynamics and interfacial properties of the electrolyte solution mixture, by taking the solvation energy of ions into account. The electrostatic potential, ion concentration and solvent composition are treated explicitly in our model. At the mean-field level, the solvation energy retains the form of Born energy which is spatially dependent in an inhomogeneous dielectric medium. The Born energy captures a key characteristic of a specific ion by its radius and valency. The difference in the solvation energy between the cations and anions leads to the local charge separation, a finite electrostatic potential difference between two coexisting phases, and the formation of an electrostatic double layer at the interface.

Ion solvation affects the phase equilibrium of the solvent mixture. The miscibility of the mixture can either increase or decrease depending on the relative value between the average solvation energy $(z_- u_+ + z_+ u_-)/(z_+ + z_-)$ and $2kT$. When the dielectric constant is low for both solvents, the addition of salt ions decreases the miscibility, while when the dielectric constant for the two solvents is high and at high temperature, the addition of salt ions makes the mixture more miscible. When the dielectric constant of one solvent is high and the other is low, adding salt ions enhances the miscibility if the high-dielectric-constant solvent is the majority component and decreases the miscibility if the low-dielectric-constant solvent is the majority component.

Ion solvation has significant effect on the interfacial structure and properties of the electrolyte solution mixture. The ion distribution in the interfacial area is determined by the competition between the effects of the electrostatic double layer and the diffusive composition interface. The former effect results in accumulation of ions in the interfacial region and is more important in the dilute electrolyte solution, while the latter effect causes ions to be depleted from the interfacial region and dominates at high salt concentration. The interfacial tension, which is a sum of the electrostatic interaction part and the ion excess part, has different scaling behavior as the salt concentration changes. The ion excess is negative and is the dominant contribution in the concentrated regime,

leading to an increase in the interfacial tension that scales as $\Delta\gamma \sim c$. On the other hand, the electrostatic interaction part is dominant in the dilute solution, which scales as $\Delta\gamma \sim -c^{1/2}$. The interfacial tension has a negative minimum near 1mM, in agreement with the Jones-Ray effect observed in experiments. Moreover, for a fixed cation type, the interfacial tension decreases as the size of anion increases. The specific ion effect can be qualitatively explained by our model when the solvation energy is accounted for.

Our model uses a simple Born form for the solvation energy, with a local dielectric constant given by some composition weighted average of the two liquid components, which is derived within the framework of *continuum*, *linear* dielectrics. Such a framework cannot predict the dielectric constant of a mixture in terms of the components, nor does it account for effects such as dielectric saturation. A more molecularly-based approach accounting for the polarizability and permanent dipoles of the solvating molecules would be required to yield an more accurate expression for the solvation energy. [36, 37]

In this work, the electrolyte solution is investigated at the mean-field level, where the solvation energy retains the form of Born energy. However, the solvation energy is closely related to the fluctuation in a charged system, which includes both the local Born solvation effect and other long-range effects. A well-known example is the depletion of ions from the water-air interface caused by the image repulsion. To fully account for the solvation energy, the Green's function describing the charge correlation need to be solved for in addition to the modified PB equation, as presented in Ref. 12. Onuki[22] pointed out that the image interaction can dominate over the local solvation energy if the dielectric inhomogeneity of the two media becomes strong, especially for the liquid-gas and liquid-solid interfaces. The Green's function approach has been used for the sharp-interface model, in both the planar [38] and curved geometry.[39] Full fluctuation effects need to be incorporated in future work in order to study the interfacial behavior in these systems.

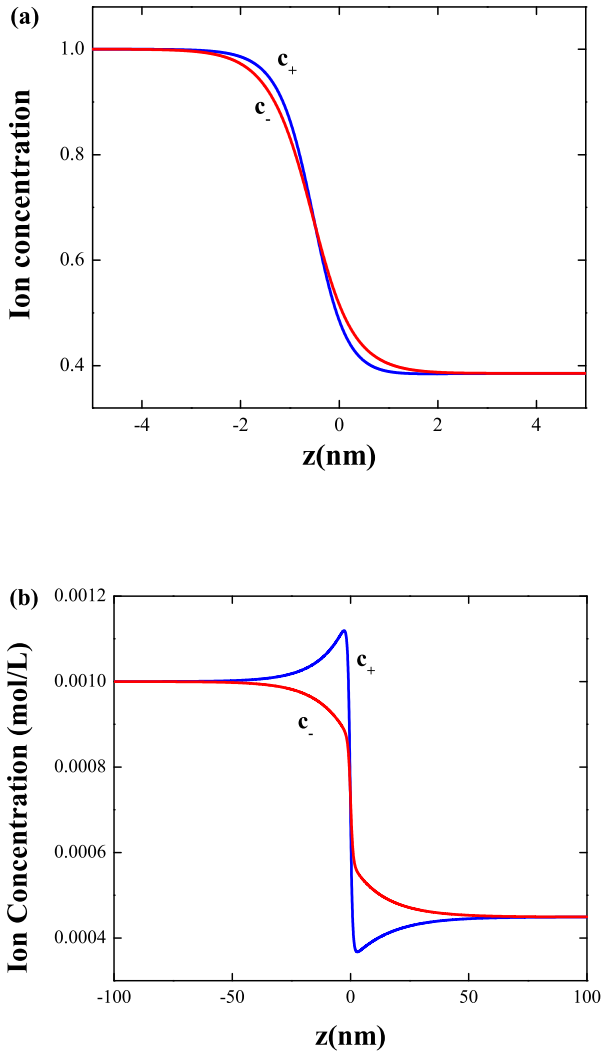

Figure 3.5: The concentration profiles of cations and anions for (a) $c_\alpha^\infty = 1$mol/L and (b) $c_\alpha^\infty = 0.001$mol/L. $\varepsilon_A = 80$, $\varepsilon_B = 40$. $z_+ = z_- = 1$, $a_+ = 0.1nm$, $a_- = 0.2nm$, $a_s = 0.5nm$, $\chi = 2.2$ and $T = 400K$.

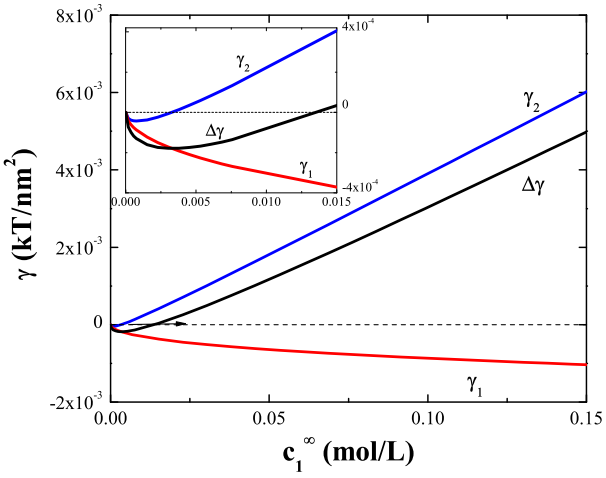

Figure 3.6: γ_1, γ_2 and $\Delta\gamma$ as functions of c_α^∞. The inset shows the behavior at low concentrations. $\varepsilon_A = 80$, $\varepsilon_B = 40$. $z_+ = z_- = 1$, $a_+ = 0.1nm$, $a_- = 0.2nm$, $a_s = 0.5nm$, $\chi = 2.2$ and $T = 400K$.

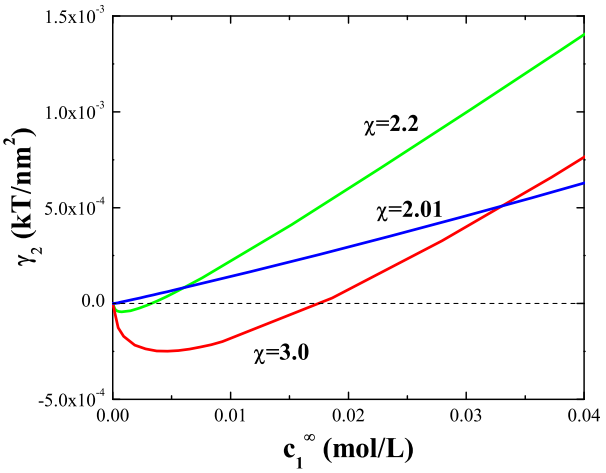

Figure 3.7: γ_2 as a functions of c_α^∞ for three different values of χ. $\varepsilon_A = 80$, $\varepsilon_B = 40$. $z_+ = z_- = 1$, $a_+ = 0.1nm$, $a_- = 0.2nm$, $a_s = 0.5nm$ and $T = 400K$.

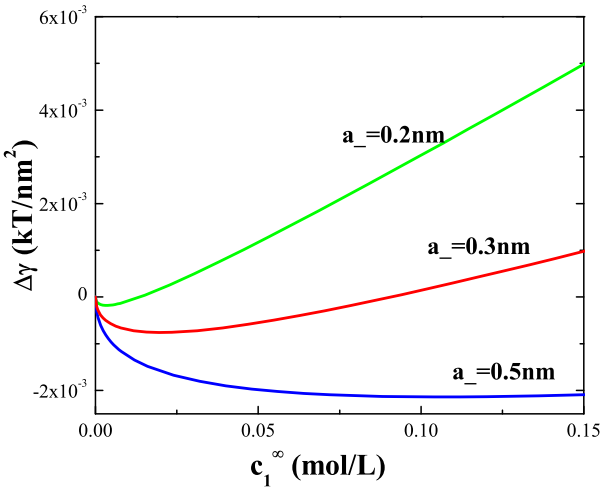

Figure 3.8: $\Delta\gamma$ as a functions of c_α^∞ for three different values of a_-. $\varepsilon_A = 80$, $\varepsilon_B = 40$. $z_+ = z_- = 1$, $a_+ = 0.1nm$, $a_s = 0.5nm$, $\chi = 2.2$ and $T = 400K$.

Bibliography

[1] J. Israelachvili, *Intermolecular and Surface Forces*, 2nd Ed. (Academic, London, 1992).

[2] D. Andelman, in *Soft Condensed Matter Physics in Molecular and Cell Biology*, W. C. K. Poon and D. Andelman, eds. (Taylor and Francis, Boca Raton, Florida, 2000); pp. 97-118.

[3] Y. Levin, Rep. Prog. Phys. **65**, 1577 (2002).

[4] B. Alberts, D. Bray, J. Lewis, M. Raff, K. Roberts, and J. D. Watson, *Molecular Biology of the Cell*, 3rd ed. (Garland, NY, 1994).

[5] I. Borukhov, D. Andelman, and H. Orland, Phys. Rev. Lett. **79**, 435 (1997).

[6] R. R. Netz and H. Orland, Euro. Phys. J. E **1**, 67 (2000).

[7] Y. Levin and J. E. Flores-Mena, Euro. Phys. Lett. **56**, 187 (2001).

[8] M. Z. Bazant, B. D. Storey, and A. A. Kornyshev, Phys. Rev. Lett. **106**, art. no. 046102 (2011).

[9] M. P. Tosi, in *Condensed Matter Physics Aspects of Electrochemistry* (World Scientific, 1991); p. 68.

[10] M. Rovere and M. P. Tosi, Rep. Prog. Phys. **49**, 1001 (1986).

[11] W. M. Gelbart, R. F. Bruinsma, P. A. Pincus, and V. A. Parsegian, Phys. Today **53**, 38 (2000).

[12] Z.-G. Wang, Phys. Rev. E **81** art. no. 021501 (2010).

[13] G. Jones and W. A. Ray, J. Am. Chem. Soc. **57**, 957 (1935); **59**, 187 (1937); **63**, 288 (1941); **63**, 3262 (1941); **64**, 2744 (1942).

[14] P. B. Petersen and R. J. Saykally, J. Am. Chem. Soc. **127**, 15446 (2005).

[15] M. Boström, W. Kunz, and B. W. Ninham, Langmuir **21**, 2619 (2005).

[16] M. Boström M, D. R. M. Williams, B. W. Ninham, Biophys. J. **85**, 686 (2003).

[17] W. L. Guest and W. C. M. Lewis, Proc. R. Soc. A **170**, 501 (1939).

[18] C. Wagner, Phys. Z. **25**, 474 (1924).

[19] L. Onsager and N. N. T. Samaras, J. Chem. Phys. **2**, 528 (1933).

[20] A. L. Nichols III and L. R. Pratt, J. Chem. Phys. **80**, 6225 (1984).

[21] M. Bier, J. Zwanikken, and R. van Roij, Phys. Rev. Lett. **101**, art. no. 046104 (2008).

[22] A. Onuki, Phys. Rev. E **73**, art. no. 021506 (2006).

[23] A. Onuki, J. Chem. Phys. **128**, art. no. 224704 (2008).

[24] Y. Levin, Phys. Rev. Lett. **102**, art. no. 147803 (2009).

[25] H. T. Davis, *Statistical Mechanics of Phases, Interfaces, and Thin Films*, (VCH Publishers, Inc. 1996).

[26] S. A. Safran, *Statistical Thermodynamics of Surfaces, Interfaces, and Membranes*, (Westview Press, 2003).

[27] P. G. de Gennes, J. Chem. Phys. **72**, 4756, (1980).

[28] M. Born, Z. Phys. **1**, 45 (1920).

[29] Y. Marcus, *Ion SolVation*, (Wiley: New York, 1985).

[30] A. R. Blythe and D. Bloor, *Electric Properties of Polymers*, (Cambridge University Press: New York, 2005).

[31] W. Kung, F. J. Solis, and M. O. de la Cruz, J. Chem. Phys. **130**, art. no. 044502 (2009).

[32] E. J. W. Verwey and K. F. Niessen, Phil. Mag. **28**, 435 (1939).

[33] Z.-G. Wang, J. Phys. Chem. B **112**(50), 16205, (2002).

[34] D. Chandler, *Introduction to Modern Statistical Mechanics*, (Oxford University Press, Oxford, 1987).

[35] D. Bhatt, J. Newman and C. J. Radke, J. Phys. Chem. B **108**, 9077, (2004).

[36] A. K. Jha and K. F. Freed, J. Chem. Phys. **128**, art. no. 034501 (2008).

[37] P. Koehl, H. Orland, and M. Delarue, J. Phys. Chem. B **113**, 5694, (2009).

[38] D. S. Dean and R. R. Horgan, Phys. Rev. E **69** art. no. 061603 (2004).

[39] R. A. Curtis and L. Lue, J. Chem. Phys. **123**, art. no. 174702 (2005).

Chapter 4

The image effects on the double layer structure and interfacial properties I. electrolyte solution near a single charged plate

It is widely accepted that the Poisson-Boltzmann (PB) theory provides an accurate description for charged surfaces in the so-called weak coupling limit. In this chapter, we show that the image charge repulsion creates a depletion boundary layer that cannot be captured by a regular perturbation approach. The correct weak-coupling theory must include the self-energy of the ion due to the image charge interaction. The image force qualitatively alters the double layer structure and properties, and gives rise to many non-PB effects, such as nonmonotonic dependence of the surface energy on concentration and charge inversion. In the presence of dielectric discontinuity, there is no limiting condition for which the PB theory is valid. This chapter is adapted in part from the manuscript R. Wang and Z.-G. Wang, submitted to *J. Chem. Phys.*.

4.1 Introduction

The electric double layer resulting from a charged surface in an aqueous solution affects a wealth of structural and dynamic properties in a wide range of physicochemical, colloidal, soft-matter and biophysical systems[1, 2, 3, 4, 5]. The standard textbook description of the electrical double layers is based on the mean-field Poisson-Boltzmann (PB) theory. At large surface-charge density, high counter-ion valency and high ion concentration – the so-called strong coupling limit – it is well recognized that PB theory fails to capture a number of qualitative effects, such as like-charge attraction[6, 7, 8] and charge inversion[9, 10, 11]. Liquid-state theories[12, 13] and other strong-coupling theories[8, 14] have been employed to account for the strong ion-ion correlations in this regime.

In the opposite limit – the weak-coupling regime – it is generally accepted that the electric double layer is well described by the PB theory[15, 17, 16, 18, 19]. Performing a perturbation expansion in the coupling parameter (to be defined below), Netz[17] demonstrated that the PB theory is the leading-order theory in the weak-coupling limit, and becomes exact in the limit of zero coupling strength. Applying Netz's approach explicitly to surfaces with dielectric discontinuity, Kanduč and Podgornik[18] concluded that, under the weak-coupling condition, the image force only enters as a small correction to the leading PB theory, which vanishes in the limit of zero coupling. In particular, the self-energy due to image charge interaction was shown not to appear in the Boltzmann factor for the ion distributions. Although these demonstrations were performed explicitly for counterion-only systems, the conclusions are generally believed to hold when salt ions are added[19]. Thus, many researchers in the electrolyte community consider the weak-coupling theory to mean the PB theory; in other words, weak coupling is considered synonymous with the validity of the PB theory.

Physically, however, a single ion in solution next to a surface of a lower dielectric plate obviously should feel the image charge repulsion even in the absence of any surface charge, and the ion distribution – the probability of finding the ion at any location – should reflect the image charge interaction through the Boltzmann factor. This was the case studied in the pioneering work of Wagner[20], and Onsager and Samaras[21] (WOS) for the surface tension of electrolyte solutions. It is rather odd that this interaction should become absent from the Boltzmann factor for the distribution of mobile ions in the weak-coupling limit when the surface becomes charged. It is also rather curious that the image interaction, which is absent from the Boltzmann factor in the Netz-Kanduč-Podgornik (NKP) approach[14, 17, 18] in the weak coupling limit, "re-emerges" in the Boltzmann factor in the strong-coupling limit, though in a different form (through a fugacity expansion)[8, 18, 19]. Taking zero-surface charge as the limiting case of the *physical* weak-coupling condition, it is clear that the NKP and WOS approaches give drastically different descriptions of the same system. It is also difficult to physically reconcile the absence of the image interaction from the

Boltzmann factor in the weak-coupling limit with its "re-emergence" in the strong coupling limit in the NKP approach.

In this work, we clarify the origin of these discrepancies by a re-examination of the role of the image charge interaction in the *physical* weak-coupling limit. We show that in the presence of a dielectric discontinuity, the *physical* weak-coupling limit is not described by the so-called weak-coupling theory if the latter is meant to be the PB or PB with small fluctuations corrections. The image charge repulsion creates a boundary layer which cannot be captured by the the NKP approach. A nonperturbative approach yields a modified Poisson-Boltzmann equation, where a screened, self-consistently determined image charge interaction appears in the Boltzmann factor for the ion concentration for any surface charge density. The WOS theory is an approximation of the more general framework presented here in the special case of zero surface charge.

To see the origin of the boundary layer, we start by an analysis of the relevant length scales for the counterion-only system. Consider a charged planar surface at $z = 0$ with charge density σ separating an aqueous solution ($z > 0$) from an semi-infinite plate ($z < 0$). The solvent and plate are taken to be dielectric continuum with dielectric constant ε_S and ε_P, respectively. Now consider a counterion of valency q at distance z away from the surface. The attraction between the test ion and the charged surface is $E_{sur} = 2\pi q l_B \sigma z = z/l_{GC}$, whereas the repulsion due to its image charge is $E_{im} = fq^2 l_B/(2z)$, where $l_B = e^2/(4\pi\varepsilon_0\varepsilon_S kT)$ is the Bjerrum length with ε_0 denoting the vacuum permittivity, $l_{GC} = 1/2\pi q\sigma l_B$ is the Gouy-Chapman length and $f = (\varepsilon_S - \varepsilon_P)/(\varepsilon_S + \varepsilon_P)$ represents the dielectric contrast between the two media. Balancing E_{sur} with E_{im} results in a characteristic length:

$$d = (f/2)^{1/2}\, q\, (l_B l_{GC})^{1/2} \tag{4.1}$$

Introducing the coupling parameter $\Xi = q^2 l_B/l_{GC}$[**?**], we see $d \sim l_B \Xi^{-1/2}$ and $d/l_{GC} \sim \Xi^{1/2}$. Thus, as the coupling strength Ξ goes to zero, d itself diverges, but the ratio of d to l_{GC} (noting that l_{GC} is the characteristic length scale for the double layer in the PB theory) goes to zero. This is a typical feature of a *boundary layer*. Physically, the competition between the surface charge attraction and the image charge repulsion gives rise to a depletion boundary layer. Since the perturbation approach performs an expansion in powers of Ξ[14, 17, 18] (which results from nondimensionalizing all the lengths by the longest length scale l_{GC}), information within the smaller length-scale – the depletion boundary layer – is lost. Although this analysis is performed explicitly for the counterion-only system, the depletion boundary layer persists when salt ions are introduced.

4.2 Theory

The presence of a boundary layer necessitates a nonperturbative treatment. Using the renormalized Gaussian variational approach[22], one of us[23] derived a general theory for a general system with

a fixed charge distribution $\rho_s(\mathbf{r})$ in the presence of mobile cations with charge q_+e and anions with charge q_-e , in a dielectric medium of a spatially varying dielectric function $\varepsilon(\mathbf{r})$. The key result of the theory is the following set of self-consistent equations for the mean electrostatic potential $\psi(\mathbf{r})$ (nondimensionized by kT/e), the correlation function (Green function) $G(\mathbf{r},\mathbf{r}')$, and the self-energy $u_\pm(\mathbf{r})$ of mobile ions:

$$-\nabla\cdot(\epsilon\nabla\psi) = \rho_s + \Gamma\lambda_+ q_+ \mathrm{e}^{-q_+\psi-u_+} - \Gamma\lambda_- q_- \mathrm{e}^{q_-\psi-u_-} \tag{4.2}$$

$$-\nabla\cdot[\epsilon\nabla G(\mathbf{r},\mathbf{r}')] + 2I(\mathbf{r})G(\mathbf{r},\mathbf{r}') = \delta(\mathbf{r}-\mathbf{r}') \tag{4.3}$$

$$u_\pm(\mathbf{r}) = \frac{1}{2}\int d\mathbf{r}'d\mathbf{r}'' h_\pm(\mathbf{r}-\mathbf{r}')G(\mathbf{r}',\mathbf{r}'')h_\pm(\mathbf{r}''-\mathbf{r}) \tag{4.4}$$

where ϵ is the scaled permittivity as $\epsilon = kT\varepsilon_0\varepsilon(\mathbf{r})/e^2$. $\lambda_\pm$ is the fugacity of cations and anions determined from the bulk salt concentration. The function Γ is introduced to constrain the mobile ions to the solvent region. $I(\mathbf{r}) = \left[q_+^2 c_+(\mathbf{r}) + q_-^2 c_-(\mathbf{r})\right]/2$ is the local ionic strength, with the concentration of cations and anions given by

$$c_\pm(\mathbf{r}) = \lambda_\pm\Gamma\exp\left[\mp q_\pm\psi(\mathbf{r}) - u_\pm(\mathbf{r})\right] \tag{4.5}$$

The short-range charge distribution function $h_\pm(\mathbf{r}-\mathbf{r}')$ on the ion in Eq. 4.4 is introduced to yield a finite Born solvation energy[23]. For our purpose, we will eventually take the point-charge limit.

Eq. 4.2 has the same form as the PB equation, but now with the self-energy of the ions appearing in the Boltzmann factor. The self-energy given by Eq. 4.4 is a unified expression that includes the Born energy of the ion, the interaction between the ion and its ionic atmosphere, as well as the distortion of the electric field by a spatially varying dielectric function, the latter taking the form of image charge interaction near a dielectric discontinuity. In general, the self energy is spatially varying if there is spatial inhomogeneity in either the dielectric constant or the ionic strength. The grand free energy is:

$$\begin{aligned} W &= -\int d\mathbf{r}\,(c_+ + c_-) + \frac{1}{2}\int d\mathbf{r}\psi\,(\rho_s - q_+c_+ + q_-c_-) \\ &+ \int d\mathbf{r} I(\mathbf{r})\int_0^1 d\eta\,[G(\mathbf{r},\mathbf{r};\eta) - G(\mathbf{r},\mathbf{r})] \end{aligned} \tag{4.6}$$

where η is a "charging" variable. $G(\mathbf{r},\mathbf{r};\eta)$ is the same-point Green's function obtained from solving the equation similar to Eq. 4.3 by replacing the term $I(\mathbf{r})$ in Eq. 4.3 with $\eta I(\mathbf{r})$.

We now specify to the charged plate with dielectric discontinuity in contact with an electrolyte solution. The fixed external charge density is then $\rho_s(\mathbf{r}) = \sigma\delta(z)$. We take the surface charge to be positive. Both Γ and $\varepsilon(\mathbf{r})$ are step functions: $\Gamma = 0$ and $\varepsilon(\mathbf{r}) = \varepsilon_P$ for $z < 0$; $\Gamma = 1$ and $\varepsilon(\mathbf{r}) = \varepsilon_S$

for $z > 0$. In the solvent region ($z > 0$), Eq. 7.3 becomes

$$-\epsilon_S \frac{\partial^2 \psi(z)}{\partial z^2} = \lambda_+ q_+ \mathrm{e}^{-q_+\psi - u_+} - \lambda_- q_- \mathrm{e}^{q_-\psi - u_-} \tag{4.7}$$

with the boundary condition $(\partial\psi/\partial z)_{z=0} = -\sigma/\epsilon_S$. Since the solvent has a uniform dielectric constant, the Born energy is constant and can be absorbed into the reference chemical potential. The remaining contribution is finite in the point-charge limit (setting $h_\pm(\mathbf{r}-\mathbf{r}') = q_\pm\delta(\mathbf{r}-\mathbf{r}')$), which yields the nontrivial part of the self energy as $u_\pm = (q_\pm^2/2)\lim_{\mathbf{r}'\to\mathbf{r}}[G(\mathbf{r},\mathbf{r}') - 1/(4\pi\epsilon_S|\mathbf{r}-\mathbf{r}'|)]$. For low ionic strengths, to a good approximation, Eq. 4.3 can be solved analytically using the WKB approximation[24]: the Green's function assumes the same functional form as the solution for constant ionic strength, but with the ionic strength replaced by its local value. With the approximate $G(\mathbf{r},\mathbf{r}')$, the self energy can be simplified to the following intuitive form:

$$u_\pm(z) = \frac{q_\pm^2}{8\pi\epsilon_S}\left[-\kappa(z) + \frac{f\mathrm{e}^{-2\kappa(z)z}}{2z}\right] \tag{4.8}$$

where $\kappa(z) = [2I(z)/\epsilon_S]^{1/2}$ is the inverse of the local Debye screening length. The first term in the self energy accounts for the interaction with the local ionic atmosphere, and the second term is the image-charge interaction, which is repulsive for $f > 0$. Far away from the plate surface ($z \to \infty$), the ion concentration approaches the bulk value $c_\pm^b$, so from Eq. 4.5, the fugacity of the ions is given by $\lambda_\pm = c_\pm^b \exp\left[-q_\pm^2\kappa_b/(8\pi\epsilon_S)\right]$ where κ_b is the inverse screening length in the bulk and we have set $\psi_b = 0$. Although the theory is derived explicitly with added salt, application to the counterion-only system is straightforward through an ensemble transformation[17].

4.3 Results and discussions

By using the variational approach, we have shown that the image charge effect appears explicitly in the Boltzmann factor, which will affect the double layer structure and the interfacial properties. In this section, we will apply our theory to electrolyte solution in contact with a weakly charged plate, for both the system containing only counterions and the system with added salts.

4.3.1 Counterion-only system

For the counterion-only system, the PB theory admits an analytical solution for the counterion distribution: $c(z) = 1/\left[2\pi l_B q^2 (z^2 + l_{GC}^2)\right]$, which is characterized by a single length scale, the Gouy-Chapman length. Our theory predicts a qualitatively different behavior when there is dielectric discontinuity as shown in Figure 4.1. The presence of the depletion boundary layer inside the Gouy-Chapman length is clear. Within the depletion boundary layer ($z < d$), image charge repulsion is

dominant and ions are excluded from the plate surface. In the point-charge model, the self energy diverges to infinity at the plate surface; thus the ion concentration vanishes at $z = 0$. Beyond the depletion boundary layer ($z > d$), surface charge attraction prevails and the ion concentration approaches the PB profile sufficiently far away from the surface.

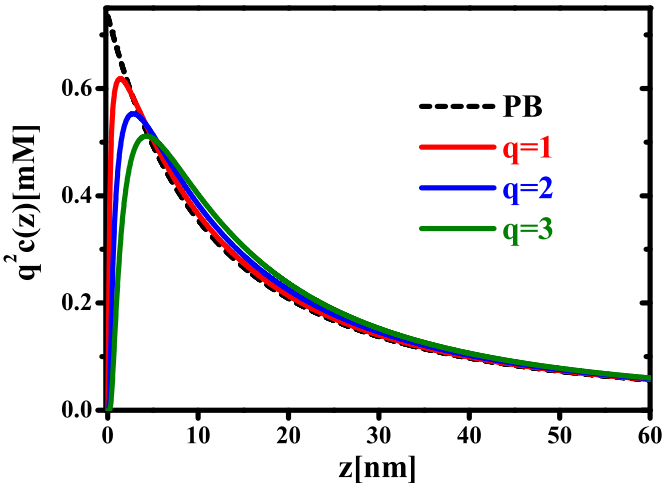

Figure 4.1: Ion concentration for the counterion-only system. $\varepsilon_S = 80$, $\varepsilon_P = 2.5$ and $\sigma = 1e/100nm^2$. The Gouy-Chapman length is kept constant for counterions of different valencies.

The PB theory predicts a universal profile $q^2c(z)$ for counterions of different valencies when the Gouy-Chapman length is kept the same. In this case, as can be easily seen from Eq. 4.1 and confirmed from Figure 1, the boundary layer thickness increases linearly with the valency. Thus, the boundary-layer problem becomes more severe for ions of high valency.

4.3.2 Added symmetric salt

When there are added salt ions in the solution, the image force affects the distribution of both the counterions and coions. The PB theory predicts that the double layer structure is characterized by the Debye screening length κ^{-1} under the condition that $\kappa^{-1} \ll l_{GC}$. In contrast, we find two regimes depending on the relative width of the screening length and the boundary layer thickness, which is itself affected by the screening. At low salt concentration, $\kappa^{-1} \gg d$ and ion depletion is confined in a boundary layer very close to the plate surface; both the ion distribution and electrostatic potential approach the profile predicted by PB beyond the boundary layer. As the salt concentration increases, the width of the depletion boundary-layer becomes comparable to the screening length and the two length scales remain comparable thereafter; the image charge interaction then affect the entire range of the double layer. In Figure 4.2 we show the ion distribution of a $0.1M$ 1:1 electrolyte calculated by our theory. The contrast with the PB result is quite striking.

The change in the double layer structure will affect a wealth of interfacial properties. As an

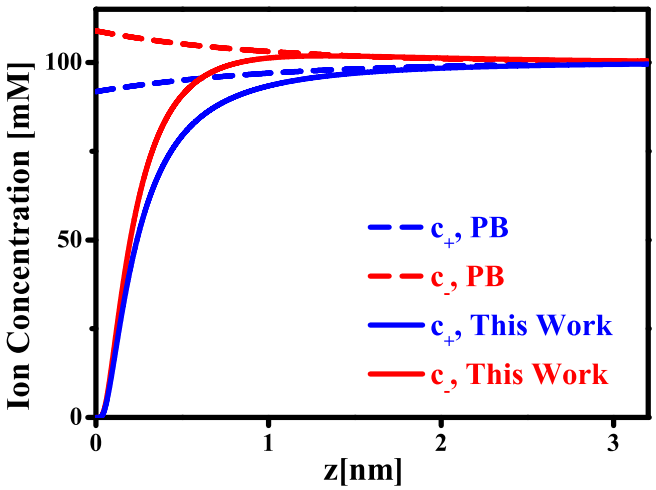

Figure 4.2: Ion concentration profile for 1:1 electrolyte solution with $c^b = 0.1M$ for a system with added salt. $\varepsilon_S = 80$, $\varepsilon_P = 2.5$ and $\sigma = 1e/100nm^2$.

example, we show in Figure 4.3 the surface excess free energy $f_s = \int_0^\infty (w - w^b)dz$ (where w is the grand free energy density and w^b is its bulk value) as a function of the salt concentration. The PB theory predicts a monotonic decrease of f_s that scales approximately with $(c^b)^{-1/2}$, which arises from the electric field contribution in the free energy due to the surface charge[25, 26]. With the inclusion of image charge interaction, our theory shows that f_s changes nonmonotonically. At low salt concentration ($c^b < 10^{-3}M$), f_s calculated by our theory follows closely the PB result; this is because the region affected by the image charge repulsion is relatively narrow compared to the screening length, giving a relatively small contribution to the surface excess energy when integrated over the entire solution. As the salt concentration increases ($c^b > 10^{-2}M$), our theory predicts a sign change in the slope of f_s vs. c^b: f_s increases with increasing c^b, *opposite to* the PB result. In this concentration regime, the width of the depletion boundary layer is comparable to the Debye screening length, and the entire double layer region is affected by the image charge interaction as shown in Figure 4.2. The increase in f_s is now largely due to the depletion (i.e., negative adsorption) of mobile ions. The slope of $\log(f_s)$ vs $\log(c^b)$ is less than 1 because of the increased screening of the image force as the salt concentration increases. The sign change of $\partial f_s/\partial c^b$ corresponds to the crossover in the length scale relationship from $\kappa^{-1} \gg d$ to $\kappa^{-1} \approx d$. As the excess surface energy determines the spreading of a liquid drop on the solid plate, this result implies a qualitatively different behavior for the spreading of a drop of electrolyte solution than that predicted by the PB theory. We also note that the nonmonotonic behavior discussed here shares the same physics as the Jones-Ray effect[25, 27, 26] for the interfacial tension observed at the water/air and water/oil interfaces.

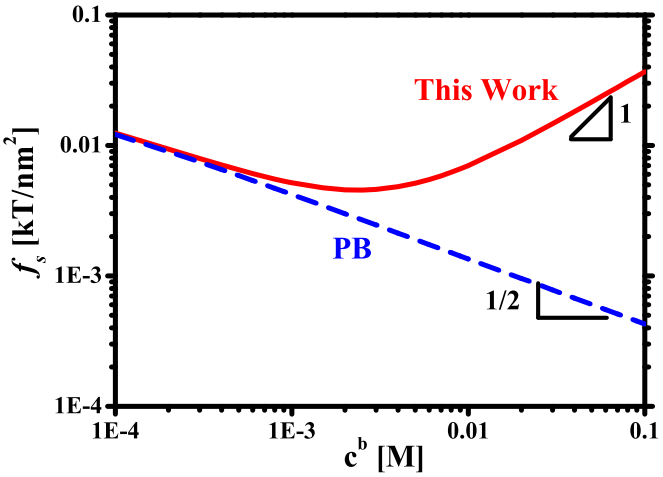

Figure 4.3: The surface energy f_s for a system with added 1:1 salt. $\varepsilon_S = 80$, $\varepsilon_P = 2.5$ and $\sigma = 1e/100nm^2$.

4.3.3 Added asymmetric salt

The effects of image charge become more complex if the salt ions are of unequal valency. Because of the quadratic dependence of the image force on the valency, the higher-valent ions are pushed further away from the surface, necessitating a compensation by the lower-valent ions in the space in between. The difference in the image force between the counterions and the coions induces additional charge separation and hence electric field within the depletion boundary layer. The induced net charge within the boundary layer alters the effective surface charge, which can affect the double layer structure outside the boundary layer. For the case where the coions are of higher valency than the counterions, the induced electric field due to unequal ion depletion counteracts the field generated by the surface charge. With the increase of the salt concentration, the induced field can exceed that generated by the bare surface charge, leading to a sign change in the effective surface charge known as charge inversion. The double layer structure becomes qualitatively different from that predicted by the PB theory as shown in Figure 4.4: the electrostatic potential is of the opposite sign to the PB result. Excess counterions accumulate in the depletion boundary layer, overcharging the plate surface, while the coions are enriched outside the boundary layer, serving to screen the inverted surface charge. In this case, the PB theory qualitatively fails to describe the entire double layer structure.

4.4 Conclusion

We show that the image charge repulsion creates a depletion boundary layer near a dielectric surface, which cannot be captured by a regular perturbation method. Using a nonperturbative approach

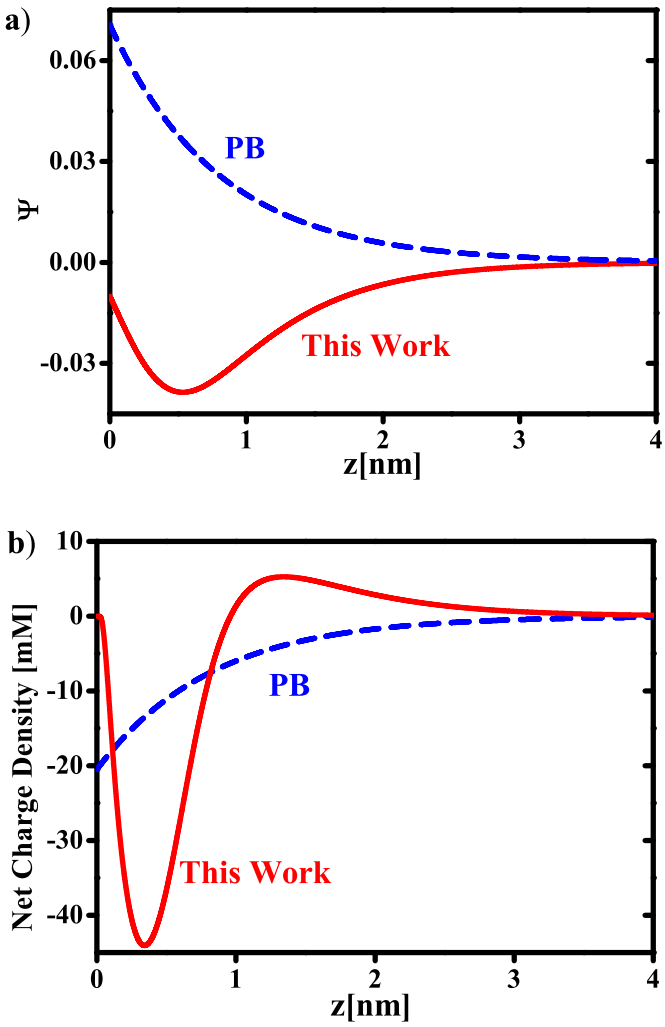

Figure 4.4: Charge inversion for a 0.05M 2:1 electrolyte solution near a positively charged plate. (a) Dimensionless electrostatic potential and (b) net charge density ($q_+c_+ - q_-c_-$). $\varepsilon_S = 80$, $\varepsilon_P = 2.5$ and $\sigma = 1e/100nm^2$.

based on Gaussian variational functional formulation, we find that the self energy of the ion, which includes contributions from both the image charge interaction and the interionic correlation, appears explicitly in the Boltzmann factor for the ion distribution, resulting in a self-energy modified Poisson-Boltzmann equation as the appropriate theory for describing the *physical* weak-coupling condition. This image-charge self energy is not diminished by reducing the surface or the ionic strength in the solution; in the presence of a significant dielectric discontinuity, there is no limiting condition for which the PB theory is valid. For zero surface charge, our theory reduces to the WOS theory upon further approximations, e.g., by using the constant bulk screening length for the image force potential. Thus, our theory provides both the justification for the WOS theory and means for systematically improving the WOS theory, for example, by including the mean electrostatic potential

generated by the charge separation in salt solutions with unequal valency or other asymmetries between the cation and anions, such as different size and polarizability[28].

The weak-coupling condition in the presence of dielectric discontinuity covers many soft-matter and biophysical systems. Many phenomena, such as the surface tension of electrolyte solutions[29], salt effects on bubble coalescence[30], and the ion conductivity in artificial and biological ion-channels[31], cannot be explained, even qualitatively, by the PB theory. The presence of the image charge interaction results in a very different picture of the electrical double layer from that provided by the PB theory, and can give rise to such phenomena as like-charge attraction and charge inversion even in the weak-coupling condition[32]; these phenomena have usually been associated with the strong-coupling condition. The PB theory has played a foundational role in colloidal and interfacial sciences: the DLVO theory, interpretation of the zeta potential, experimental determination of the surface charge and the Hamaker constant, are all based on the PB theory[1]. With the inclusion of the image charge interaction, some of the well known and accepted results will have to be reexamined.

Bibliography

[1] J. N. Israelachvili, *Intermolecular and surface forces*, 2nd Ed. (Academic, London, 1992).

[2] W. M. Gelbart, R. F. Bruinsma, P. A. Pincus and V. A. Parsegian, *Phys. Today*, **53**, 38-44 (2000).

[3] Y. Levin, *Rep. Prog. Phys.*, **65**, 1577-1632, (2002).

[4] B. Honig and A. Nicholls, *Science*, **268**, 1144-1149 (1995).

[5] G. M. Luo, S. Malkova, J. Yoon, D. G. Schultz, B. H. Lin, M. Meron, I. Benjamin, P. Vanysek and M. L. Schlossman, *Science*, **311**, 216-218 (2006).

[6] R. Kjellander, S. Marelja, R. M. Pashley and J. P. A. Quirk, *J. Chem. Phys.*, **92**, 4399-4407 (1990).

[7] W. R. Bowen and A. Q. Sharif, *Nature*, **393**, 663-665 (1998).

[8] Y. S. Jho, M. Kanduč, A. Naji, R. Podgornik, M. W. Kim and P. A. Pincus, *Phys. Rev. Lett.*, **101**, 188101 (2008).

[9] P. Kekicheff, S. Marcelja, T. J. Senden and V. E. Shubin, *J. Chem. Phys.*, **99**, 6098-6113 (1993).

[10] T. T. Nguyen, A. Y. Grosberg and B. I. Shklovskii, *Phys. Rev. Lett.*, **85**, 1568-1571 (2000); A. Y. Grosberg, T. T. Nguyen and B. I. Shklovskii, *Rev. Mod. Phys.*, **74**, 329-345 (2002).

[11] K. Besteman, M. A. G. Zevenbergen, H. A. Heering and S. G. Lemay, *Phys. Rev. Lett.*, **93**, 170802 (2004).

[12] R. Kjellander, T. Akesson, B. Jonsson and S. Marelja, *J. Chem. Phys.*, **97**, 1424-1431 (1992).

[13] J. W. Zwanikkena and M. Olvera de la Cruz, *Proc. Natl. Acad. Sci. USA*, **110**, 5301-5308 (2013).

[14] A. Naji, S. Jungblutb, A. G. Moreirac and R. R. Netz, *Physica A*, **352**, 131-170 (2005).

[15] P. Attard, D. J. Mitchell and B. W. Ninham, *J. Chem. Phys.*, **88**, 4987-4996 (1988); P. Attard, D. J. Mitchell and B. W. Ninham, *J. Chem. Phys.*, **89**, 4358-4367 (1988).

[16] J. C. Neu, *Phys. Rev. Lett.*, **82**, 1072-1074 (1999).

[17] R. R. Netz, *Eur. Phys. J. E*, **5**, 557-574 (2001).

[18] M. Kanduč and R. Podgornik, *Eur. Phys. J. E*, **23**, 265-274 (2007).

[19] A. Naji, M. Kanduč, J. Forsman and R. Podgornik, *J. Chem. Phys.*, **139**, 150901 (2013).

[20] C. Wagner, Phys. Z. **25**, 474 (1924).

[21] L. Onsager and N. N. T. Samaras, *J. Chem. Phys.*, **2**, 528 (1933).

[22] R.R. Netz and H. Orland, *Eur. Phys. J. E*,**11**, 301C311, (2003).

[23] Z. -G. Wang, *Phys. Rev. E*, **81**, 021501 (2010).

[24] F. P. Buff and F. H. Stillinger, *J. Chem. Phys.*, **39**, 1911-1923 (1963); G. M. Bell and S. Levine, *J. Chem. Phys.*, **49**, 4584-4599 (1968); S. L. Carnie and G. M. Torrie, *Adv. Chem. Phys.*, **56**, 141-253 (1984).

[25] A. Onuki, *J. Chem. Phys.* **128**, art. no. 224704 (2008);

[26] R. Wang and Z.-G. Wang, *J. Chem. Phys.* **135**, 014707 (2011).

[27] G. Jones and W. A. Ray, *J. Am. Chem. Soc.* **59**, 187 (1937); M. Bier, J. Zwanikken and R.van Roij, *Phys. Rev. Lett.* **101**, 046104 (2008);.

[28] Y. Levin, A. P. dos Santos and A. Diehl, *Phys. Rev. Lett.* **103**, 257802 (2009).

[29] W. Kunz, P. Lo Nostro, and B.W. Ninham, *Curr. Opin. Colloid Interf. Sci.* **9**, 1 (2004); B. C. Garrett, *Science* **303**, 1146 (2004).

[30] V. S. J. Craig, B. W. Ninham and R. M. Pashley, *Nature* **364**, 317 (1993).

[31] A. Parsegian, *Nature*, **221**, 844-846 (1969); T. Bastug and S. Kuyucak, *Biophys. J.*, **84**, 2871-2882 (2003); S. Buyukdagli, M. Manghi and J. Palmeri, *Phys. Rev, Lett.*, **105**, 158103, (2010).

[32] R. Wang and Z. -G. Wang, *J. Chem. Phys.*, **139**, 124702, (2013).

Chapter 5

The image effects on the double layer structure and interfacial properties II. electrolyte solution between two charged plates

The study of the electrical double layer lies at the heart of soft matter physics and biophysics. In this chapter, we address the effects of the image charges on the double layer structure and forces. For electrolyte solutions between two neutral plates, we show that depletion of the salt ions by the image charge repulsion results in short-range attractive and long-range repulsive forces. If cations and anions are of different valency, the asymmetric depletion leads to the formation of an induced electrical double layer. In comparison to a 1:1 electrolyte solution, both the attractive and the repulsive parts of the interaction are stronger for the 2:1 electrolyte solution. For two charged plates, the competition between the surface charge and the image charge effect can give rise to like-charge attraction and charge inversion. These results are in stark contrast with predictions from the Poisson-Boltzmann theory. This chapter is adapted from our paper, R. Wang and Z.-G. Wang, *J. Chem. Phys.* **139**, 124702 (2013).

5.1 Introduction

The study of the electrical double layer resulting from a charged surface is at the heart of colloid and interface sciences[1, 2, 3, 4, 5, 6, 7, 8]. Standard textbook theories of the electrical double layer are based on the Poisson-Boltzmann (PB) theory, a mean-field theory that describes a system in terms of the mean electrostatic potential and the average concentration of the mobile ions. At large surface-charge density, high counter-ion valency and high ion concentration – the so-called strong coupling limit – the PB theory fails to capture a number of qualitative effects observed in experiments and simulation, such as like-charge attraction[9, 10, 11, 12, 13] and charge inversion[14, 15, 16, 17, 18]. In this regime, integral-equation methods[19, 20] and other strong-coupling theories[24] have been employed to account for the strong interionic correlations. Under weak-coupling conditions, it is generally accepted that the electrical double layer is well described by the PB theory[21, 22, 23, 24, 25, 26]. However, a number of phenomena involving double layers under the weak-coupling conditions, such as the long-range electrostatic attraction between two neutral plates[27], the slow ion transport in the ion channels[28, 29], and salt effects on bubble coalescence in water[30, 31], cannot be explained, even qualitatively, by the PB theory.

An obvious effect missing in the PB theory is the self energy of the mobile ions[32]. The self energy consists of a local contribution due to the interaction between the ion and the local dielectric medium and a long-range contribution arising from the fluctuation in the electrostatic potential around the test ion. For systems with dielectric discontinuity, which is commonplace because of the much lower dielectric constant of air, lipid membranes and colloidal particles ($\varepsilon \sim 1$) than that of the aqueous solution ($\varepsilon \sim 80$), the distortion of the electrostatic potential at the interface known as the image charge effect is an important component of the self energy. The image charge effect plays a key role in the surface tension of electrolyte solutions[33, 34, 35, 36, 37] and the adsorption of polyelectrolytes[38].

Here, we examine the electrical double layer structure and forces between two neutral or like-charged plates by accounting for the image charge effects under weak-coupling conditions. For neutral surfaces, we show that the image charge effect results in depletion of the ions near the surface, which gives rise to short-range attraction and long-range repulsion between the plates. If cations and anions are of different valency, the unequal depletion induces charge separation and generates an electrostatic potential. For two like-charged plates, we predict like-charge attraction and charge inversion as a result of the competition between the surface charge and the image charge effect. All these results are in stark contrast with predictions from the usual PB theory.

We considered two parallel plates of infinite thickness of dielectric constant ε_P, immersed in an electrolyte solution, of dielectric constant ε_S, separated by a distance D. We set $x = 0$ at the mid-plane between the two plates, so the two plate surfaces are located at $x = \pm D/2$. Following

the standard model for electrical double layer, the surfaces of the two plates are taken to have a smeared-out charge density σ ($\sigma = 0$ for a neutral surface). Mobile cations and anions are taken as point particles with charge z_+e and z_-e, respectively. The electrolyte solution between the two plates (referred to as the "inner solution" hereafter) is connected with an "outer" bulk reservoir of concentration $c_\pm^b$. Each mobile ion in the solution generates an infinite series of image charges because of the dielectric discontinuity as illustrated in Figure 5.1.

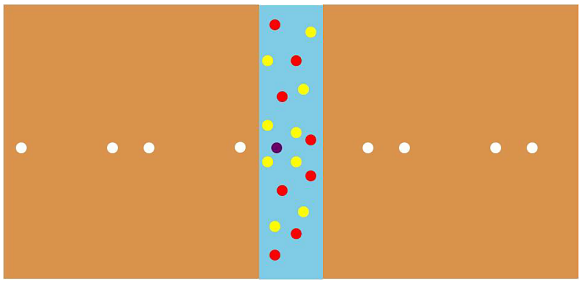

Figure 5.1: Schematic of mobile ions between two charged plates. The purple sphere represents a test ion; white spheres represent its image charges.

5.2 Theory

We treat the electrostatics of our system in the framework of the weak-coupling theory[32, 39, 40, 41], which accounts for the leading fluctuation effects in an electrolyte solution. This theory treats the *physical* weak-coupling condition (low surface charge density, low valency of ions and low ion concentrations), which can be derived either through a cluster expansion[39] or a variational approach[32]. We comment that the term "weak-coupling theory" used in this work is different from the meaning associated by some researchers in the electrolyte community with that in the work of Netz[23]. Netz considered the counterion-only system by treating the fluctuation effects through a systematic perturbation expansion using the coupling parameter $\Xi \equiv 2\pi z^3 l_B^2 \sigma_s$, where z is the counterion valency, l_B is the Bjerrum length and σ_s is the surface charge density. Netz showed that the mean-field PB theory is the leading order theory for small Ξ and becomes exact in the limit of $\Xi \to 0$. Applying the Netz approach explicitly to a surface with dielectric continuity, Kanduč and Podgornik [26] arrived at a similar result, concluding that the image force only enters as a correction to the leading PB theory. In the weak-coupling theory we employ here, the fluctuation effect on the ion distribution and free energy is treated self-consistently and nonperturbatively, leading to the appearance of the image force effect in the Boltzmann factor. In our theory, we find no limiting condition for which PB theory is valid for the system we consider.

The weak-coupling theory used in this work involves two approximations: first, the hierarchy of multi-ion correlation functions is closured at the two-body level, known as the Loeb closure[42], and

second, the fluctuation part of the electrostatic potential treated at the Debye-Hückel level[43] – the interaction between a test charge with its own fluctuation part of the electrostatic potential gives rise to a self-energy that includes the image charge interaction. The weak-coupling theory has also been formulated more systematically using field-theoretical method by a renormalized Gaussian-fluctuation variational approach[32, 44], which yields a set of self-consistent equations for the mean electrostatic potential $\psi(\mathbf{r})$, the correlation function (Green function) $G(\mathbf{r},\mathbf{r}')$ and the self energy $u_{\pm}(\mathbf{r})$ of mobile ions. These self-consistent equations are derived in Ref.[32] for a general system of ions with charge distribution function $h_{\pm}(\mathbf{r}-\mathbf{r}')$ in a spatially varying dielectric medium, which, for the present two-plate system, takes the following form:

$$\begin{aligned} &-\nabla\cdot[\varepsilon_0\varepsilon(\mathbf{r})\nabla\psi(\mathbf{r}] = \rho_{ex}(\mathbf{r}) \\ &+\Gamma(\mathbf{r})\left(e\lambda_+ z_+ \mathrm{e}^{-\beta z_+ e\psi-\beta u_+} - e\lambda_- z_- \mathrm{e}^{\beta z_- e\psi-\beta u_-}\right) \end{aligned} \tag{5.1}$$

$$-\nabla\cdot[\varepsilon_0\varepsilon(\mathbf{r})\nabla G(\mathbf{r},\mathbf{r}')] + 2\Gamma(\mathbf{r})I(\mathbf{r})G(\mathbf{r},\mathbf{r}') = \delta(\mathbf{r}-\mathbf{r}') \tag{5.2}$$

$$u_{\pm}(\mathbf{r}) = \frac{z_{\pm}^2 e^2}{2}\int d\mathbf{r}'d\mathbf{r}'' h_{\pm}(\mathbf{r}-\mathbf{r}')G(\mathbf{r}',\mathbf{r}'')h_{\pm}(\mathbf{r}-\mathbf{r}'') \tag{5.3}$$

where the spatially varying $\varepsilon(\mathbf{r})$ is

$$\varepsilon(\mathbf{r}) = \begin{cases} \varepsilon_S & for \ \mid x \mid < \frac{D}{2} \\ \varepsilon_P & for \ \mid x \mid > \frac{D}{2} \end{cases}$$

$\rho_{ex}(\mathbf{r}) = \sigma\delta(x \pm D/2)$ denotes the surface charge density at the two plate surfaces, $\Gamma(\mathbf{r})$ is a step-like function to confine the mobile ions within the region between two plates:

$$\Gamma(\mathbf{r}) = \begin{cases} 1 & for \ \mid x \mid < \frac{D}{2} \\ 0 & for \ \mid x \mid \geq \frac{D}{2} \end{cases}$$

and $\lambda_{\pm}$ is the fugacity of cations and anions determined from the salt concentration in the outer bulk reservoir. $I(\mathbf{r})$ in Eq 5.2 is the local ionic strength,

$$I(\mathbf{r}) = \frac{\beta e^2}{2}\left[z_+^2 c_+(\mathbf{r}) + z_-^2 c_-(\mathbf{r})\right] \tag{5.4}$$

with the number concentration of cations and anions $c_{\pm}(\mathbf{r})$ given by

$$c_{\pm}(\mathbf{r}) = \lambda_{\pm}\mathrm{e}^{\mp\beta z_{\pm} e\psi(\mathbf{r})-\beta u_{\pm}(\mathbf{r})} \tag{5.5}$$

The appearance of the self energy in the Boltzmann factor reflects the nonlinear feedback effects of

the fluctuation in the renormalized Gaussian variational approach, an aspect that was missing in a perturbation expansion [21, 22, 23, 26]. A detailed and in-depth discussion of this point will be given in a future publication.

Inside the semi-infinite plate($\mid x \mid > \frac{D}{2}$), Eq 5.1 is simplified to the Laplace equation $\varepsilon_0\varepsilon_P\nabla^2\psi(\mathbf{r}) = 0$, which yields a constant ψ in this region due to the requirement that ψ remain finite as $x \to \pm\infty$. Integrating Eq 5.1 across an infinitesimally thin region enclosing the dielectric interface generates the boundary condition as $\mathbf{n} \cdot \nabla\psi = -\sigma/\varepsilon_0\varepsilon_S$ where $\mathbf{n}$ is the unit outward normal of the plate surface.

The self energy given by Eq 5.3 is the reversible work required to assemble the given charge distribution on an ion at the spatial location $\mathbf{r}$ by bringing in the constituent charges from an infinitely dispersed state, where the interaction is zero. This is a unified expression that includes the Born energy of the ion, the interaction between the ion and its ionic atmosphere, as well as self-interaction due to the distortion of the electric field by a spatially varying dielectric function, the latter taking the form of image charge interaction near a sharp dielectric discontinuity. For a spatially inhomogeneous medium, a finite charge distribution in the ion results in a finite value for the short-range part of the self energy in the form of a local Born solvation energy[32]. Since the solvent in the gap has a uniform dielectric constant, the Born energy amounts to a constant shift in the reference chemical potential. It is then more convenient to take the point-charge limit $h_\pm(\mathbf{r} - \mathbf{r}') = \delta(\mathbf{r} - \mathbf{r}')$. Then Eq 5.3 is simplified to

$$u_\pm(\mathbf{r}) = \frac{z_\pm^2 e^2}{2} G(\mathbf{r}, \mathbf{r})$$

The point-charge limit produces a diverging self energy of the ion, which can be regularized by subtracting the same-point Green function in the bulk, as done in Ref.[44]. The finite part of the self energy that only includes the image charge and interaction with other ions is now:

$$u_\pm(\mathbf{r}) = \frac{z_\pm^2 e^2}{2} \lim_{\mathbf{r}' \to \mathbf{r}} \left[G(\mathbf{r}, \mathbf{r}') - \frac{1}{4\pi\varepsilon_0\varepsilon_S|\mathbf{r} - \mathbf{r}'|} \right] \tag{5.6}$$

Equations 1-3 constitute a complete set of equations for describing the electrostatics of our system, the general solution of which requires extensive numerical calculation. To avoid solving the high-dimensional Green function, Stillinger and Buff[40] proposed an approximate solution to Eq. 5.2 based on the WKB (Wentzel-Kramers-Brillouin) approximation: the Green function is first solved for a constant ionic strength, but in the resulting expression the ionic strength is replaced by its local value that depends on the local ion concentrations. With the approximate $G(\mathbf{r}, \mathbf{r}')$, the self energy can be written as a function of the one-dimensional coordinate x along the normal of the

plate surface in the following form

$$u_{\pm}(x) = \frac{e^2 z_{\pm}^2}{8\pi\varepsilon_0\varepsilon_S}\left[-\kappa(x) + J\left(x, \kappa(x)\right)\right]$$

where

$$J\left(x, \kappa(x)\right) = \sum_{m=2,4,6\ldots} \frac{2f^m \mathrm{e}^{-\kappa(x)(mD)}}{mD} + \sum_{m=1,3,5\ldots} f^m \left[\frac{\mathrm{e}^{-\kappa(x)(mD+2x)}}{mD+2x} + \frac{\mathrm{e}^{-\kappa(x)(mD-2x)}}{mD-2x}\right] \tag{5.7}$$

with $f = (\varepsilon_S - \varepsilon_P)/(\varepsilon_S + \varepsilon_P)$ representing the dielectric discontinuity. $\kappa(\mathbf{r}) = [2I(\mathbf{r})/\varepsilon_0\varepsilon_S]^{1/2}$ is the inverse of the local screening length. The first term in the self energy accounts for the local ionic atmosphere surrounding the test ion at the level of the Debye-Hückel theory[43]. The second term represents the accumulated effects of interaction from all the image charges generated by a test ion. In our case $f > 0$, so all image-charge interactions are repulsive.

In the outer bulk reservoir, ψ is set to zero. From Eq 5.5, the fugacity of the ions is related to the bulk salt concentration via: $\lambda_{\pm} = c_{\pm}^b \mathrm{e}^{-\beta z_{\pm}^2 e^2 \kappa_b/8\pi\varepsilon_0\varepsilon_S}$ where κ_b is the inverse screening length in the bulk. By solving equations 5.1, 5.5 and 5.7 iteratively, we obtain the mean electrostatic potential $\psi(x)$ and the ion distribution $c_{\pm}(x)$. Finally, the grand potential per area is constructed as:

$$\beta G = \int dx[\frac{\beta\varepsilon_0\varepsilon_S}{2}(\nabla\psi)^2 + c_+ \ln\frac{c_+}{\lambda_+} - c_+ + c_- \ln\frac{c_-}{\lambda_-} - c_- + F_{fl}] \tag{5.8}$$

where $F_{fl} = \kappa^2 \int_0^1 [\alpha J(\alpha\kappa) - \alpha\kappa] d\alpha/4\pi$ is the fluctuation contribution obtained by the charging method [41, 45]. The force per unit area between the two plates is given by $p = -(\partial G/\partial D)_{\lambda_\pm} - p_b$ where p_b is the bulk osmotic pressure.

5.3 Ion depletion and depletion force

We first study the behavior of equal-valency cations and anions ($z_+ = z_-$) between two neutral plates. Because the cation and anion have equal self energy in this case, the is no charge separation, and the mean electrostatic potential is everywhere zero. However, from Eq. 5.4, the image charge repulsion increases the self energy of ions in the inner solution, and consequently ions are depleted to the outer bulk solution (i.e. $c(x) < c^b$). The image charge effect is stronger near the interface and as the separation distance D decreases; see Figures 5.2(a)-5.2(c). The depletion is nearly complete close to the interface and when the gap is sufficiently small. In contrast, the PB theory predicts a

trivial uniform ion concentration of the bulk value.

The mid-plane value of the ion concentration $c(0)$ as a function of the separation is shown in Figures 5.2(d) and 5.2(e), which follows the analytical relation $c(0)/c^b = (1 - fe^{-\kappa(0)D})^{z_\pm^2 l_B/D}$, where l_B is the Bjerrum length of the liquid and is approximately 0.7nm for water. For small separations, nearly all the ions are depleted from the inner solution as shown by Figure 5.2(a) and the initial plateau of the curves in Figures 5.2(d) and 5.2(e)). A length scale D_1 for the onset of this regime can be obtained by the location of the fastest rise from the plateau (i.e., maximum of $\partial^2 c(0)/\partial D^2$) with the result $D_1 = -z_\pm^2 l_B \ln(1-f)/(3+\sqrt{3})$ ($\kappa_b D_1 \ll 1$). Note that D_1 increases with decreasing ε_S and is independent of the salt concentration. In the limit of large separation, the higher order image charge effect from the opposing surface becomes negligible compared to the first image charge of the ion; this defines a length scale D_2, which to leading order is given by the screening length $D_2 = \kappa_b^{-1}$. For $D > D_2$, the image charge effect is restricted to a depletion layer of thickness $D_2/2$ from the plate surface (see Figure 5.2(c)), and the mid-plane concentration approaches the bulk value. Intermediate separation is defined by $D_1 < D < D_2$, where the image charge interaction affects the entire region between the two plates but the mid-plane concentration is not too much lower than the bulk value; see Figures 2(b).

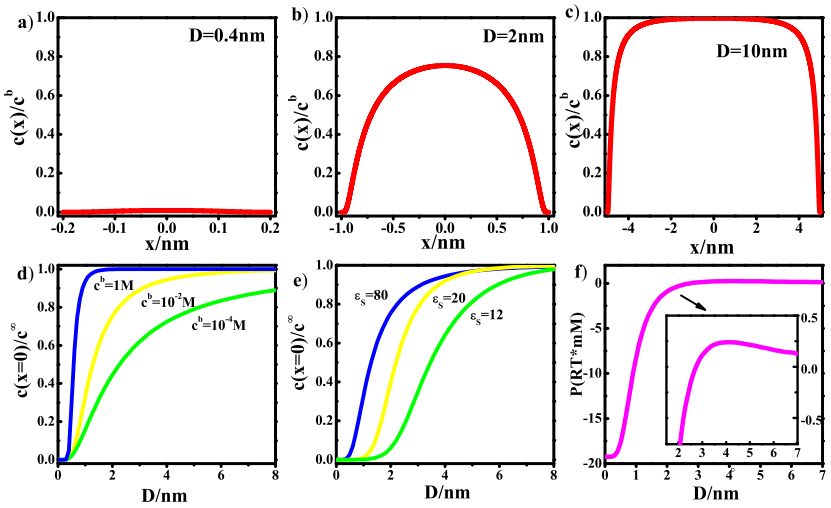

Figure 5.2: Ion depletion and depletion force between two neutral plates with $\varepsilon_P = 2.5$, $z_+ = z_- = 1$. (a)-(c): Effect of varying D on the ion concentration profile, $\varepsilon_S = 80$ and $c^b = 0.01M$. (d) and (e) Mid-plane value $c(0)/c^b$ as a function of D for several values of c^b and ε_S, respectively. (f) Pressure between two plates as a function of D (in units of the osmotic pressure of a 1 mM ideal solution). The inset shows the change from attraction to repulsion.

Ion depletion leads to an attractive well at short distances. The bottom of the well, of depth $2c^b$ extends to separation D_1, beyond which the attraction decays with the scale of the screening length;

see Figure 5.2(f). Interestingly, on this length scale and beyond, the interaction becomes repulsive as shown in the inset. This phenomenon can be understood from the ion profile at large separation: while the middle portion of the profile has reached the bulk plateau, the thickness of the depletion layer still shrinks slightly with increasing separation because of the decaying influence of higher order image charges. Thus increasing D by δD in plate separation brings more than $2c^b\delta D$ ions per plate area to the inner solution from the reservoir, which gives rise to the repulsive force between the two plates. We note that a similar behavior and explanation were given in the work of Tamashiro and Pincus[57] who pointed out that the transition of the depletion force from short-range attraction to long-range repulsion is a result of the disappearance of the overlapping of the depletion layer. However, their work used the PB theory; the depletion free energy used in their work was introduced artificially and extraneously without resorting to an explicit physical origin. The force profile shown in Figure 5.2(f) has also previously been reported by Bell and Levine[41]. Our work provides the first study of the ion profiles and analysis of the length scales for the image-charge induced depletion.

5.4 Asymmetric depletion and induced electrical double layer

The image charge contribution to the self energy is quadratic in the valency of the ions. Thus, for an asymmetric salt with unequal valency, the distribution of the cations and anions will be different, leading to charge separation near the wall. Figure 5.3(a) show charge separation for a 2:1 electrolyte solution. The divalent cations are pushed further away from the wall than the monovalent anions, resulting in the formation of an effective double layer with a finite induced surface potential, even though there is no fixed surface charge. The induced electrostatic potential in the electric double layer (Figure 5.3(b)), with the sign determined by $z_-^2 - z_+^2$, can be understood as a response of the system to the difference in the self energy between the cations and anions so as to maintain overall charge neutrality. The situation is similar to the Galvani potential across the interface between two coexisting salt solutions and the local charge separation at the interface [32, 48, 49], which are induced by the solvation energy difference between the cations and the anions. As shown in Figure 5.3(c), the potential is stronger at smaller separation D and approaches an asymptotic value of the single surface for large D. The induced electrostatic potential depends primarily on the dielectric constants of the media and valency of the ions; it depends weakly on the bulk concentration c^b as a result of screening. In comparison to a 1:1 electrolyte solution, both the attractive and the repulsive parts of the interaction are stronger for the 2:1 electrolyte solution with the same total number of ions.

Ref. [57] considered unequal depletion of the cations and anions by artificially choosing two different depletion potentials respectively for the cations and anions near the surface. Although their system is for 1:1 salts, and these depletion potentials were not given an explicit physical origin,

inasmuch as unequal depletion of cations an anions leads to charge separation and generates an induced surface potential, and the interaction force is attractive at short range but repulsive at long range, their results are similar to ours reported in this section.

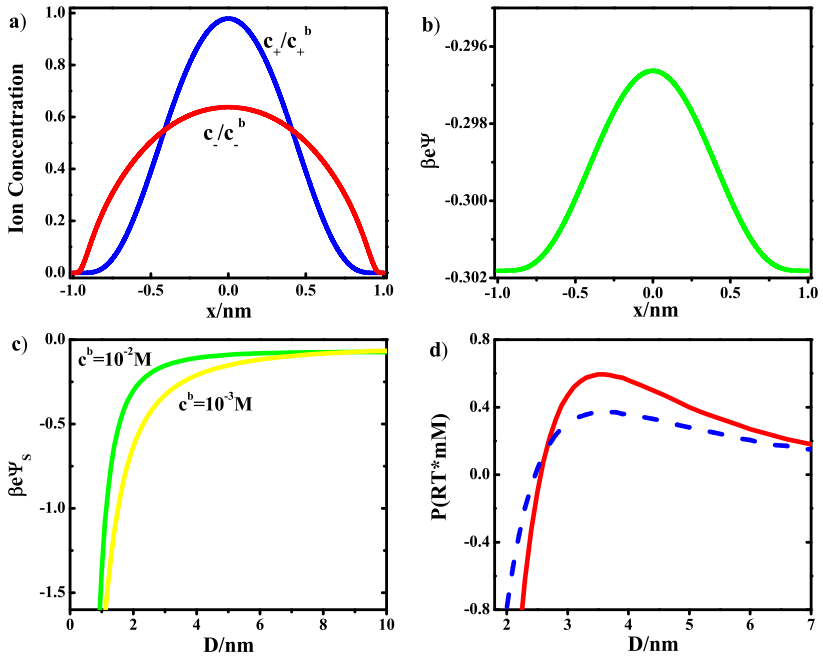

Figure 5.3: The induced electrical double layer of 2:1 electrolyte solution between two neutral plates. (a) and (b): Ion concentration profile and dimensionless electrostatic potential profile for $D = 2nm$. $\varepsilon_S = 80$, $\varepsilon_P = 2.5$, c^b=0.01M. (c): Induced electrostatic potential at the plate surface ψ_S as a function of D. (d) Pressure as a function of D (in units of the osmotic pressure of a 1 mM ideal solution) for a $0.01M$ 2:1 electrolyte solution (solid line) in comparison with a $0.015M$ 1:1 electrolyte solution (dash line). The comparison is made under condition of equal amount of ions in bulk.

Complex ion depletion behavior arises when the salt solution is a mixture of 1:1 electrolyte and 2:1 electrolyte. Cations of different valency are strongly correlated and their distributions markedly differ from the profiles when each electrolyte is present alone; see Figure 5.4. Compared to the profiles of when each electrolyte is present alone, the concentration of monovalent cations in the gap increases while the concentration of divalent cations is considerably reduced; a large portion of divalent cations are replaced by the monovalent cations which have lower self energy.

5.5 Like-charge attraction and charge inversion

We now consider plates whose surfaces are weakly charged. For concreteness, we take the surface charges to be positive. Here, the counterions are attracted to the surface due to Coulomb forces;

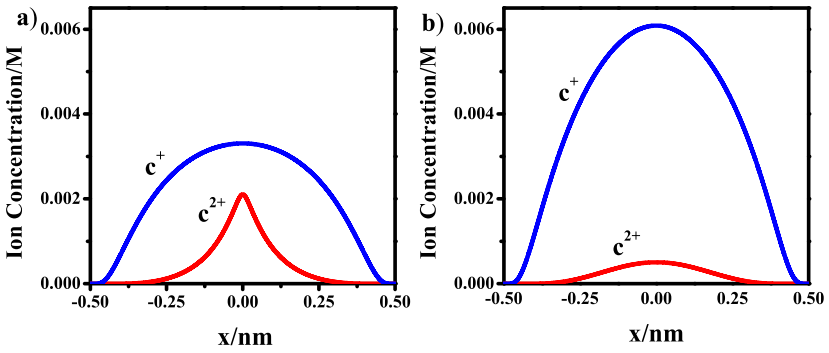

Figure 5.4: Concentration profiles for monovalent (blue) and divalent (red) cations. (a): Cation profiles for 0.01M 1:1 electrolyte alone and 0.01M 2:1 electrolyte alone in the reservoir. (b): Cation profiles when both 1:1 electrolyte and 2:1 electrolyte are present with the same respective concentration in the reservoir as in (a).

however, image force repulsion is always operative and tends to exclude the counterions from the surface. The co-ions are more strongly repelled by the surface since both the surface charge and the image charge act in the same direction. The interplay between these factors leads to rich and complex behavior in the double layer structure and the interaction forces between two like-charged plates. The role of surface charge becomes more important as the surface charge density increases, while the image charge effect gets stronger with the increase of salt concentration and counterion valency.

Figures 5.5(a) and 5.5(b) show the double layer structure for a 1:1 electrolyte solution between two weakly charged surfaces at two separation distances. For small separation distances ($D = 1nm$), the ion concentration profiles calculated by our theory drastically differ from the PB mean-field results, and are dominated by the image charge effect. Excess counterions are not accumulated at the plate surface but are instead pushed to the middle of the gap. For large D, the dominance of the image charge effect is confined to a depletion layer near the plate surface (see Figure 5.5(b)). Due to the image repulsion, counterions cannot accumulate within the depletion layer, which significantly reduces the screening of the surface charge on this length scale. Beyond the depletion layer, the ion concentration profiles approach the PB mean-field results.

The PB mean-field theory predicts purely repulsive force between two like-charged plates for all separation distances[1, 2, 25]. However, by incorporating the image charge effect, the force profile (see Figures 5.5(c) and 5.5(d)) develops an attractive well at small plate separations under conditions of small surface charge density or high salt concentration, as a consequence of the depletion of the mobile ions. Attraction between like-charged surfaces observed in experiments and simulations[9, 10, 11, 12, 13] have previously been explained by the correlation effects in the strong coupling

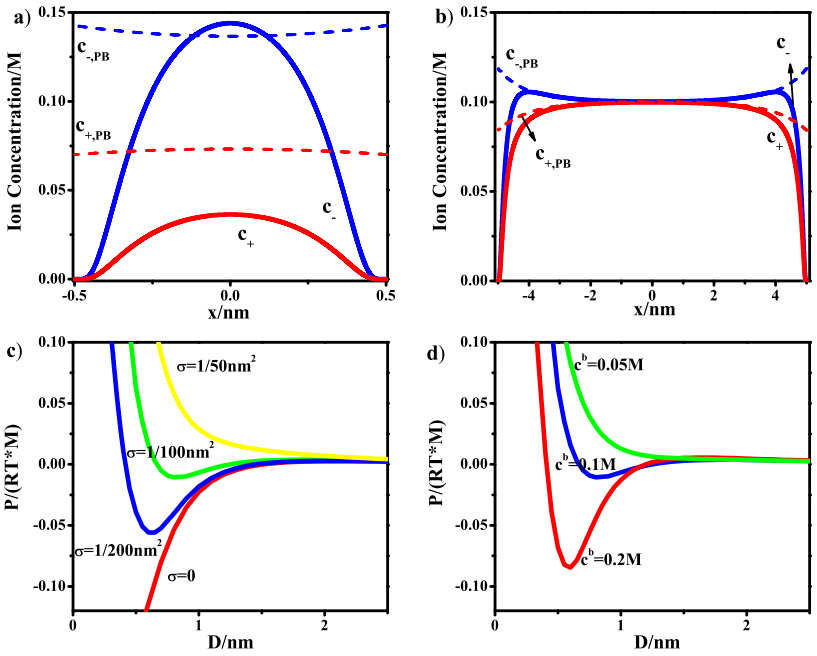

Figure 5.5: Electrical double layer structure and force for 1:1 electrolyte solution between two charged plates.(a) and (b): Ion concentration profiles for $D = 1nm$ and $D = 10nm$, respectively. $\sigma = 1e/50nm^2$, $c^b = 0.1M$. Pressure as a function of D (in units of the osmotic pressure of a 1 M ideal solution) for (c) Effects of surface charge density σ at $c^b = 0.1M$, and (d) Effects of c^b at $\sigma = 1e/100nm^2$.

regime due to the formation of 2D crystal-like layer of multivalent counterions in the vicinity of highly charged surfaces[24]. However, here we show that attraction can also appear under the weak-coupling condition with monovalent ions.

The competition between the surface charge and the image charge effect can give rise to another counter-intuitive phenomenon known as charge inversion. In the diffuse electrical double layer predicted by the PB mean-field theory, the local charge in the inner solution is always of the opposite sign to the surface charge regardless of the ion valency. However, if the co-ions have higher valency than the counterions, the stronger image charge repulsion for the co-ions pushes them farther away from the surface, necessitating a greater amount of counterions to fill the space in between. With the increase of salt concentration, the accumulated counterions near the plate surface may exceed the amount that is required to neutralize the surface charge, giving rise to a sign change in the local electrostatic potential. We define $\tau(x) = \sigma + \int_{-D/2}^{x} \rho(x')dx'$ as the local accumulative charge density (integrated from the surface) ($\tau(-D/2) = \sigma$ and $\tau(0) = 0$). The double layer structures for 2:1 electrolyte solutions of different salt concentrations are shown in Figures 6(a) and 6(b). At low salt concentration ($c^b = 0.015M$), the electrostatic potential profile is positive and convex everywhere; $\tau(x)/\sigma$ decays monotonously from the plate surface to the mid-plane, indicating the normal neutralization of the surface charge. As the salt concentration increases to a critical value ($c^b_{cr} = 0.022M$ for the given surface charge and plate separation), ψ shows a plateau in the middle region as $\tau(x)$ approaches zero. For salt concentrations exceeding this critical value, charge inversion occurs: ψ is convex near the plate surface but becomes concave in the middle region. Excess counterions overcharge the plate surface as reflected by the negative $\tau(x)$. The co-ions accumulate outside this diffuse layer of inverted surface charge and serve to screen it. The critical salt concentration c^b_{cr} for charge inversion increases with the increase of σ as shown in Figure 6(c). In addition, c^b_{cr} decreases as D increases, and approaches the asymptotic value of an isolated charged plate for large separation. The phenomenon elucidated here as a result of image charge effects offers an alternative explanation of charge inversion based on either counterion adsorption to the surface or the correlation effects[15, 18, 16, 17].

5.6 Conclusions

The image charge effects elucidated in this work affects a wealth of structural and dynamic behaviors in physical chemistry, colloidal science, soft-matter and biophysics. The increase of self energy caused by the image repulsion at small separations is closely related to the slow ion transport in ion channels where the lipid constituting the channel wall has a much lower dielectric constant than the aqueous solution[28, 29]. However, previous theories either ignore the screening effects by considering a single ion, or include the image force only on the test ion thus overestimating the screening effect[46, 47].

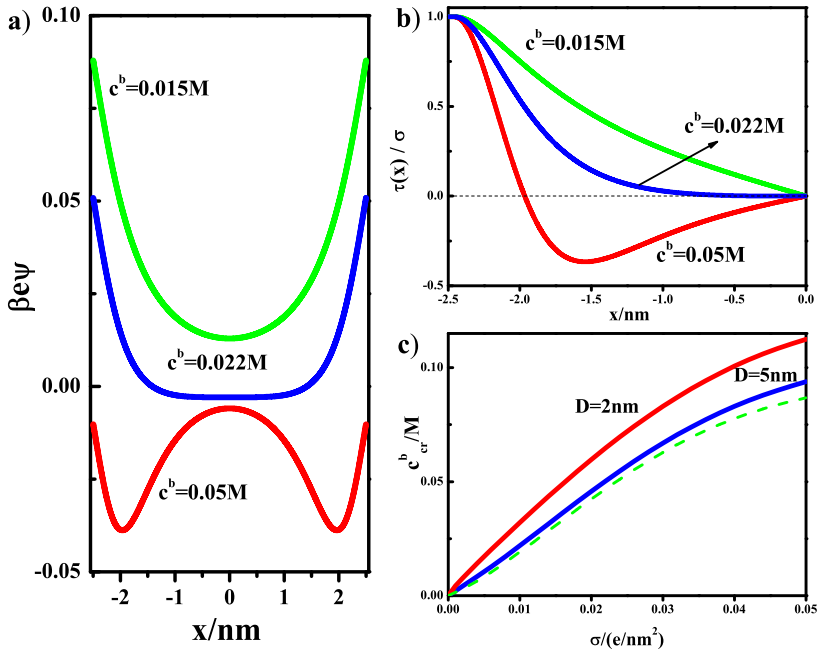

Figure 5.6: Charge inversion for 2:1 electrolyte solution between two charged plates of $\sigma = 1e/100nm^2$.(a) Dimensionless electrostatic potential profile and (b) local accumulative charge density at $D = 5nm$ for three different values of c^b. (c) Critical salt concentration for charge inversion c^b_{cr} versus σ. The dash line shows c^b_{cr} for an isolated charged plate.

The dramatic suppression of divalent ion concentration in the dielectric gap in the presence of monovalent ions demonstrated in our work suggests that (1) the study of the transport of the divalent ions must consider the presence of the monovalent ions; and (2) in channels that specifically transport divalent ions, such as the calcium channel[50, 51], there must be strong surface charge or specific ion-surface interaction to counter the image repulsion to make it favorable for the divalent ions to enter the channel. Furthermore, the image force is an important factor in any systematic theory for understanding the Jones-Ray [52, 53] and Hofmeister series[54, 35] effects for the surface tension of electrolyte solutions. In addition, the long-range repulsion between two neutral surfaces predicted by our theory provides a possible explanation to the long-standing puzzle: the effect of salts in suppressing bubble coalescence that leads to the foaminess of ocean waves[30]. Because the image force is proportional to $z_{\pm}^2$, our theory also predicts that the inhibition of bubble coalescence is more effective with the ions of high valency, in agreement with the experiment results[31].

The image charge effect on the double layer of a charged surface is twofold: depletion of the ions near the surface, giving rise to an attractive component in the interaction, and reduced screening of the surface charge, leading to increased electrostatic repulsion. Neither of these effects are captured by the PB theory. However, many important model parameters in colloidal and surface sciences such as the surface charge density and Hamaker constants are obtained by fitting the experiment data to the PB theory[1]. The surface force measurements of Kekicheff and Spalla[27] raised doubt about this procedure. In light of our results, we propose that these parameters be re-examined using our improved theory to incorporate the image charge effects. Our theory also indicates that the zeta potential predicted by the PB theory is qualitatively wrong under conditions of charge inversion. The charge-inversed double layer structure should lead to reversal in the direction of the electroosmotic flow and qualitatively change the electrophoretic mobility of charged particles[55, 56].

Bibliography

[1] J. N. Israelachvili, *Intermolecular and surface forces*, 2nd Ed. (Academic, London, 1992).

[2] D. Andelman, in *Soft Condensed Matter Physics in Molecular and Cell Biology*, W. C. K. Poon and D. Andelman, eds. (Taylor and Francis, Boca Raton, Florida, 2000).

[3] B. Honig and A. Nicholls, *Science*, **268**, 1144-1149 (1995).

[4] V. Dahirel and M. Jardat, *Curr. Opin. Colloid Interface Sci.*, **15**, 2-7 (2010).

[5] Y. Levin, *Rep. Prog. Phys.*, **65**, 1577-1632, (2002).

[6] P. Attard, *Curr. Opin. Colloid Interface Sci.*, **6**, 366-371 (2001).

[7] G. M. Luo, S. Malkova, J. Yoon, D. G. Schultz, B. H. Lin, M. Meron, I. Benjamin, P. Vanysek and M. L. Schlossman, *Science*, **311**, 216-218 (2006).

[8] E. M. Knipping, M. J. Lakin, K. L. Foster, P. Jungwirth, D. J. Tobias, R. B. Gerber, D. Dabdub and B. J. Finlayson-Pitts, *Science*, **288**, 301-306 (2000).

[9] W. R. Bowen and A. Q. Sharif, *Nature*, **393**, 663-665 (1998).

[10] W. M. Gelbart, R. F. Bruinsma, P. A. Pincus and V. A. Parsegian, *Phys. Today*, **53**, 38-44 (2000).

[11] P. Linse and V. Lobaskin, *Phys. Rev. Lett.*, **83**, 4208-4211 (1999).

[12] R. Kjellander, S. Marelja, R. M. Pashley and J. P. A. Quirk, *J. Chem. Phys.*, **92**, 4399-4407 (1990).

[13] Y. S. Jho, M. Kanduc, A. Naji, R. Podgornik, M. W. Kim and P. A. Pincus, *Phys. Rev. Lett.*, **101**, 188101 (2008).

[14] R. Messina, C. Holm and K. Kremer, *Phys. Rev. Lett.*, **85**, 872-875 (2000).

[15] K. Besteman, M. A. G. Zevenbergen, H. A. Heering and S. G. Lemay, *Phys. Rev. Lett.*, **93**, 17082 (2004).

[16] T. T. Nguyen, A. Y. Grosberg and B. I. Shklovskii, *Phys. Rev. Lett.*, **85**, 1568-1571 (2000).

[17] A. Y. Grosberg, T. T. Nguyen and B. I. Shklovskii, *Rev. Mod. Phys.*, **74**, 329-345 (2002).

[18] P. Kekicheff, S. Marcelja, T. J. Senden and V. E. Shubin, *J. Chem. Phys.*, **99**, 6098-6113 (1993).

[19] R. Kjellander, T. Akesson, B. Jonsson and S. Marelja, *J. Chem. Phys.*, **97**, 1424-1431 (1992).

[20] J. W. Zwanikkena and M. Olvera de la Cruz, *Proc. Natl. Acad. Sci. USA*, **110**, 5301-5308 (2013).

[21] P. Attard, D. J. Mitchell and B. W. Ninham, *J. Chem. Phys.*, **88**, 4987-4996 (1988).

[22] P. Attard, D. J. Mitchell and B. W. Ninham, *J. Chem. Phys.*, **89**, 4358-4367 (1988).

[23] R. R. Netz, *Eur. Phys. J. E*, **5**, 557-574 (2001).

[24] A. Naji, S. Jungblutb, A. G. Moreirac and R. R. Netz, *Physica A*, **352**, 131-170 (2005).

[25] J. C. Neu, *Phys. Rev. Lett.*, **82**, 1072-1074 (1999).

[26] M. Kanduč and R. Podgornik, *Eur. Phys. J. E*, **23**, 265-274 (2007).

[27] P. Kekicheff and O. Spalla, *Phys. Rev. Lett.*, **75**, 1851-1855 (1995).

[28] A. Parsegian, *Nature*, **221**, 844-846 (1969).

[29] T. Bastug and S. Kuyucak, *Biophys. J.*, **84**, 2871-2882 (2003).

[30] V. S. J. Craig, B. W. Ninham and R. M. Pashley, *Nature*, **364**, 317-319 (1993).

[31] V. S. J. Craig, B. W. Ninham and R. M. Pashley, *J. Phys. Chem.*, **97**, 10192-10197 (1993).

[32] Z. -G. Wang, *Phys. Rev. E*, **81**, 021501 (2010).

[33] B. C. Garret, *Science*, **303**, 1146-1147 (2004).

[34] L. Onsager and N. N. T. Samaras, *J. Chem. Phys.*, **2**, 528-536 (1934).

[35] Y. Levin, A. P. dos Santos and A. Diehl, *Phys. Rev. Lett.*, **102**, 257802 (2009).

[36] Y. Levin, *Phys. Rev. Lett.*, **102**, 147803 (2009).

[37] A. Onuki, *J. Chem. Phys.*, **128**, 224704 (2008).

[38] R. R. Netz and J. F. Joanny, *Macromolecules*, **32**, 9013-9025 (1999).

[39] S. L. Carnie and G. M. Torrie, *Adv. Chem. Phys.*, **56**, 141-253 (1984).

[40] F. P. Buff and F. H. Stillinger, *J. Chem. Phys.*, **39**, 1911-1923 (1963).

[41] G. M. Bell and S. Levine, *J. Chem. Phys.*, **49**, 4584-4599 (1968).

[42] A. L. Loeb, *J. Colloid Sci.*, **6**, 75-91 (1951).

[43] P. Debye and E. Hückel, *Phys. Z.*, **24**, 185-206 (1923).

[44] R.R. Netz and H. Orland, *Eur. Phys. J. E*, **11**, 301-311 (2003).

[45] R. A. Marcus, *J. Chem. Phys.*, **24**, 979-989 (1956).

[46] P. C. Jordan, R. G. Bacquet, J. A. McCammon and P. Tran, *Biophys. J.*, **55**, 1041-1052 (1989).

[47] G. Moy, B. Corry, S. Kuyucak and S. H. Chung, *Biophys. J.*, **78**, 2349-2363 (2000).

[48] R. Wang and Z. -G. Wang, *J. Chem. Phys.*, **135**, 014707 (2011).

[49] W. Kung, F. J. Solis and M. O. de la Cruz, *J. Chem. Phys.*, **130**, 044502 (2009).

[50] E. Gouaux and R. MacKinnon, *Science*, **310**, 1461-1465 (2005).

[51] D. Boda, M. Valisko, B. Eisenberg, W. Nonner, D. Henderson and D. Gillespie, *J. Chem. Phys.*, **125**, 034901 (2006).

[52] G. Jones and W. A. Ray, *J. Am. Chem. Soc.*, **59**, 187-198 (1937).

[53] P. B. Petersen and R. J. Saykally, *J. Am. Chem. Soc.*, **127**, 15446-15452 (2005).

[54] F. Hofmeister, *Arch. Exp. Pathol. Pharmakol.*, **24** (1888), 247-260.

[55] A. Martin-Molina, M. Quesada-Perez, F. Galisteo-Gonzalez and R. Hidalgo-Alvarez, *J. Chem. Phys.*, **118**, 4183-4189 (2003).

[56] A. Kubickova, T. Krizek, P. Coufal, M. Vazdar, E. Wernersson, J. Heyda and P. Jungwirth, *Phys. Rev. Lett.*, **108**, 186106 (2012).

[57] M. N. Tamashiro and P. Pincus, *Phys. Rev. E*, **60**, 6549-6559 (1999).

Chapter 6

The inhomogeneous screening effect near the dielectric interface

The ion distribution near the interface with dielectric discontinuity is highly anisotropic and nonuniform, giving rise to different nature of the screening effect compared to it in the bulk. Here, we develop a theory that fully accounts for the inhomogeneous screening effect near the dielectric interface. The double layer structure and interfacial properties is drastically affected by the inhomogeneous screening if the bulk Debye screening length is comparable or smaller than the Bjerrum length. The width of the depletion layer is characterized by the Bjerrum length, independent of the salt concentration. We predict that the negative adsorption of ions at the interface increases linearly with the salt concentration, which cannot be captured by neither of the bulk screening approximation and the WKB approximation. For asymmetric salt, the inhomogeneous screening enhances the charge separation in the induced double layer and significantly increases the value of the surface potential. This chapter is adapted in part from the manuscript R. Wang and Z.-G. Wang, in preparation.

6.1 Introduction

For a wide range of physicochemical, colloidal, soft-matter and biophysical systems, ions and electrostatic interactions affects a wealth of structural and dynamic properties[1, 2, 3, 4, 5, 6, 7]. The screening effect due to ion-ion correlation is perhaps one of the most important concepts in the electrostatics[8], which was introduced 90 years ago by Debye and Hückel for studying the thermodynamic properties of bulk electrolyte solution[9]. In the vicinity of a charged plate or an interface with dielectric discontinuity, the ion distribution is not uniform, making the screening effect also inhomogeneous which is different from the bulk. This inhomogeneous screening effect on the interaction between the mobile ion and the fixed surface charge has been accounted for, to a large extent, by the Poisson-Boltzmann (PB) theory[10]. However, the inhomogeneous screening effect on the interaction between mobile ions as well as between the mobile ion and its own image charge has not been studied to our knowledge.

Near a dielectric interface (e.g. the water/air interface), the screened image force creates a depletion layer, whose theoretical treatment was pioneered by Wagner, Onsager, and Samaras (WOS)[11, 12]. This problem arouse great interest in recent years because it is closely related to the ion conductivity in artificial and biological ion-channels[13, 14, 15], and the rate of ozone consumption in the Arctic[16, 17]. Approximating the inhomogeneous screening in the depletion layer by the constant bulk screening strength, the WOS theory predicts that the width of the depletion layer shrinks as the salt concentration c_b increases, which results in a concave downwards curve when the the surface tension of the electrolyte solution is plotted against c_b. However, the prediction of the WOS theory contradicts with the experiment results that the surface tension increases linearly with the salt concentration in the regime $c_b > 0.1M$[18, 19]. To force-fit the experiment data, excluded zone of constant width is artificially invoked in the previous theoretical descriptions[20, 21].

An obvious fact which is not captured by the WOS theory and the subsequent modifications is that the screening on the image charge interaction is spatially varying near the dielectric interface. Figure 6.1 illustrates the structure of the depletion layer for electrolyte solution near the dielectric interface, in which the ion concentration changes gradually from zero the the bulk value. The ionic cloud is highly anisotropic and nonuniform, giving rise to different feature of the screening near the interface in comparison with the isotropic and homogeneous screening in the bulk. Very close to the interface, ions are strongly depleted; the ionic strength around the test ion (see Test-ion 1 in Figure 6.1) is much lower than the bulk. The bulk screening approximation obviously overestimates the screening strength on this ion (or underestimates the image charge repulsion). Even for the ion approaching the bulk solution (see Test-ion 2 in Figure 6.1), the screening strength is still lower than the bulk as a result of the long-range and accumulative effect coming from the strong depletion region. This feature of the inhomogeneous screening extends the effective range of the image charge repulsion

comparing to the prediction from the bulk screening approximation. An alternative approximated treatment on the inhomogeneous screening is proposed by Buff and Stillinger[22] based on the WKB approximation, which captures the local inhomogeneity of the screening near the interface. However, the long-range and accumulative nature of the inhomogeneous screening is still lost in the WKB approximation.

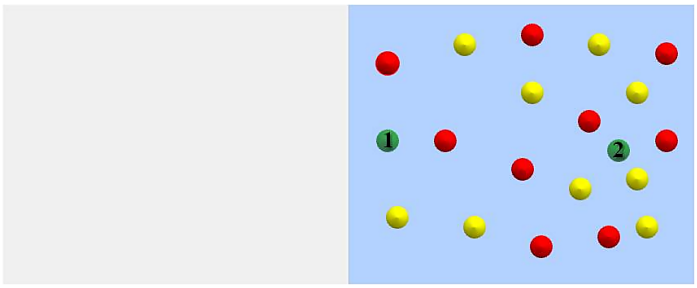

Figure 6.1: Schematic of the inhomogeneous ion distribution in the depletion layer near the dielectric interface and its effect on the screening. The red and yellow spheres represent the cations and anions, respectively. The green spheres represent the two test ions, with Test ion "1" located very close to the interface and Test ion "2" approaching the bulk solution.

In this work, we theoretically study the inhomogeneous screening effect of electrolyte solution near the liquid/air interface. By comparing the result from fully solving the Green function with the approximated methods, we show the nature of inhomogeneous screening and its effect on the depletion layer structure and interfacial properties. For the case that the bulk Debye screening length is comparable or smaller than the Bjerrum length, we show that the inhomogeneous screening drastically affects the depletion layer, which cannot be captured by either the bulk screening approximation or the WKB approximation.

6.2 Theory

In the previous work, we have shown that the image charge repulsion creates a depletion boundary layer near the dielectric interface which necessitates non-perturbative treatment[23, 24]. Using the renormalized Gaussian variational approach[25, 26], we derived a general theory for a weak-coupling system with a fixed charge distribution $\rho_s(\mathbf{r})$ in the presence of mobile cations with charge q_+e and anions with charge q_-e , in a dielectric medium of a spatially varying dielectric function $\varepsilon(\mathbf{r})$[24]. The key result of the theory is the following set of self-consistent equations for the mean electrostatic potential $\psi(\mathbf{r})$ (nondimensionized by kT/e), the correlation function (Green function) $G(\mathbf{r}, \mathbf{r}')$, and the self-energy $u_\pm(\mathbf{r})$ of mobile ions:

$$-\nabla \cdot (\epsilon \nabla \psi) = \rho_s + \Gamma \lambda_+ q_+ \mathrm{e}^{-q_+\psi - u_+} - \Gamma \lambda_- q_- \mathrm{e}^{q_-\psi - u_-} \tag{6.1}$$

$$-\nabla \cdot [\epsilon \nabla G(\mathbf{r}, \mathbf{r}')] + 2I(\mathbf{r})G(\mathbf{r}, \mathbf{r}') = \delta(\mathbf{r} - \mathbf{r}') \tag{6.2}$$

$$u_{\pm}(\mathbf{r}) = \frac{1}{2} \int d\mathbf{r}' d\mathbf{r}'' h_{\pm}(\mathbf{r} - \mathbf{r}') G(\mathbf{r}', \mathbf{r}'') h_{\pm}(\mathbf{r}'' - \mathbf{r}) \tag{6.3}$$

where ϵ is the scaled permittivity as $\epsilon = kT\varepsilon_0\varepsilon(\mathbf{r})/e^2$. $\lambda_{\pm}$ is the fugacity of cations and anions determined from the bulk salt concentration. The function Γ is introduced to constrain the mobile ions to the solvent region. $I(\mathbf{r}) = \left[q_+^2 c_+(\mathbf{r}) + q_-^2 c_-(\mathbf{r})\right]/2$ is the local ionic strength, with the concentration of cations and anions given by

$$c_{\pm}(\mathbf{r}) = \lambda_{\pm}\Gamma \exp\left[\mp q_{\pm}\psi(\mathbf{r}) - u_{\pm}(\mathbf{r})\right] \tag{6.4}$$

The short-range charge distribution function $h_{\pm}(\mathbf{r} - \mathbf{r}')$ on the ion in Eq. 7.3 is introduced to yield a finite Born solvation energy. For our purpose, we will eventually take the point-charge limit.

Eq. 7.1 is the self-energy modified Poisson-Boltzmann (PB) equation, reflecting that the ion distribution is determined by the competition between the mean electrostatic potential and the self energy. The correlation between the two point charge (i.e. the Green function in Eq. 7.2) has the contribution from both the direct Coulomb interaction and the long-range image charge interaction due to the distortion of the electric field at the dielectric interface. The self-energy given by Eq. 7.3 is a unified expression that includes the Born energy of the ion, the interaction between the ion and its ionic atmosphere, as well as the image charge interaction near a dielectric discontinuity. As shown in Eqs. 7.2 and 7.3, the inhomogeneity in the ionic strength affects the solution of the Green function as well as the self energy, which will consequently affect the double layer structure through Eq. 7.1 especially when the fixed charge density is small.

We now specify to electrolyte solution in contact with a low dielectric medium through a sharp interface (located at $z = 0$). Mobile ions are exclusive from the low dielectric side as illustrated in Figure 6.1. Both Γ and $\varepsilon(\mathbf{r})$ are step functions: $\Gamma = 0$ and $\varepsilon(\mathbf{r}) = \varepsilon_P$ for $z < 0$; $\Gamma = 1$ and $\varepsilon(\mathbf{r}) = \varepsilon_S$ for $z > 0$. In the solvent region ($z > 0$), Eq. 7.1 becomes

$$-\epsilon_S \frac{\partial^2 \psi(z)}{\partial z^2} = \lambda_+ q_+ \mathrm{e}^{-q_+\psi - u_+} - \lambda_- q_- \mathrm{e}^{q_-\psi - u_-} \tag{6.5}$$

with the boundary condition $(\partial\psi/\partial z)_{z=0} = -\sigma/\epsilon_S$. Since the solvent has a uniform dielectric constant, the Born energy is constant and can be absorbed into the reference chemical potential. The remaining contribution is finite in the point-charge limit (setting $h_{\pm}(\mathbf{r} - \mathbf{r}') = q_{\pm}\delta(\mathbf{r} - \mathbf{r}')$), which yields the nontrivial part of the self energy as

$$u_{\pm} = \frac{q_{\pm}^2}{2} \lim_{\mathbf{r}' \to \mathbf{r}} \left[G(\mathbf{r}, \mathbf{r}') - \frac{1}{4\pi\epsilon_S |\mathbf{r} - \mathbf{r}'|} \right] \tag{6.6}$$

To solve the Green function in the planar geometry, it is convenient to set up a cylindric coordinate

(r, z, z'). Performing 2D Fourier transform to Eq. 7.2 with respect to the variable r yields:

$$G(r, z, z') = \frac{1}{2\pi} \int_0^\infty k dk J_0(kr) \hat{G}(k, z, z') \tag{6.7}$$

where J_0 is the zero-order Bessel function. $\hat{G}(k, z, z')$ satisfies:

$$-\frac{\partial^2 \hat{G}(k, z, z')}{\partial z^2} + (\kappa^2(z) + k^2)\hat{G}(k, z, z') = \frac{1}{\epsilon_S}\delta(z, z') \tag{6.8}$$

for $z > 0$, with the boundary condition $\epsilon_S \partial \hat{G}/\partial z + k\epsilon_P \hat{G} = 0$ at $z = 0$. $\kappa(z) = [2I(z)/\epsilon_S]^{1/2}$ is the inverse of the local Debye screening length.

Two approximated approaches are adopted in the literature to avoid numerically solving the high-dimensional Green function. The first one is the bulk screening approximation[7, 12, 20, 21], which replaces the spatially varying screening length $\kappa(z)$ in Eq. 6.8 by the constant bulk screening length κ_b. With the bulk screening approximation, the Green function has an approximated analytical solution as

$$\hat{G}(k, z, z') = \frac{1}{2\epsilon_S \omega} \left[\mathrm{e}^{-\omega|z-z'|} + \Delta \mathrm{e}^{-\omega(z+z')} \right] \tag{6.9}$$

where $\omega = \sqrt{\kappa_b^2 + k^2}$ and $\Delta = (\epsilon_S \omega - \epsilon_P k)/(\epsilon_S \omega + \epsilon_P k)$. Substituting Eq. 6.9 into Eq. 7.7 leads to the following intuitive form of the self energy for $\epsilon_S \gg \epsilon_P$:

$$u_\pm(z) = \frac{q_\pm^2}{8\pi\epsilon_S} \left(-\kappa_b + \frac{f \mathrm{e}^{-2\kappa_b z}}{2z} \right) \tag{6.10}$$

with $f = (\epsilon_S - \epsilon_P)/(\epsilon_S + \epsilon_P)$ denoting the dielectric contrast. The second approximated approach is proposed by Buff and Stillinger based on the WKB approximation[22, 23, 27]: the Green function assumes the same functional form as the analytical solution for a constant ionic strength (Eq. 6.9 or Eq. 6.10), but with the ionic strength replaced by its local value.

In this work, we also perform the full numerical calculation of the Green function by using the finite difference method[28] (the numerical details are given in Ref. [29]). It should be noticed that the free-space Green function $-\partial^2 \hat{G}_0/\partial z^2 + k^2 \hat{G}_0 = \delta(z, z')/\epsilon_S$ also need to be numerically solved accompanying with Eq. 6.8 to remove the singularity of the same-point Green function, which gives rise to the nondivergent part of the self energy as:

$$u_\pm(z) = \frac{q_\pm^2}{4\pi} \int_0^\infty \left[\hat{G}(k, z, z) - \hat{G}_0(k, z, z) \right] k dk \tag{6.11}$$

6.3 Results and Discussions

In this section, we apply our theory to electrolyte solution near the liquid/air interface in the absence of fixed surface charge ($\rho_s = 0$). Two kinds of liquid are considered in the calculation: the more polar

water with $\varepsilon_S = 80$ and the less polar medium with $\varepsilon_S = 20$. The dielectric constant of air is set to be 1. We first study electrolyte solutions with equal-valent cations and anions, in which there is no charge separation and the electrostatic potential is everywhere zero. Then we investigate electrolyte solutions containing asymmetric salt, where the difference in the image force between the cations and anions induces charge separation and hence electric field. The difference between the results from fully solving the Green function and results obtained by the approximated methods (the bulk screening approximation and the WKB approximation) reveals the nature of the inhomogeneous screening and its effects on the double layer structure and interfacial properties.

The image charge effect creates a depletion boundary layer near the dielectric interface, in which there are two length scales: the Bjerrum length $l_B = 1/(4\pi\epsilon_S)$ (approximately 7 $\mathring{A}$ in water) and the bulk Debye screening length κ_b^{-1}. Within the Bjerrum length, the ion is strongly repelled by its own image charge; whereas beyond the bulk Debye screening length, the image charge repulsion is significantly reduced due to the screening from other ions. The effect of inhomogeneous screening on the ion distribution is twofold. First, the screening strength within the Bjerrum length is weaker than that in the bulk, giving rise to stronger image repulsion and more depletion of ions. Second, the low ion concentration within the Bjerrum length has long-range and accumulative effect on the screening strength beyond the Bjerrum length, which extends the range of the depletion layer. Figures 6.2(a) and 6.2(b) show the effect of inhomogeneous screening on the ion distribution of 1:1 electrolyte solution near the water/air interface. At low salt concentration, $\kappa_b^{-1} \gg l_B$ and the ion concentration profiles calculated by the three methods collapse onto each other as shown in Fig 6.2(a). The effect of inhomogeneous screening on the depletion layer structure is insignificant in this case, because the screening strength itself is very small even in the bulk, which makes the accurate treatment of the screening ineffective. In addition, the effect of strong ion depletion within the Bjerrum length decays in a short range compared to the Debye screening length. The long-range behavior of the double layer is still characterized by the bulk Debye screening length.

In contrast, κ_b^{-1} becomes comparable to l_B and even smaller than l_B thereafter as the salt concentration increases; the inhomogeneous screening affects the entire range of the depletion layer as shown in Fig 6.2(b). Close to the interface ($z < l_B$), the ion concentration calculated by fully solving the Green function is significantly lower than the result of the bulk screening approximation, because the local screening strength is obviously smaller than the bulk. Although this short-range effect is also captured by the WKB approximation, neither of the two approximated methods captures the long-range nature of the screening effect on the ion depletion. The depletion layer calculated by fully solving the Green function extends to the range much longer than the bulk Debye screening length, which drastically differs from the results of the two approximated methods. The screening strength beyond κ_b^{-1} is still lower than the bulk value due to the anisotropic ionic cloud near the dielectric interface and the accumulative effect from the low ionic strength whin l_B. Therefore, the long-range

behavior of the depletion layer cannot be characterized by the bulk Debye screening length in this case, which is different from the situation in the bulk electrolyte solution. Moreover, Levine and Bell state that the WKB approximation provides the lower bound of the screening. In light of our results, this statement is not valid as far as the long-range part of the ion distribution is concerned. Both the bulk screening approximation and the WKB approximation overestimate the long-range part of the screening and underestimate its effect on the image charge repulsion.

As the dielectric constant of the liquid decreases, the Bjerrum length increases ($l_B \sim \varepsilon_S^{-1}$), whereas the bulk Debye screening length decreases ($\kappa_b^{-1} \sim \varepsilon_S^{1/2}$). As shown by Fig 6.2(c), the inhomogeneous screening in the less polar liquid affects the ion distribution at much lower salt concentration and the depletion layer is extended to much longer range compared to water. We note that salt ions tend to form bound ion pairs in the low dielectric medium. Here, the concentration of ions only refer to the dissociated free ions. The effect of strong dipole the ion pair possesses on the screening of the free ion is not considered in this work.

Applying Gibbs construction on the ion concentration profile, we define $d = \int_0^\infty [c_b - c(z)]\, dz/c_b$ to characterize the average distance of ion depletion. d as a function of the salt concentration (and κ_b^{-1}) is shown in Figure 6.3 for both the water/air interface and the less polar liquid/air interface. For the entire regime of salt concentration, the two approximated methods predict that d decreases as c_b increases; the characteristic length for the depletion layer is scaled by the bulk Debye screening length ($d \sim \kappa_b^{-1}$). In contrast, d calculated by fully solving the Green function deviates significantly from the results of the approximated methods as κ_b^{-1} becomes comparable to l_B. Thereafter, d approaches a constant as c_b keeps increasing, which indicates that the image charge repulsion affected by the inhomogeneous screening creates a depletion layer that maintains a constant width in the regime of $\kappa_b^{-1} < l_B$. The characteristic length of the ion depletion is scaled by the Bjerrum length ($d \sim l_B$) in stead of the bulk Debye screening length, which is independent of the salt concentration. This result is qualitatively different from the prediction obtained by the bulk screening approximation and the WKB approximation. The characteristic length in the less polar liquid behaves the same as it in the water (see figure 6.3(b)), except that the deviation of the numerical result from the approximated methods occurs at lower salt concentration ($< 10^{-3}M$) and the inhomogeneous screening becomes longer range.

The change in the structure of the depletion layer due to the inhomogeneous screening will affect the interfacial properties. In Figure 6.4, we show the negative adsorption of ions ($-\Gamma = \int_0^\infty [c(z) - c_b]\, dz$) as a function of salt concentration at the water/air interface, which is closely related to the salt effect on the interfacial tension. Because of the shrinking of the depletion layer as c_b increases, the method by using the bulk screening approximation predicts that $-\Gamma$ is a concave downwards function of c_b. This is also the prediction given by the WOS theory[11, 12]. However, the prediction of the WOS theory contradicts with the experiment results which shows that both

$-\Gamma$ and the interfacial tension of the 1:1 electrolyte solution increases linearly with c_b in the regime of $0.1M < c_b < 1M$[18, 19]. To force-fit the experimental data, excluded zone with constant width is artificially invoked for the ions in the previous theoretical descriptions[20, 21]. By fully accounting for the inhomogeneous screening effect, the result obtained by numerically solving the Green function predicts that the width of the depletion layer is constant in the regime of $0.1M < c_b < 1M$, and $-\Gamma$ increases linearly with c_b (see Figure 6.4), which is in agreement with the experiment results. In light of our results, we suggest that the inhomogeneous screening effect provides an explanation on the linear increase of the surface tension with the salt concentration, which cannot be explained by the approximated treatment on the screening effect.

Due to the square-root dependence of the screening strength on the valency, the way of treating the inhomogeneous screening has larger influence on the depletion of the multi-valent ions than the monovalent ions. In the previous work, we show for the asymmetric salt that the difference in the image force between the cations and anions induces charge separation and hence electric field within the depletion layer[23, 24]. This difference in the image force can be enhanced by the inhomogeneous screening effect as shown in Figure 6.5. For 2:1 electrolyte solution near the water/air interface, the divalent cations calculated by fully solving the Green function are pushed further away from the interface comparing to the approximated methods (see Figure 6.5(a)). The monovalent anions are also driven further away from the interface to reduce the charge separation. It should be noted that, due to the existence of the divalent ions, the inhomogeneous screening effect on the distribution of the monovalent ions is more significant in the 2:1 electrolyte solution than the 1:1 electrolyte solution for the same salt concentration. The inhomogeneous screening also significantly affects the induced electrostatic potential as shown in Figure 6.5(b). The value of the surface potential $\mid \psi(0) \mid$ calculated by fully solving the Green function is 65% larger than that obtained by using the bulk screening approximation, which can make essential difference in predicting the zeta potential of the colloid surfaces[1] and interesting the Jones-Ray effect in the surface tension of electrolyte solution[30, 31, 32, 33].

6.4 Conclusion

In this work, we have presented a theory that fully accounted for the inhomogeneous screening effect near the dielectric interface. The effect of inhomogeneous screening on the image charge repulsion and the depletion layer structure is twofold. First, the ionic cloud in the depletion layer is highly anisotropic with much lower ionic strength than the bulk; this local inhomogeneity gives rise to less screening on the image force and stronger ion depletion. Second, the strong ion depletion near the interface has accumulative effect on the long-range screening strength, which extends the effective range of the image force. We show that the depletion layer structure is drastically affected by

the inhomogeneous screening if the bulk Debye screening length is comparable or smaller than the Bjerrum length. In this case, both the bulk screening approximation and the WKB approximation fail to describe the depletion layer structure and the interfacial properties. The characteristic length of the depletion layer is scaled by the Bjerrum length, which is independent of the salt concentration. We predict that the negative adsorption of ions at the liquid/air interface increases linearly with the salt concentration if the inhomogeneous screening is fully accounted for, which is in agreement with the experiment results. The inhomogeneous screening effect becomes more significant for the less polar solvent and for the ions of higher valency. Applying our theory to the 2:1 electrolyte solution, we show that the charge separation in the induced double layer is enhanced by the inhomogeneous screening, giving rise to significant change in the surface potential.

Inhomogeneity of the ion distribution near the interface with dielectric discontinuity widely exists in many soft-matter and biophysical systems. The inhomogeneous screening is an intrinsic component of the electrostatic contribution, which, however, has not been fully accounted for in the previous study. An accurate treatment of the inhomogeneous screening is important to understand the electrostatic behaviors in these systems. In addition, there are other non-electrostatic contributions such as cavity energy[34, 35], hydration[21], and dispersion forces[36] for the ions near the interface. However, there is still debate on the existence and relative importance of these non-electrostatic contributions[3]. Only by systematically and accurately treating the electrostatic contribution which is essential in a charged system, we can evaluate the relative importance of the non-electrostatic contributions.

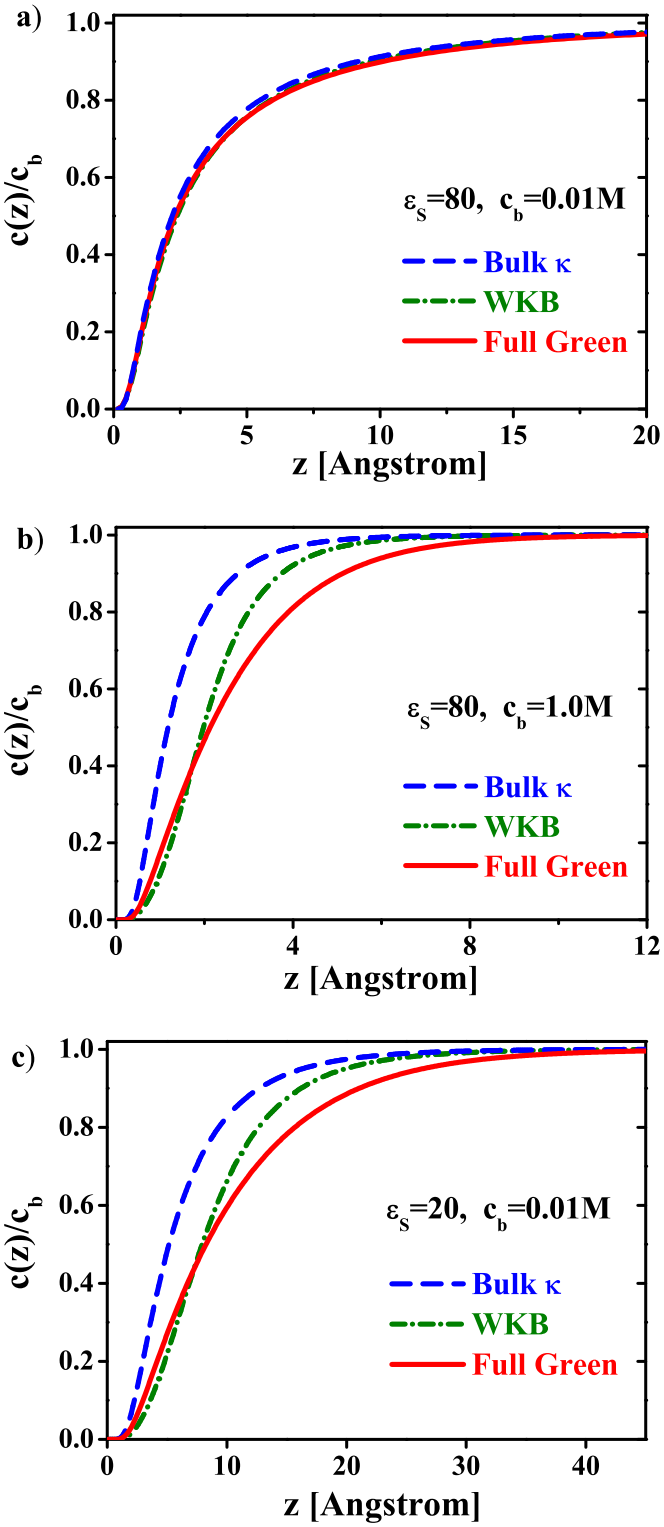

Figure 6.2: The effect of inhomogeneous screening on the ion distribution of 1:1 eletrolyte solution near the dielectric interface. (a) and (b) are for the water/air interface with $\varepsilon_S = 80$ and $\varepsilon_P = 1$. The bulk salt concentration c_b is $0.01M$ in (a) and $1.0M$ in (b). The liquid in (c) is less polar medium with $\varepsilon_S = 20$, and $c_b = 0.01M$. Notations "Bulk κ" and "WKB" refer to the results obtained by using the bulk screening approximation and WKB approximation, respectively. The notation "Full Green" refers to the results calculated by numerically solving the Green function.

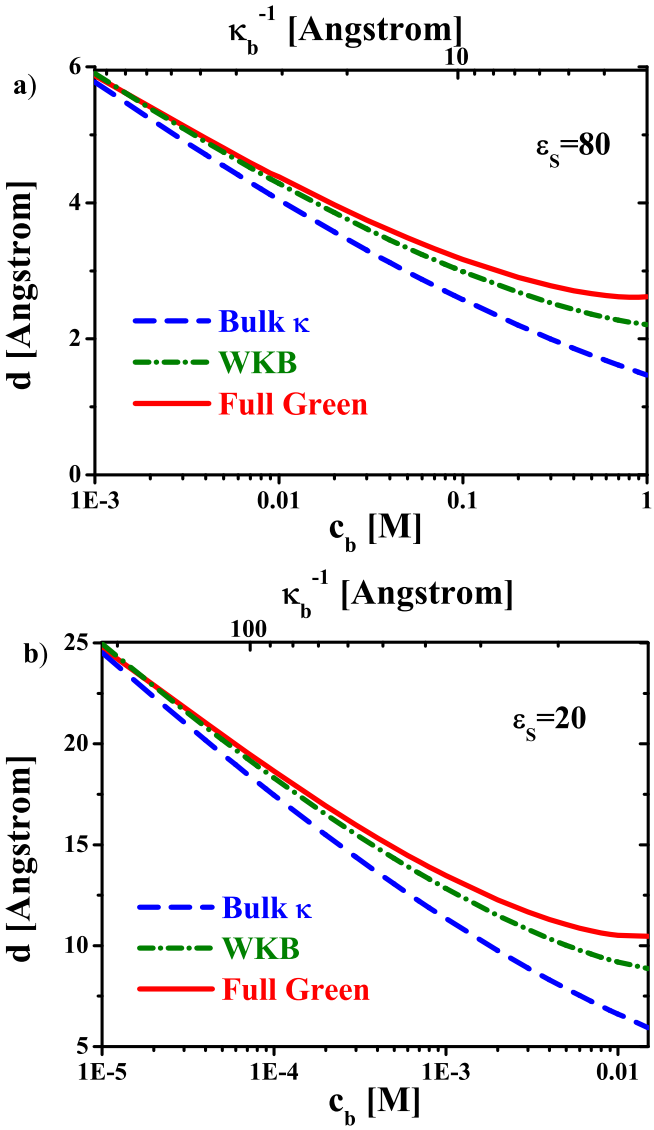

Figure 6.3: The characteristic length of ion depletion as a function of salt concentration and bulk Debye screening length for (a) the water/air interface ($\varepsilon_S = 80$) and (b) the less polar liquid/air interface ($\varepsilon_S = 20$).

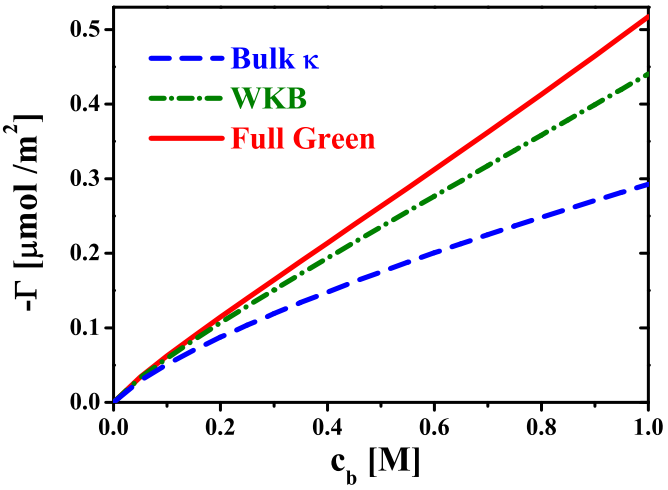

Figure 6.4: The effect of inhomogeneous screening on the negative adsorption of ions at the water/air interface.

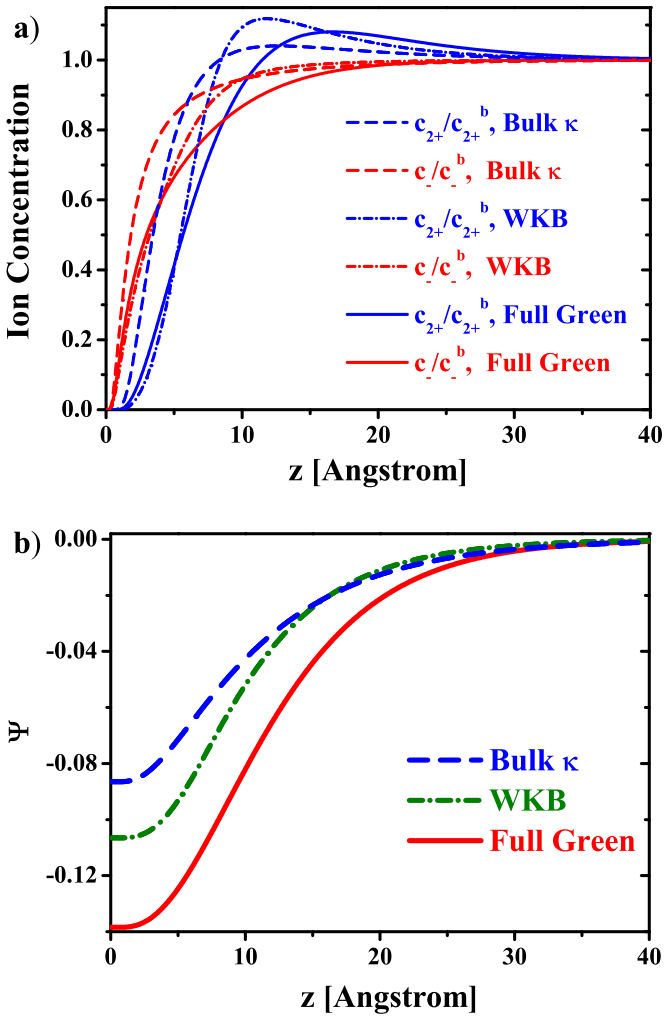

Figure 6.5: The inhomogeneous screening effect on the depletion layer structure of 0.05M 2:1 electrolyte solution near the water/air interface. (a) Ion concentration scaled by $c_{\pm}^{b}$ and (b) dimensionless electrostatic potential.

Bibliography

[1] J. N. Israelachvili, *Intermolecular and surface forces*, 2nd Ed. (Academic, London, 1992).

[2] W. M. Gelbart, R. F. Bruinsma, P. A. Pincus and V. A. Parsegian, *Phys. Today*, **53**, 38-44 (2000).

[3] P. L. Nostro and B. W. Ninham, *Chem. Rev.* **112**, 2286 (2012).

[4] B. Honig and A. Nicholls, *Science*, **268**, 1144-1149 (1995).

[5] M. Z. Bazant, B. D. Storey, and A. A. Kornyshev, Phys. Rev. Lett. **106**, art. no. 046102 (2011).

[6] G. M. Luo, S. Malkova, J. Yoon, D. G. Schultz, B. H. Lin, M. Meron, I. Benjamin, P. Vanysek and M. L. Schlossman, *Science*, **311**, 216-218 (2006).

[7] J. W. Zwanikkena and M. Olvera de la Cruz, *Proc. Natl. Acad. Sci. USA*, **110**, 5301-5308 (2013).

[8] Y. Levin, *Rep. Prog. Phys.*, **65**, 1577-1632, (2002).

[9] P. Debye and E. Hückel, *Phys. Z.*, **24**, 185-206 (1923).

[10] D. Andelman, in *Soft Condensed Matter Physics in Molecular and Cell Biology*, W. C. K. Poon and D. Andelman, eds. (Taylor and Francis, Boca Raton, Florida, 2000).

[11] C. Wagner, Phys. Z. **25**, 474 (1924).

[12] L. Onsager and N. N. T. Samaras, *J. Chem. Phys.*, **2**, 528 (1933).

[13] A. Parsegian, *Nature*, **221**, 844-846 (1969).

[14] T. Bastug and S. Kuyucak, *Biophys. J.*, **84**, 2871-2882 (2003).

[15] S. Buyukdagli, M. Manghi and J. Palmeri, *Phys. Rev, Lett.*, **105**, 158103, (2010).

[16] J. H. Hu, Q. Shi, P. Davidovits, D. R. Worsnop, M. S. Zahniser and C. E. Kolb, *J. Phys. Chem.*, **99**, 8768 (1995).

[17] E. M. Knipping, M. J. Lakin, K. L. Foster, P. Jungwirth, D. J. Tobias, R. B. Gerber, D. Dabdub, and B. J. Finlayson-Pitts, *Science*, **288**, 301, (2000).

[18] N. Matubayasi, K. Yamamoto, S. Yamaguchi, H. Matsuo and N. Ikeda, *J. Colloid Interface Sci.*, **214**, 101 (1999).

[19] N. Matubayasi, K. Tsunemoto, I. Sato, R. Akizuki, T. Morishita, A. Matuzawa, and Y. Natsukari, *J. Colloid Interface Sci.*, **243**, 444 (2001).

[20] Y. Levin and J. E. Flores-Mena, Europhys. Lett. 56, 187 (2001).

[21] Y. Levin, A. P. dos Santos and A. Diehl, *Phys. Rev. Lett.* **103**, 257802 (2009).

[22] F. P. Buff and F. H. Stillinger, *J. Chem. Phys.*, **39**, 1911-1923 (1963).

[23] R. Wang and Z. -G. Wang, *J. Chem. Phys.*, **139**, 124702, (2013).

[24] R. Wang and Z. -G. Wang, in preparation.

[25] R.R. Netz and H. Orland, *Eur. Phys. J. E*,**11**, 301C311, (2003).

[26] Z. -G. Wang, *Phys. Rev. E*, **81**, 021501 (2010).

[27] G. M. Bell and S. Levine, *J. Chem. Phys.*, **49**, 4584-4599 (1968).

[28] Z. L. Xu, M. M. Ma and P. Liu, *Phys. Rev. E*, **90**, 013307 (2014).

[29] Eq. 6.8 is solved with 2000 grid points along the z axis for each k. The Dirac delta function is approximated by Kronecker delta. The numerical integration of Eq. 6.11 is performed by using the Simpson method with 200 grid points in the k space.

[30] A. Onuki, *J. Chem. Phys.* **128**, art. no. 224704 (2008);

[31] G. Jones and W. A. Ray, *J. Am. Chem. Soc.* **59**, 187 (1937).

[32] M. Bier, J. Zwanikken and R.van Roij, *Phys. Rev. Lett.* **101**, 046104 (2008).

[33] R. Wang and Z.-G. Wang, *J. Chem. Phys.* **135**, 014707 (2011).

[34] K. Lum, D. Chandler, and J. D. Weeks, *J. Phys. Chem. B* **103**, 4570 (2005); D. Chandler, *Nature* **437**, 640 (2005).

[35] S. Rajamani, T. M. Truskett, and S. Garde, *Proc. Natl. Acad. Sci. U.S.A.* **102**, 9475 (2005).

[36] M. Boström, D. R. M. Williams and B. W. Ninham, *Langmuir* **17**, 4475 (2001).

Chapter 7

Continuous Self Energy of Ions at the Dielectric Interface: the Specific Ion effect

By treating both the short-range (solvation) and long-range (image force) electrostatic forces as well as charge polarization induced by these forces in a consistent manner, we obtain a simple theory for the self energy of an ion that is continuous across the interface. Along with nonelectrostatic contributions, our theory enables a unified description of ions on both sides of the interface. Using intrinsic parameters of the ions, we predict the specific ion effect on the interfacial affinity of halogen anions at the water/air interface, and the strong adsorption of hydrophobic ions at the water/oil interface, in agreement with experiments and atomistic simulations. This chapter is adapted from our paper, R. Wang and Z.-G. Wang, *Phys. Rev. Lett.* **112**, 136101 (2014).

7.1 Introduction

The interfacial activities of salt ions are of great importance in physical chemistry, colloidal science and biophysics[1]. Many interfacial phenomena, such as the surface tension of electrolyte solution[2, 3], salt effects on bubble coalescence[4] and effectiveness of salts on the stability of proteins solutions and colloidal suspensions[5, 6], exhibit strong dependence on the chemical identity of the ions. Although this "specific ion effect" has been known for over a century[7], a systematic, unified and predictive theory remains an outstanding challenge. Current theories are system dependent and require adjustable parameters to force-fit experimental data[8, 9, 10, 11, 12, 13, 14, 15, 16].

A key factor that determines the ion distribution at the dielectric interface and other interfacial properties is the self energy of a single ion[17]. The self energy consists of electrostatic and non-electrostatic contributions, such as cavity energy, hydration and dispersion forces. While the effects and the theoretical treatments of these nonelectrostatic contributions are still debatable [8], the constituent components in the electrostatic self energy have become clear in recent years[18, 19, 20]. The problem is then in the accurate and consistent treatment of the electrostatic effects. Such a treatment is essential both because the electrostatic part is a major component in the self energy of an ion, and because the relative importance of the nonelectrostatic contributions can only be evaluated when the electrostatic contribution is treated accurately.

A major contribution in the electrostatic self energy is the image interaction, whose treatment was pioneered by Wagner, Onsager and Samaras (WOS)[21, 22]. The WOS theory predicts depletion of ions from the water/air interface due to the image charge repulsion and qualitatively explains the increase of surface tension with the salt concentration. However, this theory fails to capture the initial decrease with salt concentration in the surface tension known as the Jones-Ray effect[23, 24], and the systematic dependence on the identity of the ions[2, 3]. A major weakness in the WOS theory and its subsequent modifications is modeling the ion as a point charge, which results in a discontinuous self energy across the dielectric interface. The self energy diverges to positive infinity on approaching the interface from the water side and to negative infinity on approaching from the air(oil) side. To avoid this unrealistic behavior, the ion distribution is artificially restricted to lie only in the water phase, which makes the theory inapplicable to hydrophobic ions and liquid-liquid interfaces. This artificial cut-off also affects the electrostatic potential gradient across the interface, which is shown essential to the Jones-Ray effect[25, 26].

Another important effect is the finite polarizability of the ions. Simulation by Jungwirth and Tobias[27, 28] showed that the polarizability of ions is a key contribution to their differential affinity to the interface. Levin and coworkers [18, 19, 20] developed a model of polarizable ions near a dielectric interface that are able to explain several interfacial properties of aqueous electrolyte solutions. In their model, charge polarization in the ion is included to optimize the short-range Born

energy. However, near a dielectric interface, the long-range image force can be sufficiently strong to contribute to charge polarization. Furthermore, their model does not account for the image force on the air(oil) side of the interface, thus making it difficult to extend the theory to hydrophobic ions and liquid/liquid interfaces.

In this chapter, we present a unified theory that treats all the electrostatic contributions: the Born solvation energy, the image charge interaction, and ion polarizability in a single, consistent framework. Along with the relevant nonelectrostatic contributions, we apply our theory to air/water and liquid/liquid interfaces.

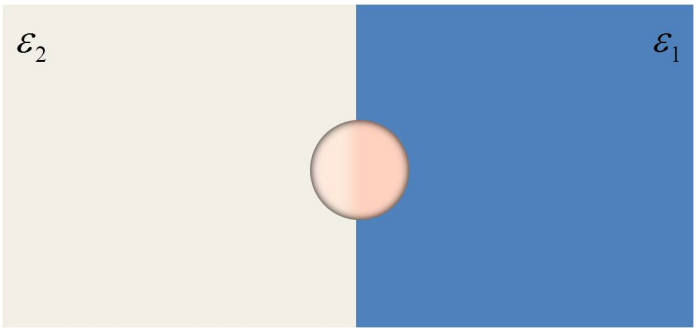

Figure 7.1: Schematic description of the model system. The charge distribution on the ion is illustrated by the shade.

7.2 Electrostatic Self Energy

As illustrated in Figure 7.1, we consider a single ion in the vicinity of a sharp interface, located at $z = 0$, between two semi-infinite regions ($\Re_1$ and $\Re_2$) with respective dielectric constant ε_1 and ε_2 ($\varepsilon_1 > \varepsilon_2$). We take the elementary charge e as the unit of charge, and kT as the unit of energy. The ion is taken as a sphere of radius a centered at $\mathbf{r}_c$, with charge distribution $\rho(\mathbf{r}, \mathbf{r}_c)$, which satisfies $\int d\mathbf{r}\rho(\mathbf{r}, \mathbf{r}_c) = \nu_\pm$ with $\nu_\pm$ the valency of the ion ("+" for cation and "−" for anion). The ion is polarizable; therefore, the charge distribution will be self-adjusted to the local dielectric environment.

The electrostatic self energy u_{el} can be written as two parts: $u_{el} = u_{int} + u_{pol}$, where u_{int} accounts for the sum of the Coulomb interactions in the constituent charges on the ion and u_{pol} is the energy cost of charge polarization. u_{int} is given by:

$$u_{int}(\mathbf{r}_c) = 2\pi l_B \int d\mathbf{r} \int d\mathbf{r}' \rho(\mathbf{r}, \mathbf{r}_c) G(\mathbf{r}, \mathbf{r}') \rho(\mathbf{r}', \mathbf{r}_c) \tag{7.1}$$

where $l_B = e^2/4\pi\varepsilon_0 kT$ is the Bjerrum length in the vacuum and ε_0 is the vacuum permitivity. $G(\mathbf{r}, \mathbf{r}')$ is the Green's function: the electrostatic potential at $\mathbf{r}$ due to a unit point charge at $\mathbf{r}'$. It satisfies the Poisson equation $-\nabla \cdot [\varepsilon(\mathbf{r})\nabla G(\mathbf{r}, \mathbf{r}')] = \delta(\mathbf{r} - \mathbf{r}')$. Depending on whether $\mathbf{r}$ and $\mathbf{r}'$ are

in the same region, $G(\mathbf{r},\mathbf{r}')$ is given by

$$G(\mathbf{r},\mathbf{r}') = \begin{cases} \frac{1}{4\pi\varepsilon_\alpha|\mathbf{r}-\mathbf{r}'|} + \frac{\Delta_{\alpha\beta}}{4\pi\varepsilon_\alpha|\mathbf{r}-\mathbf{r}^\star|} & \mathbf{r},\mathbf{r}' \in \Re_\alpha \\ \frac{1}{2\pi(\varepsilon_\alpha+\varepsilon_\beta)|\mathbf{r}-\mathbf{r}'|} & \mathbf{r} \in \Re_\beta, \mathbf{r}' \in \Re_\alpha \end{cases} \tag{7.2}$$

α and β can be either 1 or 2, and $\Delta_{\alpha\beta} = (\varepsilon_\alpha - \varepsilon_\beta)/(\varepsilon_\alpha + \varepsilon_\beta)$ is the dielectric contrast. $\mathbf{r}^\star = (x', y', -z')$ is the location of the image of $\mathbf{r}'$ with respect to the interface. The first term on the r.h.s of Eq. 7.2 is the direct Coulomb interaction and will generate the local Born solvation energy upon integration over the charge distribution. The last term in the first line of Eq. 7.2 is the image charge interaction, which can be either positive or negative depending on whether the point charge is located on the high dielectric side or low dielectric side; thus it either enhances or counteracts the solvation energy effect.

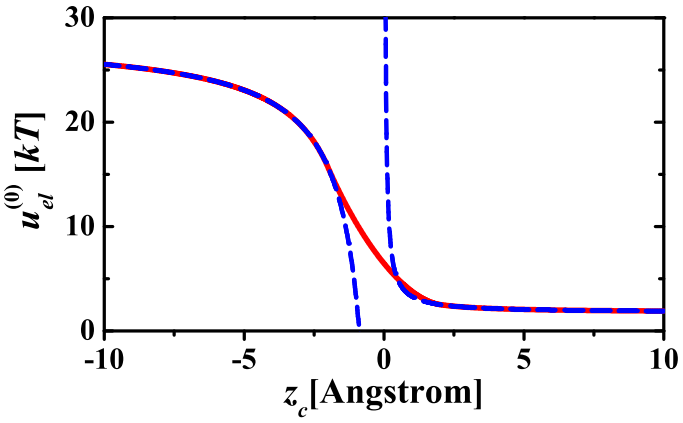

Figure 7.2: Electrostatic self energy, $u_{el}^{(0)}$, of a monovalent ion with uniform surface charge distribution, calculated by our model (solid line) and the point charge model (dash line). $\varepsilon_1 = 80$, $\varepsilon_2 = 5$ and $a = 2\mathring{A}$.

In the point-charge model $\rho(\mathbf{r},\mathbf{r}_c) = \nu_\pm \delta(\mathbf{r}-\mathbf{r}_c)$, Eq. 7.2 gives $u_{int}(\mathbf{r}_c) = 2\pi l_B \nu_\pm^2 G(\mathbf{r}_c,\mathbf{r}_c)$, which produces divergences in both the local Born solvation energy and in the image charge interaction as $z_c \to 0$ from either side of the interface. The use of a finite charge distribution avoids both types of divergences. Figure 7.2 shows the result for the electrostatic self energy, $u_{el}^{(0)}$, calculated for a nonpolarizable, uniform surface charge distribution on the ion (thus $u_{el}^{(0)} = u_{int}$). For comparison, we include the results from the point-charge model, adjusted by the bulk Born energy $\nu_\pm^2 l_B/2a\varepsilon_\alpha$ on each side. While $u_{el}^{(0)}$ calculated by the two models are consistent in the bulk region ($\mid z_c \mid > a$), qualitative and dramatic differences are seen in the interfacial region – the most relevant region for the interfacial activities of the ions. Interestingly, $u_{el}^{(0)}$ for an ion located exactly at the interface ($z_c = 0$) is significantly lower than the mean of the Born energy in two bulk regions, reflecting the asymmetry in the image force between the two dielectric media.

Polarization of the ion allows the charge distribution to self-adjust to its local dielectric environment, which decreases u_{int} relative to that for a fixed uniform charge distribution. However, this redistribution incurs an energy penalty u_{pol}. Levin [18] proposed a phenomenological model for u_{pol} by taking reference to the perfectly conducting sphere and making a Landau type of symmetry argument to describe this energy penalty. In our notation u_{pol} is:

$$u_{pol}(\mathbf{r}_c) = \frac{(\gamma_0 - \gamma)}{2v\gamma} \int d\mathbf{r} \left[\frac{\rho(\mathbf{r}, \mathbf{r}_c)}{\rho_0} - 1 \right]^2 \tag{7.3}$$

where γ is the polarizability of the ion, $\gamma_0 (= a^3)$ is the polarizability of a perfectly conducting sphere of the same radius as the ion[29], v is the volume of the ion, and ρ_0 is the charge density for the uniform spherical distribution on the ion surface. The form of the coefficient in Eq. 7.3 was so constructed as to reproduce the known limiting behavior, i.e., that it should be zero for the perfectly conducting sphere and infinity for a nonpolarizable ion.

Putting together Eqs. 7.1 and 7.3, we obtain the general expression for u_{el} with arbitrary charge distribution on the ion. The optimal distribution is then obtained from $\delta u_{el}(\mathbf{r}_c)/\delta\rho(\mathbf{r}, \mathbf{r}_c) = 0$. To avoid the complexity of solving the high dimensional integral equation from this condition, we make a variational trial function for $\rho(\mathbf{r}, \mathbf{r}_c)$. We assume that polarization apportions respectively f and $1 - f$ of the total ionic charge ($f \in [0, 1]$) uniformly to the two hemispheres of the ion separated by the xy plane at z_c, i.e.,

$$\rho(\mathbf{r}, \mathbf{r}_c) = \begin{cases} 2f\rho_0(\mathbf{r}) & for\ z \geq z_c \\ 2(1-f)\rho_0(\mathbf{r}) & for\ z < z_c \end{cases} \tag{7.4}$$

where $\rho_0(\mathbf{r}) = \nu_{\pm}\delta(\mid \mathbf{r} - \mathbf{r}_c \mid -a)/4\pi a^2$ is the uniform surface distribution on the sphere. The deviation of f from 1/2 measures the degree of polarization of the ionic charge. Substituting the trial function Eq. 7.4 into Eqs. 7.1 and 7.3, $u_{el}(\mathbf{r}_c)$ can be simplified to a quadratic function of f, which can be easily minimized to yield a position-dependent charge fraction $f(\mathbf{r}_c)$. This optimal charge fraction $f(\mathbf{r}_c)$ is then used to evaluate $u_{el}(\mathbf{r}_c)$. Since the electrostatic interaction includes the local Born solvation energy and the long-range image force, the resulting polarization reflects the combined effects of these terms. Figure 7.3 shows the charge polarization and the electrostatic self energy of I^- ($a_{I^-} = 2.26\mathring{A}$, $\gamma_{I^-} = 6.9\mathring{A}^3$). In the immediate vicinity of the interface ($\mid z_c \mid < a$), I^- is highly polarized. Charge polarization significantly lowers u_{el} compared with the nonpolarizable ion. Beyond the immediate vicinity of the interface ($\mid z_c \mid > a$), polarization is driven by the long-range image force, and f decays to 1/2 as the ion approaches the bulk. While the effect of charge polarization on u_{el} is small on the high dielectric side beyond $z_c = a$, u_{el} of the polarizable ion is appreciably lower than the nonpolarizable ion on the low dielectric side slightly beyond $z_c = -a$, as a result of stronger and longer-range image force in this region.

For comparison, in Figure 7.3(b) we also include result from Levin's polarizable ion model[18].

u_{el} in Levin's theory only extends to $z_c = -a$, whereas our theory yields a continuous u_{el} across the interface to the bulk air(oil) phase; this will be important when there is appreciable ion partition in the oil phase. In addition, u_{el} on the low dielectric side is significantly higher in our theory than from Levin's theory because the relocation of charge from $z < 0$ to $z > 0$ changes the image force from attractive to repulsive, which is not accounted for in Levin's theory. The difference becomes more pronounced with increasing dielectric contrast.

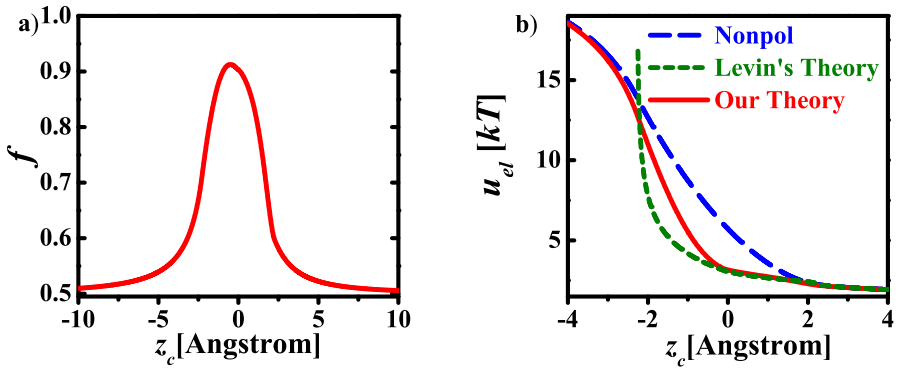

Figure 7.3: (a) Charge polarization f, and (b) electrostatic self energy u_{el}, for I^-. For comparison, we include Levin's theory[18] and a nonpolarizable ion of the same radius as I^- (dash line). $\varepsilon_1 = 80$, $\varepsilon_2 = 5$.

The calculations so far concern only the electrostatic contributions to the self energy, which will not be affected by the addition of nonelectrostatic effects. The total self energy of the ion is the sum of the electrostatic and nonelectrostatic parts:

$$u(\mathbf{r}_c) = u_{el}(\mathbf{r}_c) + u_{ne}(\mathbf{r}_c) \tag{7.5}$$

We now include the appropriate nonelectrostatic contributions to discuss the interfacial behavior of different ions at the water/air and water/oil interfaces respectively.

7.3 Water/Air Interface

For the nonelectrostatic self energy at the water/air interface, we take the simplest form of cavity energy[30, 31, 18], which is the work required to create a cavity for the ion where the water molecules are excluded. It is given by[30, 31, 18]

$$u_{ne}^{w/a}(\mathbf{r}_c) = \begin{cases} \kappa a^3 & z_c \geq a \\ \frac{\kappa a^3}{4}\left(\frac{z_c}{a}+1\right)^2\left(2-\frac{z_c}{a}\right) & a > z_c \geq -a \\ 0 & z_c < -a \end{cases} \tag{7.6}$$

with $\kappa \approx 0.3\mathring{A}^{-3}$ from bulk simulation[32]. $u_{ne}^{w/a}$ provides the driving force for the ion to migrate from the bulk water to the interface; this driving force is larger for larger ions. The self energy profile of the ion across the interface is determined by the competition between the cavity energy and the electrostatic self energy, the former preferring the ion to reside on the air side and the latter favoring it being on the aqueous side.

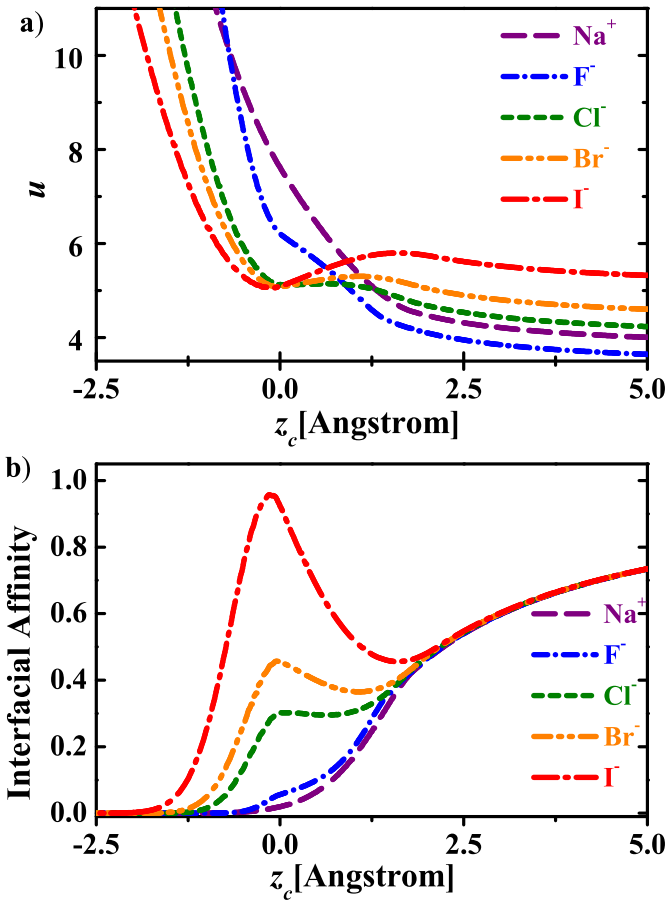

Figure 7.4: (a) Self energy and (b) interfacial affinity of F^-, Cl^-, Br^-, I^- and Na^+ at the water/air interface. $\varepsilon_1 = 80$, $\varepsilon_2 = 1$.

Figure 7.4(a) shows u for four halogen anions and the alkali-metal Na^+. We use the Born radius 2.26, 2.05, 1.91, 1.46 and 1.80 $\mathring{A}$[33], and the polarizability 6.90, 4.53, 3.50, 0.97 and 0.18 $\mathring{A}^3$[27, 28], respectively for I^-, Br^-, Cl^-, F^- and Na^+. For the larger and more polarizable ions, such as I^- and Br^-, the gain in cavity energy at the relatively low cost of electrostatic self energy leads to a local minimum at the interface in the self energy profile, which is consistent with the result of MD simulation using a polarizable potential model[34, 35]. For small and less polarizable ions, such as F^- and Na^+, u is monotonic and increases rapidly as the ion moves from the aqueous phase to air. Our theory predicts a more repulsive u_{el} for these ions on the water side than in Ref. [18],

which has the same qualitative effect as the hydration effect considered in Ref. [19, 20] for predicting the surface tension. For more complex ions such as IO_3^-, explicit treatment of hydration may be necessary[19, 20]. However, the quantitative importance of hydration needs to be reevaluated with our more accurate electrostatic self energy.

The self energy of an ion is closely related to the concentration profile of the ions. While a full treatment has to include the interaction between the ions, which leads to screening of the the image forces, we can obtain a qualitative picture of the ion distribution by defining the interfacial affinity as $e^{-[u(z_c)-u(\infty)]}$ to characterize the relative probability of finding the ion in the interfacial region to the bulk. In Fig. 3(b), we show the interfacial affinity for the halogen anions and Na^+. It is clear that our theory captures the known specific ion effect, which follows precisely the reverse Hofmeister series: $I^- > Br^- > Cl^- > F^-$[2, 3, 7]. The local peak in the interfacial affinity of I^- and Br^- ions is consistent with results of electron spectroscopy experiments [36] and computer simulations using polarizable fields [27, 28]. In addition, the interfacial affinity of halogen anions is larger than that of Na^+, from which we expect local charge separation and an induced electrical double layer at the interface in a NaX solution, with the halogen anions accumulating right around the location of the interface and the Na^+ ions next to it on the water side. The electrostatic potential gradient due to charge separation has been shown to be key to explaining the Jones-Ray effect[25, 26].

7.4 Water/Oil Interface

With a continuous self energy, our theory naturally applies to the liquid/liquid interface. In addition to cavity energy, dispersion forces have been suggested to be an important contribution to the nonelectrostatic self energy at the water/oil interface[8, 9, 20]. These nonelectrostatic contributions set a chemical potential difference between the two bulk phases in addition to the Born energy difference. Phenomenologically, these nonelectrostatic effects can be captured by a single parameter B with a crossover in the interfacial region that can be approximated by the interpolation scheme proposed by Levin and coworkers[18, 19, 20]. Similar to Eq. 7.6, we may write the nonelectrostatic self energy in the form:

$$u_{ne}^{w/o}(\mathbf{r}_c) = \begin{cases} B & z_c \geq a \\ \frac{B}{4}\left(\frac{z_c}{a}+1\right)^2\left(2-\frac{z_c}{a}\right) & a > z_c \geq -a \\ 0 & z_c < -a \end{cases} \tag{7.7}$$

Restricting our consideration to cavity energy and dispersion force, and taking the reference energy to be 0 in the bulk oil, $B = v^w - v^o + A_{eff}(\gamma/\gamma_0)$[20], where v^w is the cavity energy in water, which scales with the cavity volume for small cavity sizes ($a < 4\mathring{A}$) and with the surface area for

larger cavities[30, 31]. v^o is the cavity energy in oil, which is primarily due to the surface energy between the ion and oil[37, 38]. A_{eff} is the effective Hamaker constant for the water/oil interface, estimated to be about $4kT$[20] for a typical oil-water system. Alternatively, we can treat B as an adjustable parameter from the bulk partitioning of the ions between water and oil.

We defer a more general study of ions at the water/oil interface to a future study. Here we consider a special case of hydrophobic ions. Schlossman and coworkers observed strong adsorption of hydrophobic ions at the water/oil interface by X-ray reflectivity[11, 12, 13, 14], from which it is inferred that there is an attractive well for the self energy on the oil side. However, no explanation has been given to the origin of this attractive well. Within our theory, this phenomenon can be easily understood as arising from the long-range image charge attraction of the hydrophobic ions in the low-dielectric oil phase. Figure 7.5 shows the self energy and interfacial affinity of a hydrophobic ion calculated by our theory with $B = 33kT$, estimated using $A_{eff} = 4kT$, surface tension of water and surface tension of the oil used in the experiment[39]. As the ion approaches the interface from the oil side, u decreases because of the image charge attraction, and then increases rapidly due to the unfavorable contact with the aqueous environment. The peak in the interfacial activity on the oil side of the interface corresponds to minimum in the self energy with depth of about $5.8kT$, in good agreement with the experimental results[11, 12, 13, 14]. We note that although the choice of B will affect bulk partitioning of the ions, the depth of the attractive well is quite insensitive to the precise numerical value as long as B is large enough to ensure hydrophobicity of the ion. This clearly demonstrates the electrostatic origin of the strong adsorption of hydrophobic ions on the oil side of the interface, as the nonelectrostatic contributions (as depicted by the dash line) do not contain an attractive well.

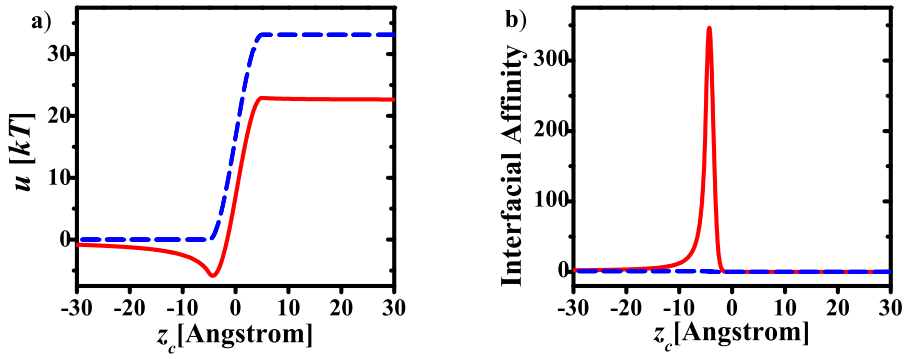

Figure 7.5: (a) Self energy and (b) interfacial affinity of a hydrophobic ion at the water/oil interface relative to the bulk oil. The dash line shows the results calculated by the nonelectrostatic contribution alone. $a = 5\mathring{A}$, $\gamma/\gamma_0 = 0.5$, $\varepsilon_1 = 80$ and $\varepsilon_2 = 5$. $B = 33kT$[39].

7.5 Conclusion

In conclusion, by treating both the short-range (solvation) and long-range (image force) electrostatic forces as well as charge polarization induced by these forces in a consistent manner, we obtain a simple continuous electrostatic self energy across the interface, making it applicable to both water/air and liquid-liquid interfaces. A systematic and accurate treatment of the electrostatic self energy is essential for evaluating the relative importance of the nonelectrostatic contributions. Combining the electrostatic self energy with existing models for nonelectrostatic contributions, we are able to explain a number of interfacial specific ion effects using the intrinsic parameters of the ion, such as the valency, radius, and polarizability. The self energy model developed here provides the essential ingredient in a complete theory to treat ions at finite concentration, via e.g., the weak coupling theory[40] or modified Poisson-Boltzmann theory[41], to describe the phenomena mentioned in the beginning of this chapter.

Bibliography

[1] J. N. Israelachvili, *Intermolecular and surface forces*, Academic, 1992.

[2] W. Kunz, P. Lo Nostro, and B.W. Ninham, *Curr. Opin. Colloid Interf. Sci.* **9**, 1 (2004).

[3] B. C. Garrett, *Science* **303**, 1146 (2004).

[4] V. S. J. Craig, B. W. Ninham and R. M. Pashley, *Nature* **364**, 317 (1993).

[5] Tavares, F. W., Bratko, D., Prausnitz, J. M. *Curr. Opin. Colloid Interface Sci.* **9**, 81 (2004).

[6] Gradzielski, M. *Curr. Opin. Colloid Interface Sci.* **9**, 256 (2004).

[7] F. Hofmeister, *Arch. Exp. Pathol. Pharmakol.* **24**, 247 (1888).

[8] P. L. Nostro and B. W. Ninham, *Chem. Rev.* **112**, 2286 (2012).

[9] M. Boström, D. R. M. Williams and B. W. Ninham, *Langmuir* **17**, 4475 (2001).

[10] M. Manciu and E. Ruckenstein, *Adv. Colloid Interface Sci.* **105**, 63 (2003).

[11] N. Laanait, et. al, *Proc. Natl. Acad. Sci. U.S.A.* **109**, 20326 (2012).

[12] N. Laanait, et. al, *J. Chem. Phys.* **132**, 171101 (2010).

[13] G. M. Luo et. al, *Science* **311**, 216 (2006).

[14] B. Y. Hou, et. al, *J. Phys. Chem. B* **117**, 5365 (2013).

[15] M. Bier, J. Zwanikken and R.van Roij, *Phys. Rev. Lett.* **101**, 046104 (2008).

[16] D. S. Dean and R. R. Horgan, *Phys. Rev. E* **69**, 061603 (2004).

[17] Z. -G. Wang, *Phys. Rev. E* **81**, 021501 (2010).

[18] Y. Levin, *Phys. Rev. Lett.* **102**, 147803 (2009).

[19] Y. Levin, A. P. dos Santos and A. Diehl, *Phys. Rev. Lett.* **103**, 257802 (2009); *Langmuir*, **26**, 10778 (2010).

[20] A. P. dos Santos and Y. Levin, *Langmuir*, **28**, 1304 (2012); *Faraday Disc* **160**, 75 (2013).

[21] C. Wagner, *Phys. Z.* **25**, 474 (1924).

[22] L. Onsager and N. N. T. Samaras, *J. Chem. Phys.* **2**, 528 (1934).

[23] G. Jones and W. A. Ray, *J. Am. Chem. Soc.* **59**, 187 (1937).

[24] P. B. Petersen and R. J. Saykally, *J. Am. Chem. Soc.* **127**, 15446 (2005).

[25] A. Onuki, *J. Chem. Phys.* **128**, art. no. 224704 (2008);

[26] R.Wang and Z.-G. Wang, *J. Chem. Phys.* **135**, 014707 (2011).

[27] P. Jungwirth and D. J. Tobias, *J. Phys. Chem. B* **106**, 6361 (2002).

[28] P. Jungwirth and D. J. Tobias, *Chem. Rev.* **106**, 1256 (2006).

[29] J. D. Jackson, *Classical Electrodynamics*, Wiley, 1999.

[30] K. Lum, D. Chandler, and J. D. Weeks, *J. Phys. Chem. B* **103**, 4570 (2005).

[31] D. Chandler, *Nature* **437**, 640 (2005).

[32] S. Rajamani, T. M. Truskett, and S. Garde, *Proc. Natl. Acad. Sci. U.S.A.* **102**, 9475 (2005).

[33] W. M. Latimer, K. S. Pitzer and C. M. Slansky, *J. Chem. Phys.* **7**, 108 (1939).

[34] L. X. Dang and T.-M. Chang, *J. Phys. Chem. B* **106**, 235 (2002).

[35] T.-M. Chang and L. X. Dang, *Chem. Rev.* **106**, 1305 (2006).

[36] S. Ghosal et al., *Science* **307**, 563 (2005).

[37] R. A. Pierotti, *Chem. Rev.* **76**, 717 (1977).

[38] T. T. Duignan, D. F. Parsons and B. W. Ninham, *J. Phys. Chem. B* **117**, 9421 (2013).

[39] For this large ion, the cavity energy is proportional to its surface area[30]: $v^w - v^o = 4\pi a^2(\sigma^{iw} - \sigma^{io})$, where σ^{iw} and σ^{io} are respectively the ion-water and ion-oil interfacial energy. We estimate σ^{iw} and σ^{io} in two ways. Taking the ion as a cavity (vacuum), these two surface energies can be approximated by the surface tension of water $\sigma^w = 72.8mN/m$ and the oil (1,2-Dichloroethane [14]) $\sigma^o = 38.75mN/m$. This yields $B \approx 33kT$. If we take the hydrophobic ion to be of the same material as the oil, then $\sigma^{io} = 0$. $\sigma^{iw} = \sigma^{ow}$, where $\sigma^{ow} = 28.2mN/m$ is the interfacial tension between water and 1,2-Dichloroethane[14]. This estimate gives $B \approx 28kT$.

[40] S. L. Carnie and G. M. Torrie, *Adv. Chem. Phys.* **56**, 141 (1984).

[41] D. Horinek and R. R. Netz, *Phys. Rev. Lett.* **99**, 226104 (2007).